T-3928

THE EFFECT OF DEOXIDATION SEQUENCE ON CARBON MANGANESE STEEL WELD METAL MICROSTRUCTURES

by

FANG-CHUN LIAO

T-3928

A thesis submitted to the Faculty and the Board of Trustees of the Colorado School of Mines in partial fulfillment of the requirements for the degree of Master of Sicence (Metallurgical Engineering).

Golden, Colorado
Date : June 04, 1900

Singed : Fang-Chun Liao

Fang-Chun Liao

Approved : Stephen Liu

Dr. Stephen K.C. Liu
Thesis Advisor

Golden, Colorado
Date : 6/5/90.

Signed : John Moore

Dr. John J. Moore
Professor and Head
Department of
Metallurgical Engineering

ABSTRACT

In order to investigate the individual and combined effects of aluminum and titanium on weld metal microstructures, experimental welds were made on 12.7 mm (0.5 in.) thick A516 G70 pressure vessel steel plates using E70S-3 filler wire and a low oxygen commercial flux.

Three passes were made per weld. The first pass was submerged arc welded, and the second and third passes were gas tungsten arc welded. Metallography and chemical analyses of the welds were performed. Inclusions were analyzed using carbon extraction replica and scanning electron microscopy (SEM).

In the aluminum or titanium addition series welds, the results indicated that the final weld metal microstructures are related to the inclusion size distribution and the amount of solute atoms in solid solution.

In the aluminum-titanium or titanium-aluminum (combined) addition welds, the deoxidation sequence is important in residual solute content and microstructural refinement. The amount of titanium-bearing or aluminum-bearing inclusions are an important factor to determine the acicular ferrite content. Excessive aluminum and/or titanium (in solution) increase the weld metal hardenability which results in

increased bainite content.

In summary, the deoxidation sequence plays an important role in the formation of specific types of non-metallic inclusions and in the determination of solid solution elements content, which are fundamental in microstructural refinement.

TABLE OF CONTENTS

LIST OF FIGURES

LIST OF TABLES

ACKNOWLEDGEMENTS

I wish to express my special gratitude to my advisor, Dr. Stephen Liu, for his guidance, advice, and encouragement during my graduate studies and this investigation. For above all duties as a professor, he is also a good friend.

I want to thank Dr. David L. Olson and Dr. William D. Copeland for participation in the committee.

I am also indebted to my good friend Steve Donelson and Bob Mcgrew for their help in sample preparation and microscopy work.

I would like to thank all my colleagues for their discussion and friendship, with special recognition of the following individuals :Matt Dvornak, Bumsoo Han, Shoji Okamoto, Kirk Erven, and P. R. Chidambaram.

Last, but not least, I am grateful to my family, especially my parents, my wife Yih-Shyuan and my son Frederick for their patience, understanding, and support during my studies at the Colorado School of Mines.

I. INTRODUCTION

In order to satisfy many critical engineering applications , high strength, high toughness steel weld metals have been widely investigated in recent years to determine the factors that control weld metal microstructure.

During the austenite-to-ferrite decomposition, the first transformation product is grain boundary ferrite which forms along prior austenite grain boundaries. Following, Widmanstatten sideplate ferrite nucleates and grows from grain boundary ferrite as long needle-like laths that protrude into the austenite grains. As the temperature continues to drop, fine acicular ferrite laths begin to nucleate intragranularly. Finally, the remaining austenite transforms to a variety of micro-constituents which include bainite, martensite, etc. The relative proportions of these products are strongly influenced by the nonmetallic inclusions in the weld metal.

Several models have been proposed to explain the effects of nonmetallic inclusions in the weld metal on the formation of acicular ferrite. However, the influence of deoxidizers on inclusion formation and inclusion size distribution is still not fully understood. The deoxidizers are added into

the weld pool in the form of an electrode or fluxes.

All the deoxidizers present in the weld pool compete with each other for the oxygen atoms, and the individual and combined effects of these elements in weld pool deoxidation are not clearly distinguished. This research focuses on the weld pool deoxidation sequence to better understand the relationship between weld metal microstructures and nonmetallic inclusions.

II. LITERATURE REVIEW

II.1. Solidification Structure In Low Carbon Steel Welds

Fusion welding is one of the most important joining techniques used in manufacturing. During arc welding, an electrical arc is used as the heat source to form a molten pool of metal. As the heat source moves forward, solidification will occur in the molten weld pool.

Easterling [1] has mentioned that in most of the low carbon, low alloy steels, the primary solidification product is in the form of parallel arrays of dendrites or cells.

Savage and Aronson [3] showed that solidification begins by "epitaxial growth" on the base metal grains along the fusion line. Grains generated in the weld metal have the same size and crystallographic orientation as the immediately contiguous parent plate grains across the fusion boundary [3,4]. The close composition between weld metal and parent plate results generally in a very small wetting angle [5]. This effectively decreases the energy barrier to nucleation and almost no undercooling is required to initiate solidification, Figure 1. For cubic crystal materials, the <100> directions are the preferred easy-growth directions for dendrites growth. As the heat source moves forward, the new

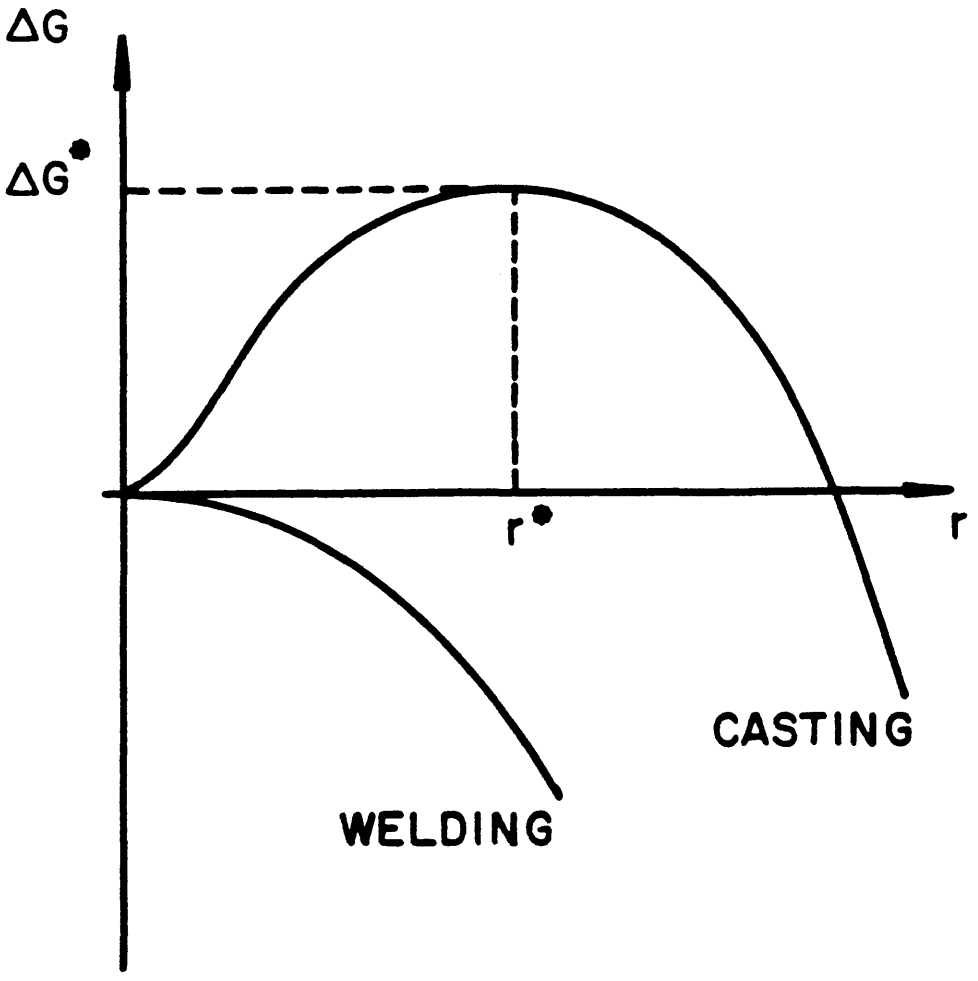

Figure 1. The different free energy during forces for casting and welding solidification. Epitaxial growth in welding processes reduce the nucleation energy barrier to zero.

and old dendrites must adjust themselves toward the maximum thermal gradient which is always normal to the fusion boundary [6].

As the weld metal temperature reaches the peritectic temperature, austenite starts to form. The reaction is :

Liquid Iron + Delta Ferrite ----> Austenite. -----(1)

Using a double etching techniques (saturated picric acid solution and 2 volume percent Nital), it is easy to observe that the δ-ferrite grains are rotated with respect to the austenite grains. This proves that the δ-ferrite grains and the austenite grains may not have occurred at the same time [5]. Due to the high temperature, the austenite grains grow until their boundaries impinge or are pinned by inclusions or precipitates. In submerged arc welding (high heat input), austenite grain growth in the heat affected zone is substantial.

II.2. Solid State Phase Transformation Structures

When the solidified carbon-manganese steel weld metal cools down , austenite decomposition will occur. Table 1 [12] is a summary of the various names used by different

Table 1. Classification and terminology of microstructures in low alloy steel weld metal [12]. (review)

Dube,C.A. Aaronson,H.I. Cochrane,R.C.	Widgery,D.J.	Abson,D.J.	Ito,Y. Watanabe,I. Kikuta,Y. etc.	Parageter,R.J. Levine,E. Choi,C.L. etc.
Allotriomorphic (Polygonal) Ferrite	Proeutectoid Ferrite	Grain Boundary Ferrite	Proeutectoid Ferrite, Grain Boundary Ferrite, Polygonal Ferrite	Proeutectoid Ferrite, Grain Boundary Ferrite, Block Ferrite
		Polygonal Ferrite	Polygonal Ferrite	Ferrite Islands
Primary & Secondary Ferrite Sideplates	Lamellar Component	Ferrite with Aligned M-A-C	Ferrite Sideplate, Lath-Like Ferrite	Ferrite Sideplate, Lath Ferrite Upper Bainite
Intragranular Ferrite Plates	Acicular Ferrite	Acicular Ferrite	Acicular Ferrite, Needle Like Ferrite,	Acicular Ferrite, Fine Bainitic Ferrite
Lath Martensite Twinned Martensite Upper Bainite	Martensite	Martensite M-A	Martensite M-A High-C Martensite, Upper Bainite	Martensite M-A Lath Ferrite

research groups for the classification of weld metal microstructures. In this research the following nomenclature is used :

(1). Grain boundary ferrite (GBF).
(2). Polygonal ferrite (PF).
(3). Widmanstatten sideplate ferrite (SP).
(4). Acicular ferrite (AF).
(5). Bainite (B).
(6). Microconstituents (MAC).

II.2.1. Grain Boundary Ferrite (GBF)

During the austenite-to-ferrite transformation, the highest temperature transformation product is GBF which nucleates along prior austenite grain boundaries. Elongated ferrite along the austenite grain boundary is also known as ferrite veins, Figure 2(a). Ferrite veining is considered detrimental to weld metal toughness because it can provide a continuous crack path through the weld metal [7,8].

II.2.2. Polygonal Ferrite (PF)

Many authors [9,10,11] consider grain boundary ferrite and polygonal ferrite as primary ferrite, because it is not

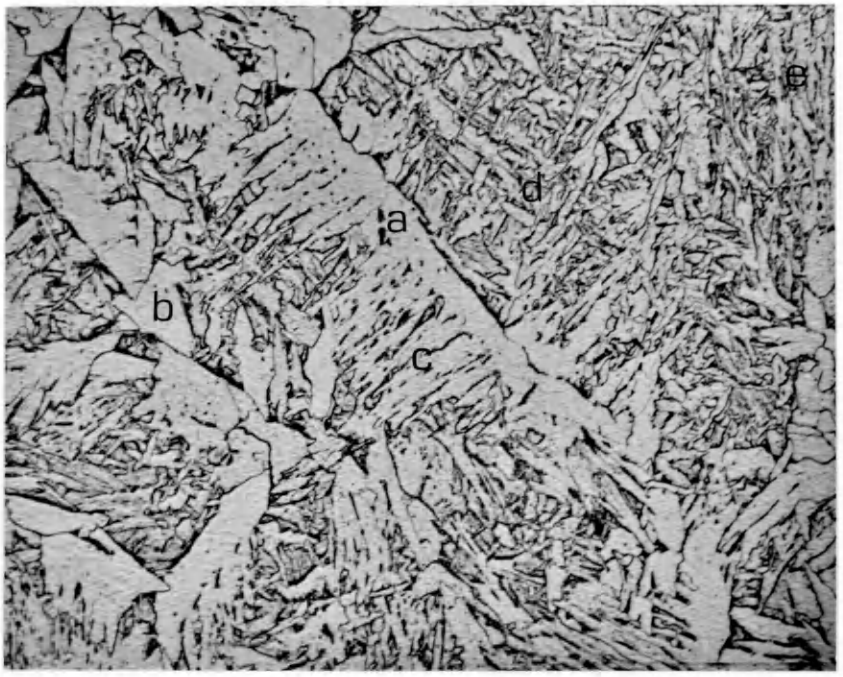

Figure 2. Optical micrographs showing the different microstructures found in C-Mn steel weld metal. a.GBF b.PF c.SP d.AF e.B

easy to distinguish those two constituents, Figure 2(b). Granular Polygonal ferrite can form intragranularly when the cooling rate is very slow or the alloy content is low [12].

II.2.3. Widmanstatten Sideplate Ferrite (SP)

Widmanstatten sideplate ferrite forms at a lower temperature than grain boundary ferrite and polygonal ferrite. Sideplate ferrite nucleates at GBF and grows as long needle-like laths that protrude into the austenite grains, as shown in Figure 2(c). The SP growth rate is controlled by the carbon diffusion away from the tips of the needles [13,14]. Between the growing needles and the parent austenite, Kurdjumov-Sachs orientation relationship is observed [15].

K-S orientation relationship :

$$(110)_{bcc} \;//\; (111)_{fcc} \;,\; [1\bar{1}1]_{bcc} \;//\; [0\bar{1}1]_{fcc}$$

Commonly the aspect ratio of the Widmanstatten sideplate ferrite needles are approximately 10:1, but laths with aspect ratios as large as 20:1 have been found [15].

II.2.4. Acicular Ferrite (AF)

As the transformation temperature continues to drop, AF laths nucleates intragranularly on non-metallic inclusions. Sometimes several ferrite laths share a nucleation site and grow outward forming a star shaped group. Most of acicular ferrite is 1 to 2 μm thick with aspect ratio varying from 3:1 to 10:1 and shown in Figure 2(d) [12]. The fine ferrite grains, high angle boundaries, and the interlocking nature of the laths explain the high toughness and high strength properties of acicular ferrite.

II.2.5. Bainite (B) And Microconstituents (MAC)

During austenite decomposition, the higher temperature transformation products continue to eject carbon and alloying elements into the untransformed austenite. This may delay further transformation of austenite. The enrichment of carbon may also lead to a variety of low transformation temperature products which include bainite, martensite, and pearlite, depending upon cooling rate and alloy components. Bainite generally forms packets associated with grain boundaries and the inclination between laths is small, as shown in Figure 2(e). Additionally, the dislocation density of bainite is high. The aspect ratio of bainite laths can be as high as

Widmanstatten sideplate ferrite [12]. Depending on the cooling rate and carbon rejection, retained austenite can also be found in a low carbon low alloy steel weld metal.

II.3. Weld Pool Deoxidation Practice

In steel making, elements with higher affinity for oxygen than iron are added to the molten bath for the purpose of deoxidation. The most common deoxidants used in steel making are aluminum, manganese, silicon, titanium, calcium, zirconium, and elements in the rare earth group. In arc welding, these elements can enter the weld pool from the base metal,electrode filler wire, or fluxes. In ladle refining of steels the deoxidation reactions occur at near isothermal and equilibrium conditions, different from that found in most welding conditions. The non-isothermal, non-equilibrium natures of arc welding make it very difficult to identify clearly the deoxidation sequence in the weld pool and the effect on weld metal microstructure.

In the submerged arc welding process, oxygen comes mainly from the flux which may contain easily reduced oxides such as iron oxide, manganese oxide, silica, etc [17]. Due to the high temperature in the weld pool these oxides quickly dissociate. At 1600°C, the solubility of oxygen in pure

molten iron is approximately 1600 ppm [18]. During solidification, the weld pool oxygen concentration established at high temperatures will readjust as a result of decreasing oxygen solubility and the combination of oxygen with deoxidizers that exist in the weld metal. Kluken and Grong [19] divided the weld pool into two reaction zones. One is the "hot" reaction zone, the weld pool right beneath the arc root, where the deoxidation products are continually separated by highly turbulent flows which sweep those products out of the weld pool. The other is the "cold" reaction zone where most of the precipitated products are entrapped in the weld metal as finely dispersed particles.

II.3.1. Richardson's Diagram

The free energies of formation of some common oxides are plotted as a function of temperature in Figure 3. Each line represents an element reacting with oxygen to form an oxide. The sequence of those curves is dependent on the affinity with oxygen of each deoxidant. Oxides described by the lower lines are more stable than the ones represented by the higher lines. Figure 3 is very useful in evaluating the relative reducing or oxidizing tendencies of metals. For example, aluminum will reduce FeO to iron at all temperatures and

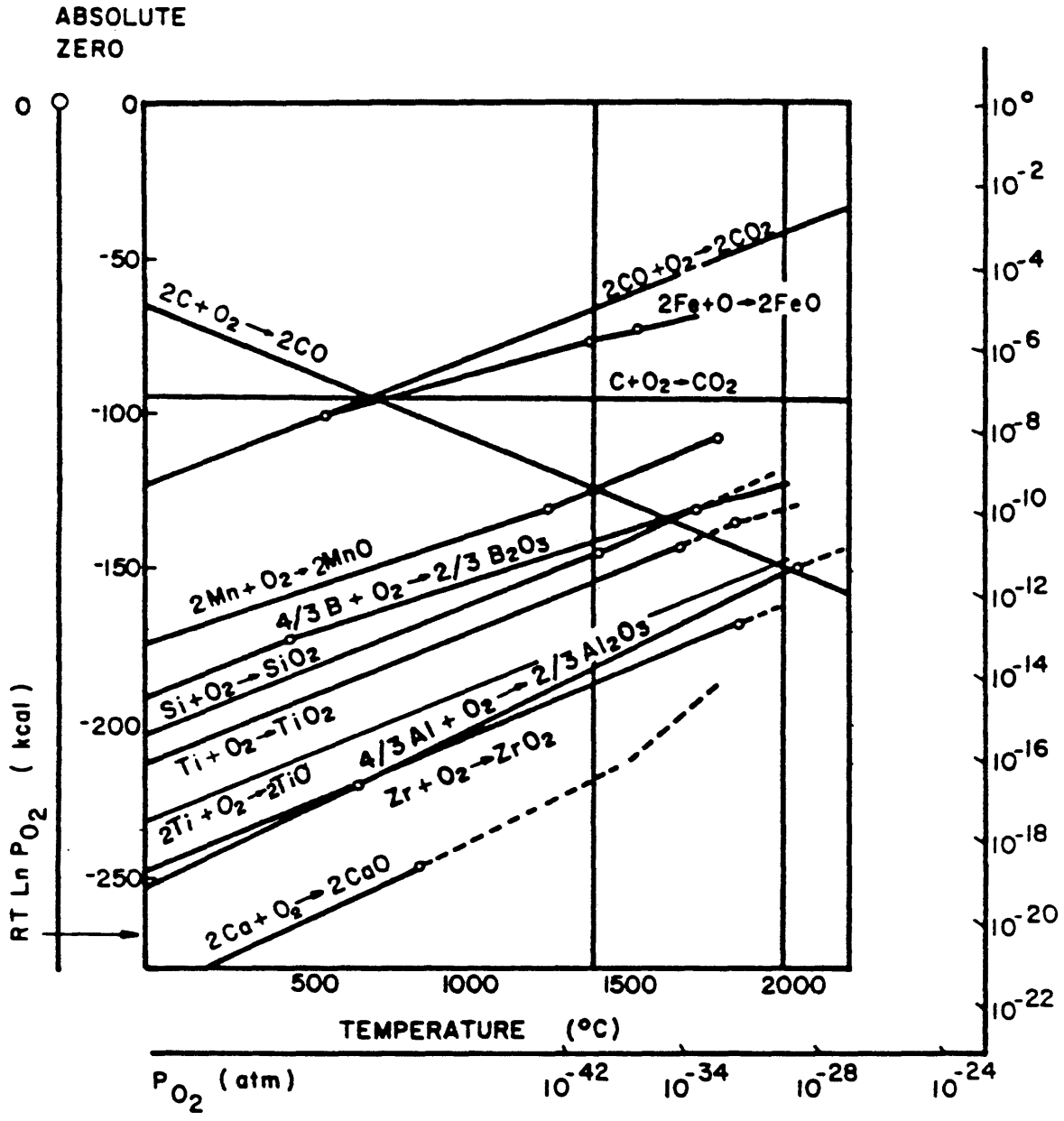

Figure 3. Richardson diagram [81] showing the stability of some major oxides commonly found in welding flux systems. (after Liu [5])

this can be considered by the free energy change of formation of Al_2O_3 and FeO.

At 1500 °C,

$$4/3\ Al_{(s)} + O_{2(g)} \rightarrow 2/3\ Al_2O_{3(s)} \quad \Delta G^\circ = -176\ kcal \quad ---(2)$$

$$2\ Fe_{(s)} + O_{2(g)} \rightarrow 2\ FeO_{(s)} \quad \Delta G^\circ = -72\ kcal \quad ---(3)$$

combining equations [(2) - (3)] ,

$$4/3\ Al_{(s)} + 2\ FeO_{(s)} \rightarrow 2/3\ Al_2O_{3(s)} + 2\ Fe_{(s)} \quad ---(4)$$
$$\Delta G^\circ = -104\ kcal$$

the ΔG° of reaction described by equation (4) is negative indicating that the reaction is thermodynamically feasible and spontaneous.

In Figure 3, the order of decreasing stability of oxides are Al_2O_3, TiO, TiO_2, SiO_2, MnO and FeO. However, arc welding does not occur isothermally, nor in equilibrium conditions, the sequence of deoxidation reactions that occur in the weld pool may be very complicated .

II.3.2. Deoxidation Reaction Products

In the welding process, the amount of oxygen in the weld metal is decreased by the addition of deoxidizers and the level of residual oxygen in liquid iron is strongly dependent on the amount and kind of deoxidants added, as illustrated in Figure 4 [20], which is a plot of equilibrium oxygen concentrations in liquid iron as a function of deoxidant contents at 1600 °C [20]. If only one deoxidant is used in the welding system, the deoxidation sequence and products are much easier to understand and predict. In reality, however, the four major deoxidants used in steel welding are manganese (Mn), silicon (Si), aluminum (Al), and titanium (Ti). As result, inclusions containing these deoxidizers are formed and the amount of alloying elements and deoxidizers strongly affects the final inclusions composition, size, and shape. As iron has the lowest affinity for oxygen, it will only react with oxygen after all deoxidizers are consumed. The degree of deoxidation of the weld metal can therefore be revealed by the level of FeO residual in the weldments.

Manganese (Mn)

In normal deoxidation condition by only Mn addition, the final deoxidation product will be rich in MnO with a small

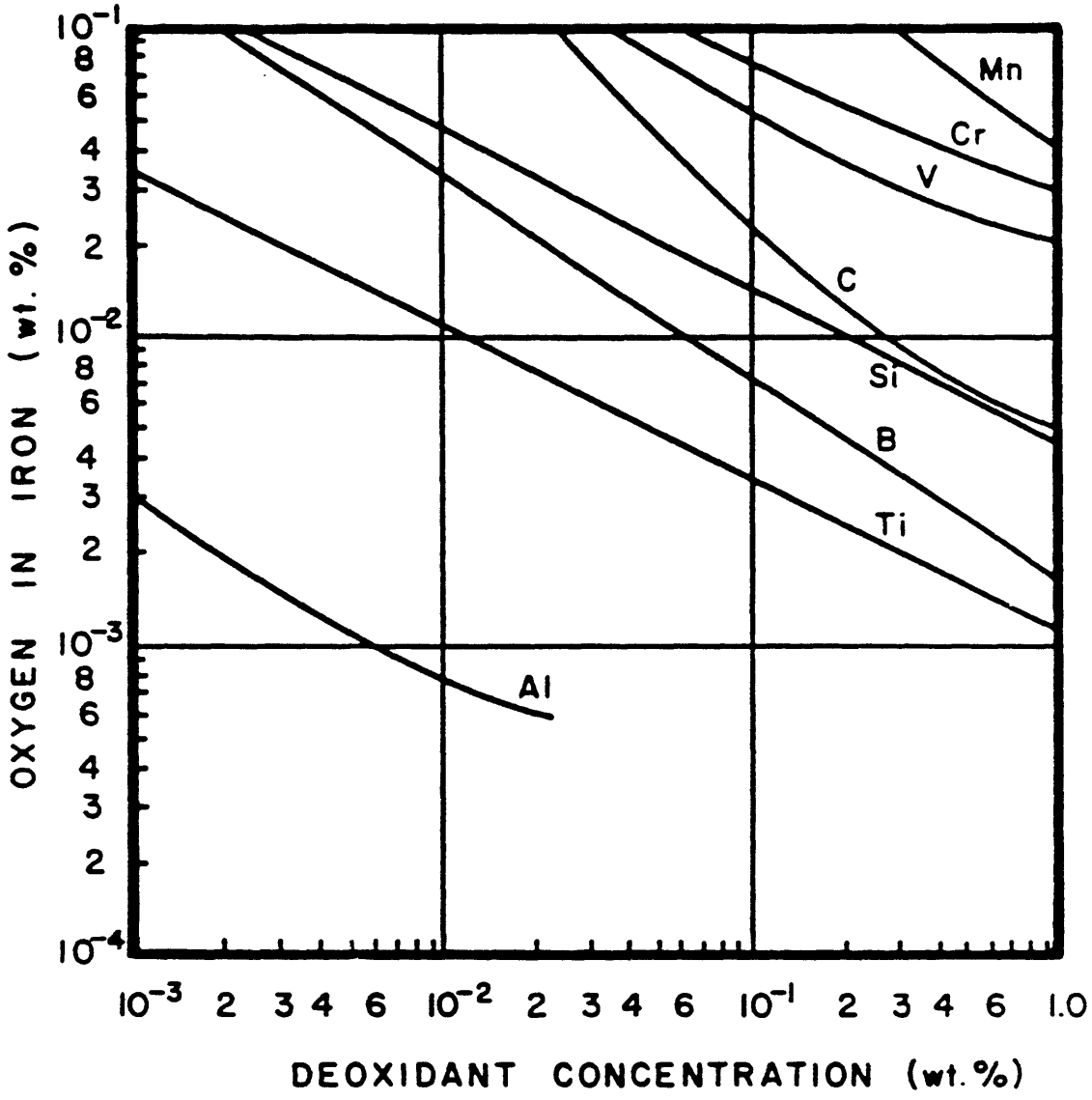

Figure 4. The equilibrium plot of the concentrations of oxygen is liquid iron as a function of deoxidant contents at 1600 °C [20].

amount of FeO [72]. The deoxidation reaction in the weld pool is shown by following equation.

$$Mn_{(l)} + FeO_{(l)} \rightarrow MnO_{(s)} + Fe_{(l)} \quad ---(5)$$

The inclusion type and shape are strongly dependent on the ratio of MnO/FeO. With high manganese level (high MnO/FeO ratio), inclusions have the tendency to have irregular morphology. But in low manganese level (low MnO/FeO ratio), the morphology of inclusions are always spherical.

Silicon (Si)

If only silicon is used as the deoxidizer in the welding system, the final deoxidation product in the weldments is the solid silica [18] and the deoxidation reaction can be written as following equation.

$$Si_{(l)} + 2FeO_{(l)} \rightarrow SiO_{2(s)} + 2\ Fe_{(l)} \quad ---(6)$$

Aluminum (Al)

In the particular case of deoxidation by only aluminum, the final products can be a compound of Al_2O_3 and FeO. Only in relatively high aluminum content welds is pure $Al_2O_{3(s)}$

formed. The deoxidation reactions in the weld pool can be written as the following two equations.

(1). In high aluminum content welds,

$$2\ Al_{(l)} + 3\ FeO_{(l)} \rightarrow Al_2O_{3(s)} + 3\ Fe_{(l)} \quad ---(7)$$

(2). In lower aluminum content welds.

$$2\ Al_{(l)} + 4\ FeO_{(l)} \rightarrow Al_2O_3 \cdot FeO_{(s)} + 3\ Fe_{(l)} \quad ---(8)$$

Titanium (Ti)

Using titanium as the only deoxidant, the deoxidation products are more complicated than the ones previously described. Increasing the weld metal titanium content, the content of titanium in the inclusions are also increased, the final form of inclusions may be TiO_2 or TiO.

However, in real arc welding processes, more than one deoxidant is added to the weld pool and the deoxidation sequence is complicated and most of the inclusions occur in a combined form, with more than one oxide compound.

II.3.3. Chemical Composition Of Inclusions

It has been known for a long time that weld metal inclusions are inhomogeneous. Generally speaking, the cores of the inclusions consist mainly of a mixture of oxides with aluminum, manganese and silicon [2,84], unless very low amounts of aluminum or substantial amounts of titanium are present. Due to the complicated chemical nature of weld metal inclusions, several ternary diagrams were used to explain the deoxidation sequences in the weld pool [19,21,22-26]. These diagrams can be divided into two major groups. The $MnO-SiO_2-Al_2O_3$ system [19,22,24,26] and the $MnO-(SiO_2+TiO_2)-Al_2O_3$ system [21,25].

Considering bulk inclusion compositions with only minor titanium content in the inclusions, the $MnO-SiO_2-Al_2O_3$ diagram can be used to describe the chemical nature of the inclusions and is shown in Figures 5 to 7. In Figure 5, the $MnO-SiO_2-Al_2O_3$ ternary system shows the stoichiometric composition of the different phases which have been reported [24]. Figure 6 shows the measured inclusion compositions in deoxidized submerged arc steel weld metals by Kluken and Grong [19]. The mean inclusion composition of their welds are located around the line where the $[\%SiO_2]$: $[\%MnO]$ ratio approximately equal to 0.94. Figure 7 represents the mean

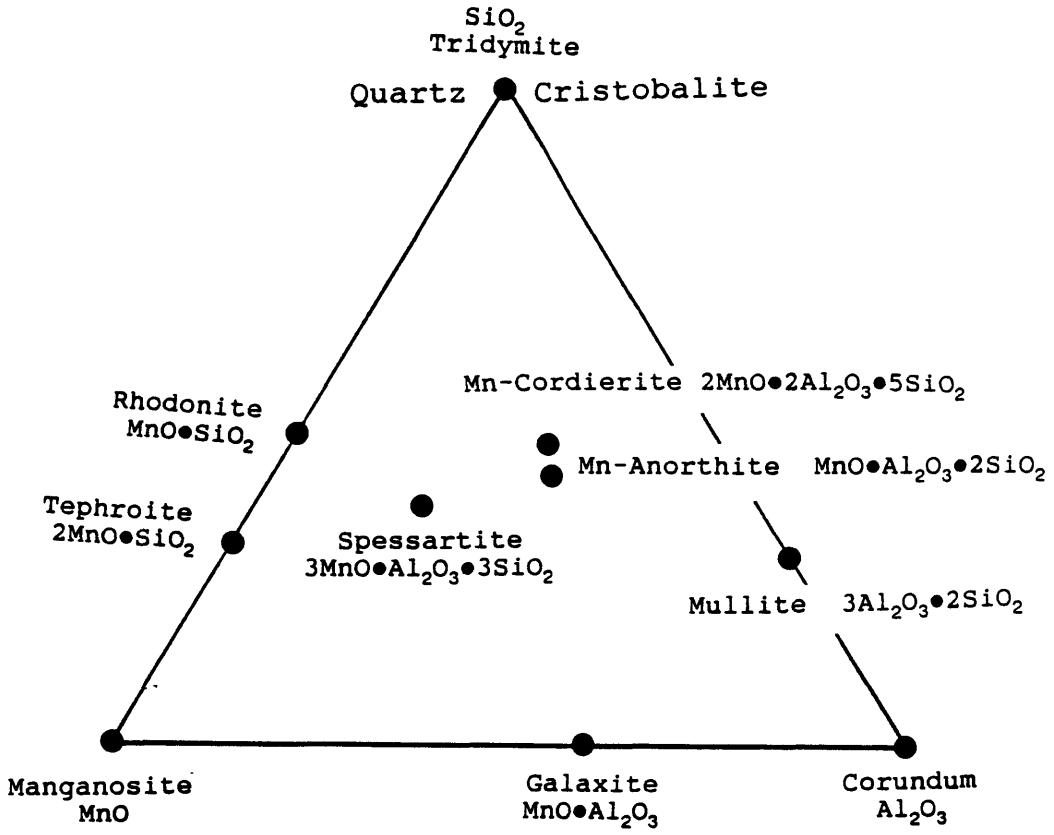

Figure 5. The stoichiometric composition of the different phases in the $MnO-SiO_2-Al_2O_3$ system. (after Keissling and Lange [24])

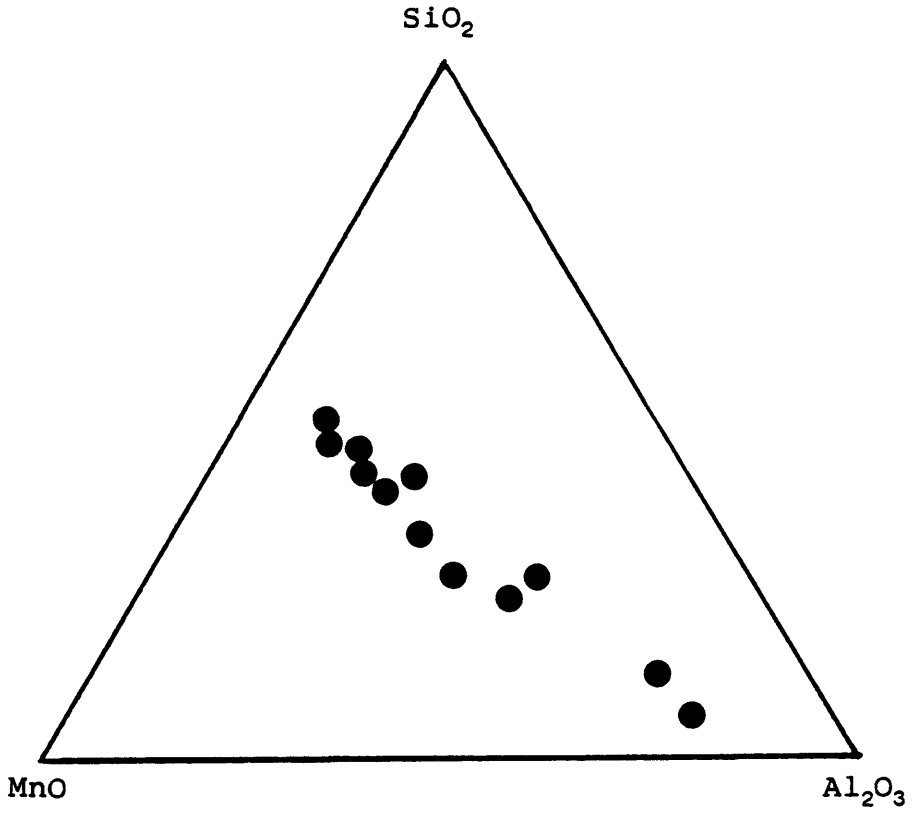

Figure 6. Measured average composition of inclusions in Si-Mn-Al-Ti deoxidized submerged arc welds. (after Kluken and Grong [19])

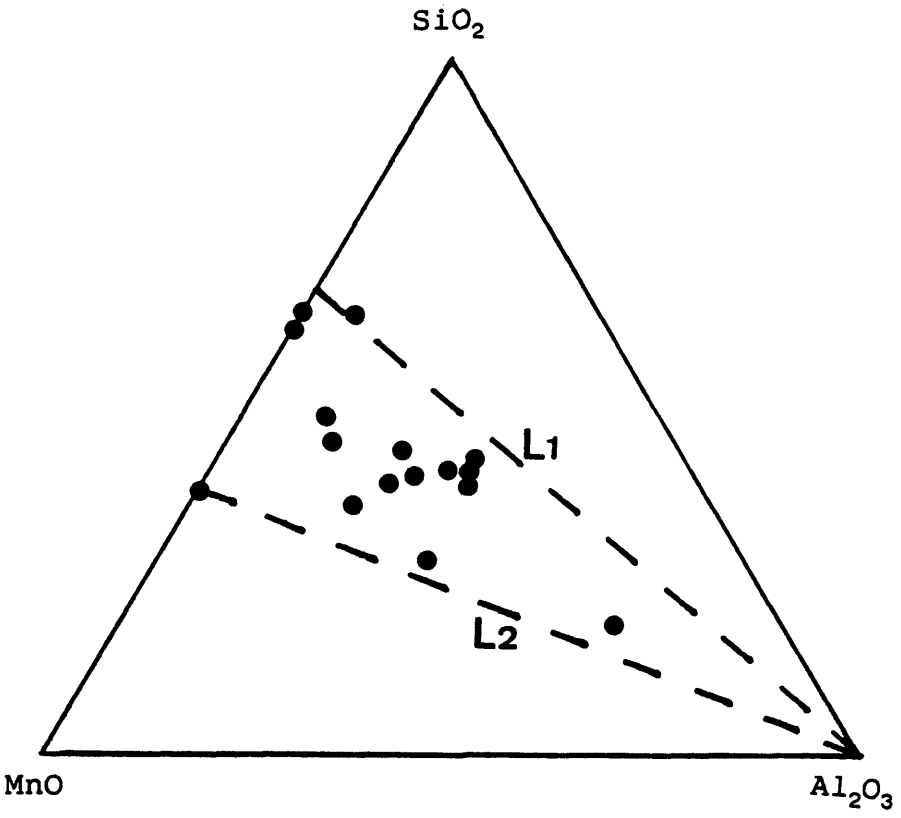

Figure 7. Summary of the analytical results regarding occurrence and plotting in the $MnO-SiO_2-Al_2O_3$ ternary system.
(after keissling and Lange [24])

compositions obtained from many different inclusions collected by Keissling and Lange. [24] The inclusion compositions seem to fall in the region limited by the two lines, L_1 and L_2, where the [%SiO_2] : [%MnO] ratios are 0.6 and 1.2. Both Figures 6 and 7 shown the similar phenomena that the majority of the inclusions have their compositions lie close to the line joining Corundum (Al_2O_3) to Rhodonite ($MnO \cdot SiO_2$) with an approximately constant [%SiO_2] : [%MnO] ratio at varied Al_2O_3 contents.

Saggese et al. [21] designed their experiments using filler wires with and without titanium and plotted the average compositions of the inclusions on the MnO-(SiO_2 + TiO_2)-Al_2O_3 ternary diagram shown in Figure 8. Again, the majority of the inclusions show constant SiO_2 to MnO ratio, despite different aluminum and titanium addition.

II.4. Inclusion Effects On Weld Metal Phase Transformations

It is generally accepted that high toughness and high strength are associated with large volume fraction of acicular ferrite (AF) in the low carbon low alloy steel weld metal microstructure [27-29]. As such, to be able to control the mechanical properties of these welds, it is necessary to understand the transformation mechanism of acicular ferrite.

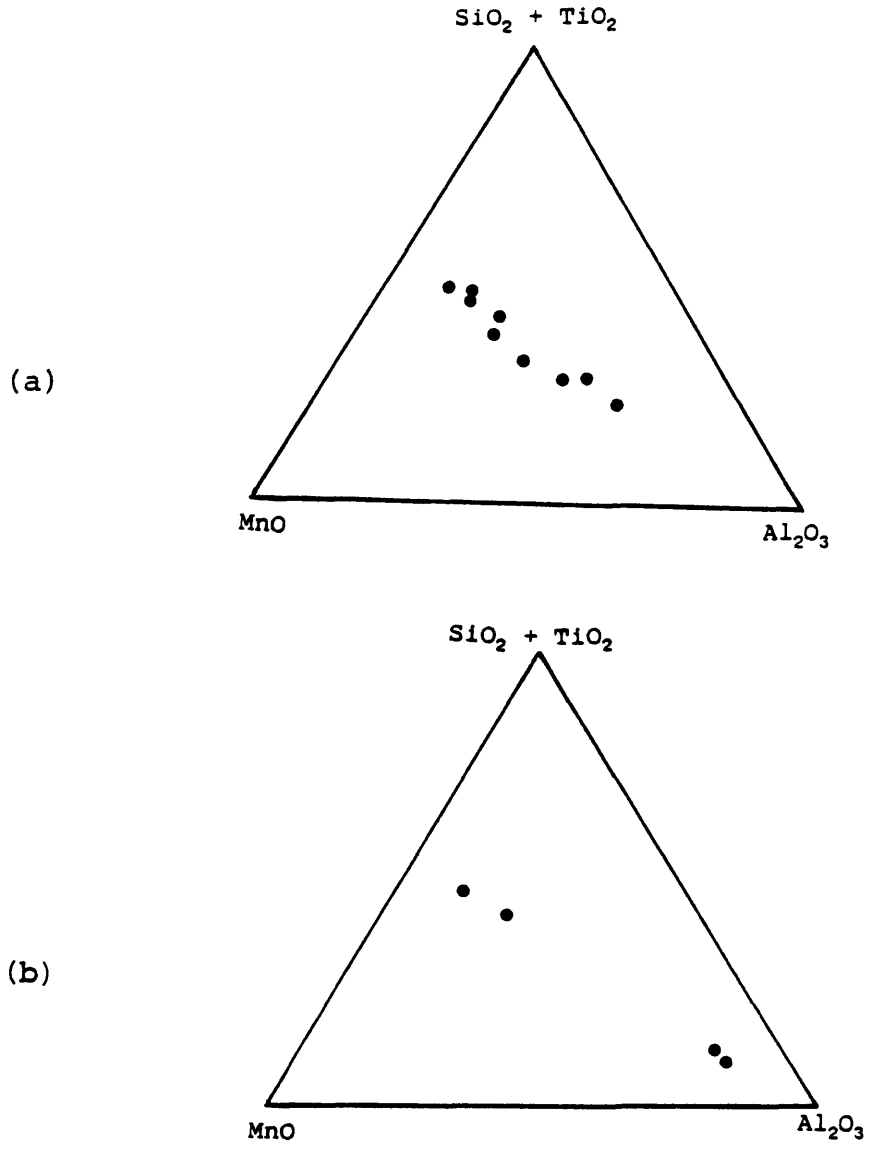

Figure 8. Measured average compositions of inclusions in submerged arc steel weld metals.
(a). filler wire with high Si content, no Ti.
(b). filler wire with low Si content, with Ti.
(after Saggese et al. [21])

The formation of AF is closely related to the oxygen content of the weld metal [30-37] and the type, volume fraction, and size distribution of the inclusions [36-38].Several models have been proposed to explain the effects of inclusions on the formation of AF. These include

(1). Austenite grain boundary pinning model.
(2). Inclusion type model.
(3). Inclusion size distribution model.
(4). Lattice disregistry model.
(5). Differential thermal strain model.

II.4.1. Austenite Grain Boundary Pinning Effect

Inclusions located at the austenite grain boundaries can affect the austenite-to-ferrite transformation. In high oxygen content welds (i.e., high inclusion volume fraction), the finer inclusions will pin the austenite grain boundaries to limit grain growth and serve as nucleation sites for higher temperature transformation products. Cochrane and Kirkwood [37], Harrison and Farrar [39], and Ferrante and Farrar [40] also offered similar explanations in their investigations. Ferrante and Farrar [40] determined that austenite grain size larger than 45 μm have the tendency to

produce the acicular ferrite. More recent studies reported larger austenite grain sizes, at the order of 100 μm, to promote acicular ferrite formation [5,86].

Inclusion size is an important factor that affects the austenite grain boundary pinning effect. Large particles are less effective in pinning than small particles. Liu [5] and Fleck [47] offered similar observations in their investigations. Zener derived a relationship between inclusion volume fraction (Vv), prior austenite grain size (D), and "effective" particle diameter (Zener diameter - ϕ) to estimate the inclusion size that is capable of pinning the austenite grain boundary.

$$\phi = 3/2 \times D \times Vv \qquad ---(9)$$

Only those particles smaller than the Zener diameter will pin the austenite grain boundary. Large particles are generally located within the austenite grains and often serve as nucleation sites for intragranular ferrite formation.

Harrison and Farrar [39] verified the relationship between oxygen content (inclusion content) and the austenite grain size using laser remelting of the weld metal. They showed that reducing the oxygen content (inclusion content)

in welds increased the austenite grain size which suggested that non-metallic inclusions may have significant effect on grain boundary pinning.

II.4.2. Inclusion Type Effect

Weld metal inclusions are chemically inhomogeneous and may contain oxides of aluminum, manganese and silicon. Pargeter [42] observed that some microstructural constituents are associated with specific type of inclusions. For example, acicular ferrite is often found related to aluminum-bearing inclusions. Several authors [21,42,43] have observed a correlation between moderately high Al_2O_3 (> 50% Al_2O_3) content inclusions and high proportions of acicular ferrite. Others [21] reported that when little titanium is present in the inclusions the amount of AF decreases as the amount of Al_2O_3 in the inclusions decreases, indicating the importance of aluminum. Above a certain amount of titanium in the inclusions (≥ 2.5% TiO) the proportion of AF was independent of inclusion Al_2O_3 content and large proportions of AF were always present. Terashima and Hart [44] obtained similar results. Both Cochrane and Keville [45] and Barritte and Edmonds [46] reported that AF content decreased when the inclusion composition changed from alumina-rich to manganese

alumina silicates. Grain boundary ferrite and Widmanstatten sideplate ferrite are always associated with inclusions that contain manganese and silicon, with or without sulfur. In submerged arc welds, inclusions covered by sulphide shells are observed to inhibit acicular ferrite nucleation [19,41]. Recently, $MnO \cdot Al_2O_3$ (galaxite) is widely accepted to be effective nucleation site for acicular ferrite formation [22]. Mills et al. [53] are also reported the same results in their investigation.

II.4.3. Inclusion Size distribution Effect

The inclusion size distribution is an important factor to determine the austenite grain size. A population with a large fraction of smaller particles can pin the grain boundary more effectively than a population with many large inclusions. Some authors [5,32] reported smaller austenite grain size with smaller mean inclusion diameters. Cochrane and Kirkwood [37] indicated that a certain size distribution of inclusions is required to obtain large volume fraction of AF. Terashima and Hart [44] suggested that inclusions with mean diameter smaller than 0.56 μm were too small to nucleate AF and that those with mean diameter larger than 0.81 μm were too large to nucleate AF.

II.4.4. Lattice Disregistry Effect

In heterogeneous nucleation, the interfacial free energy between the inclusion and the nuclei is the major energy barrier for nucleation [13,14]. The interfacial free energy is mainly due to the difference in lattice parameters between the inclusion and the new nucleated phase. Turnbull and Vonnegut [48] developed an equation to express the lattice disregistry effect and proposed that the smaller the mismatch the greater the tendency of nucleation.

$$\delta = \Delta a_0 / a_0 \qquad ---(10)$$

δ : the lattice mismatch

Δa_0 : the difference lattice parameter between the inclusion and the nucleated phase for a low index plane.

a_0 : the lattice parameter for the nucleated phase.

Bramfitt [48] modified the Turnbull and Vonnegut equation by considering the mismatch over several planes.

It was noted that constituents with a low lattice disregistry with nucleated ferrite, for example, TiO, TiN [30,49-53], galaxite ($MnO \cdot Al_2O_3$) [51,53-55], have been reported

to be effective nucleation agents for AF formation during the austenite-to-ferrite transformation. Some crystallographic data of several potential nucleating agents are listed in Table 2 [50,54].

II.4.5. Differential Thermal Contraction Effect

Due to the different thermal contraction coefficients of the inclusion and the austenite matrix, the strain energy involved in the phase transformation is expected to affect the thermodynamic driving force of nucleation. It has been found that the thermal contraction coefficient of austenite is much higher than that of the oxide inclusions [18,55]. On cooling, the austenite matrix is strained and may accelerate the austenite to ferrite transformation reaction.

Laszlo [55] and Easterling [1] studied the stresses caused by differential thermal contraction and determined these stresses using the equation below :

$$\sigma = \Gamma \bullet [\ (\alpha_{matrix} - \alpha_{inclusion}) \bullet \Delta T\ ] \quad ---(11)$$

σ :the stress generated in austenite matrix due to contraction.

Table 2. Crystallographic data for the effective nucleating agents. [50 , 54]

Compound	Crystal Structure	Lattice Parameter (Å)			Relation of Planes between Nucleating Agents and α –Fe	Planar Disregistry (%)
		a_o	b_o	c_o		
TiN	Cubic (NaCl)	4.235	--	--	$(100)_n//(100)_\alpha$ $[010]_n//[011]_\alpha$	3.8
Ti_2O	Hexagonal	2.959	--	4.845	$(0001)_n//(111)_\alpha$ $[001]_n//[110]_\alpha$	29.3
TiO	Cubic (NaCl)	4.177	--	--	$(100)_n//(100)_\alpha$ $[010]_n//[011]_\alpha$	3.0
TiO_2	Tetragonal (SnO_2)	4.594	--	2.958	$(001)_n//(110)_\alpha$ $[010]_n//[110]_\alpha$	8.8
B_2O_3	Hexagonal	4.336	--	8.340	$(0001)_n//(111)_\alpha$ $[001]_n//[110]_\alpha$	5.8
BN	Hexagonal	2.550	--	4.200	$(0001)_n//(111)_\alpha$ $[001]_n//[110]_\alpha$	37.8
Al_2O_3	Hexagonal (Cr_2O_3)	4.759	--	12.991	$(0001)_n//(111)_\alpha$ $[121]_n//[110]_\alpha$	16.0
$MnO.Al_2O_3$	Spinel	8.250	--	--	$(100)_n//(110)_\alpha$ $[010]_n//[011]_\alpha$	1.8

Note :

n :substrate

α :nucleating phase α - Fe

Γ :a proportionally factor that is a function of the elastic modules of the inclusion and austenite matrix, and inclusion geometry.

α_{matrix} :thermal expansion coefficient of the austenite matrix.

$\alpha_{inclusion}$:thermal expansion coefficient of the inclusion.

ΔT :the temperature change during coding.

The thermal expansion coefficients of some inclusions commonly found in steels are listed in Figure 9 [5]. Based on the strain energy concept, the most favorable inclusion to act as substrate for ferrite nucleation is $(MnO)_2(Al_2O_3)_2(SiO_2)_5$, because it has the largest difference in thermal expansion coefficient from austenite. However, using a gleeble thermomechanical simulator, Dallam [85] found no significant effect of thermal contraction.

II.5. Microalloying Elements Effects On Weld Metal Microstructures

It is well known that adequate alloy elements added to the weld pool decrease the amount of grain boundary ferrite. Evans [82] reported that manganese can reduce the prior austenite grain size and increase the amount of AF in the welds. The increase of AF is mainly due to the decreasing

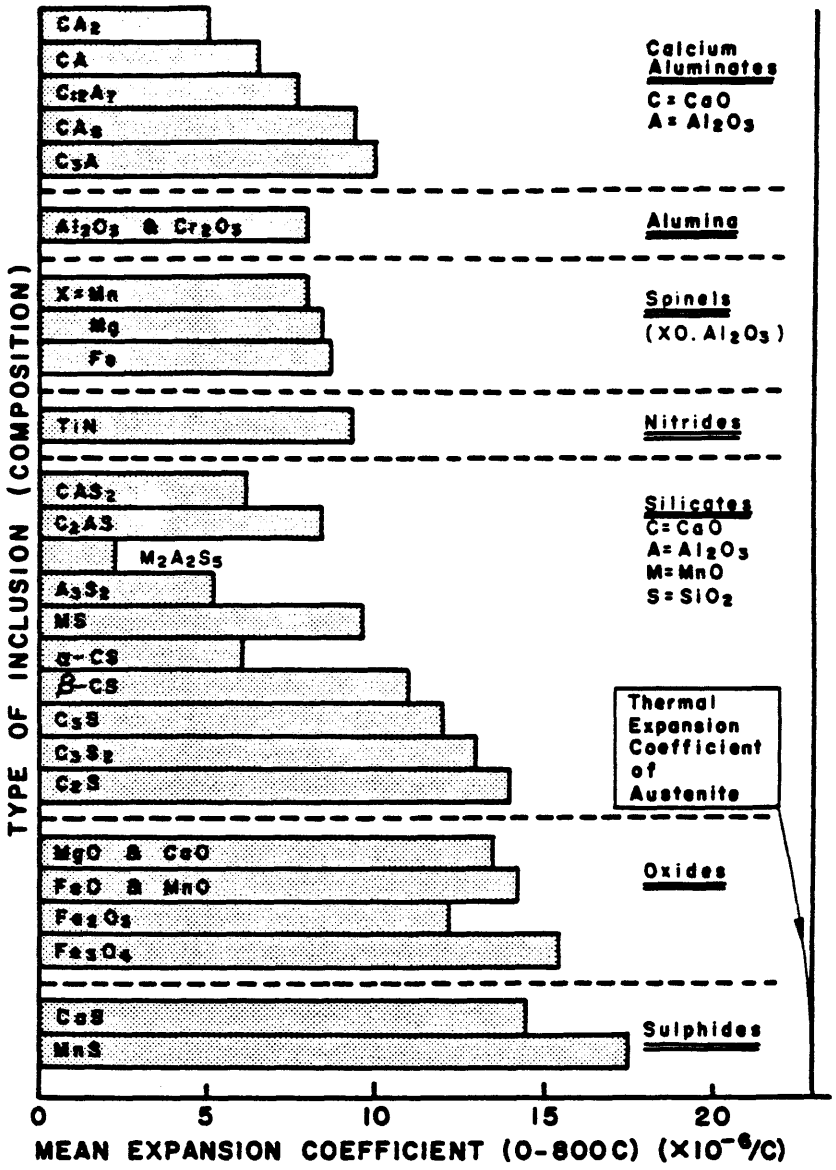

Figure 9. Thermal expansion coefficients of some commonly found inclusions in steels. (after Liu [5])

amount of GBF. Manganese not only delays the grain boundary ferrite transformation, it also depresses the bainitic transformation temperature, promoting the fine-grained acicular ferrite formation. Evans also indicated that there is an specific amount of manganese which will produce optimal toughness (approximately 1.4 wt. pct. Mn). This is shown in Figure 10. Cochrane et al. [69] also reported similar optimum manganese range (1.2-1.6 wt. pct.) to form desirable microstructures. Below this value, sideplate microstructures are generally formed.

However, a corresponding increase in acicular ferrite content [56,57] can also occur if effective intragranular nucleation sites are available within the grains. This research has the main objective of investigating the individual and combined effects of aluminum and titanium additions on weld pool deoxidation. Thus, only the effects of aluminum and titanium on inclusion formation will be discussed in the following.

II.5.1. Effects Of Aluminum

To investigate the beneficial influence which aluminum may have, Cole and Colvin [64] used a submerged arc flux that contained approximately 50% Al_2O_3 and obtained welds with fine

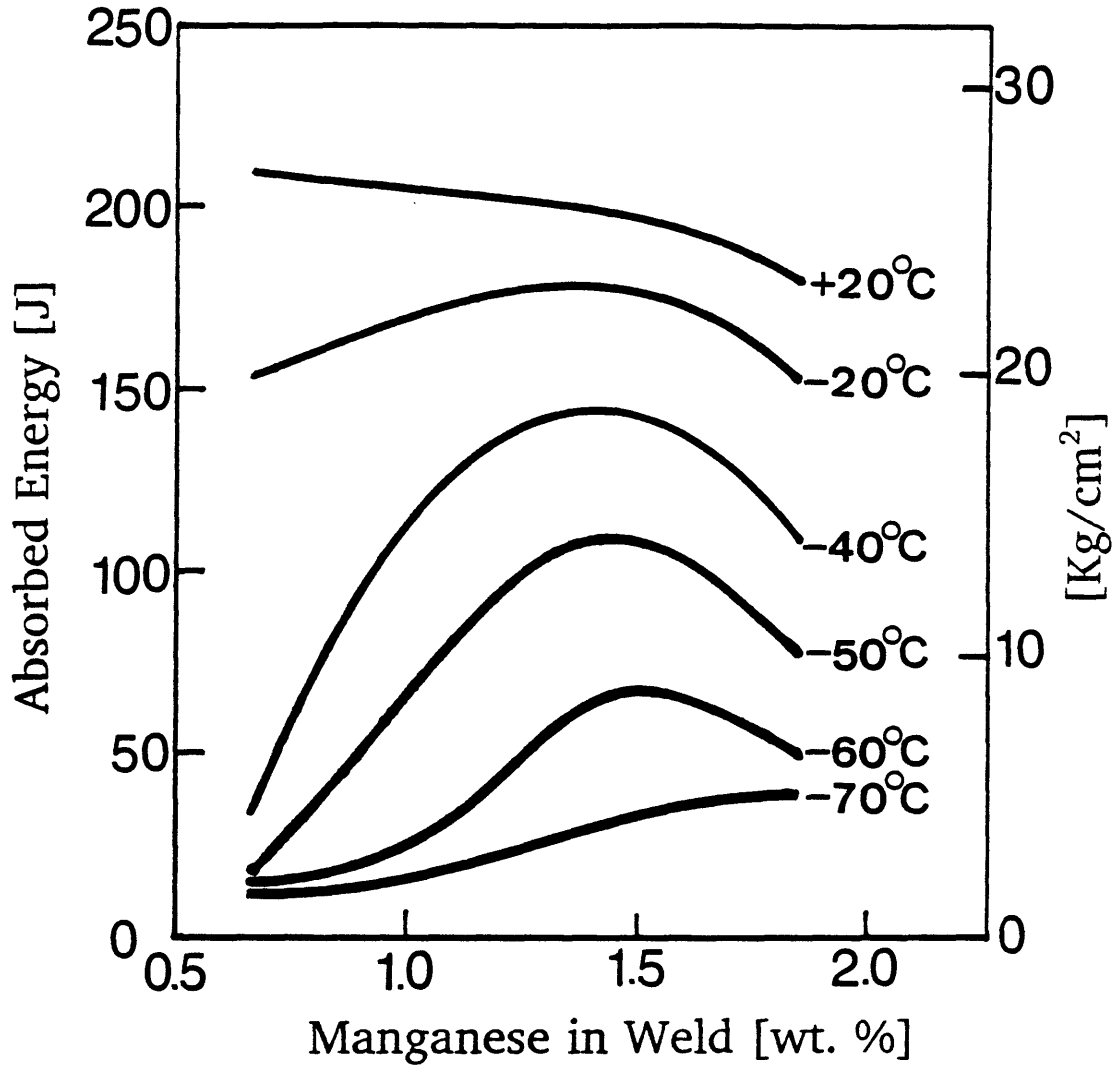

Figure 10. Effect of manganese on Charpy-V toughness tests at different temperatures. (after Evans [82])

acicular ferrite microstructure. They explained that aluminum nitride precipitates acted as effective nucleation sites for AF nucleation. Other investigators [21,42,43,65] reported that welds with inclusions with relatively high Al_2O_3 content showed high volume fraction of AF. However, several authors have observed detrimental effects of aluminum in submerged arc welds made with basic fluxes. Terashima and Hart [66] showed that increasing the aluminum content decreased the amount of titanium bearing precipitates, and the proportion of AF decreasing. Yoshino and Stout [67] reported that their microstructural coarsening was due to excesses aluminum in solid solution. Brownlee [68] showed that welds with aluminum content larger than 0.04 wt. pct. had deteriorated toughness (as a result of reduced amount of AF), Figure 11. Thus, deoxidation with aluminum should be carefully controlled to avoid the detrimental effects.

II.5.2. Effects Of Titanium

The addition of titanium to the weld metal has the effects of weld metal microstructure refinement and toughness improvement [44,60-63]. Many authors [44,50,60,61,63] suggested that the increase in toughness was due to the increase in titanium bearing nucleation sites, effective for

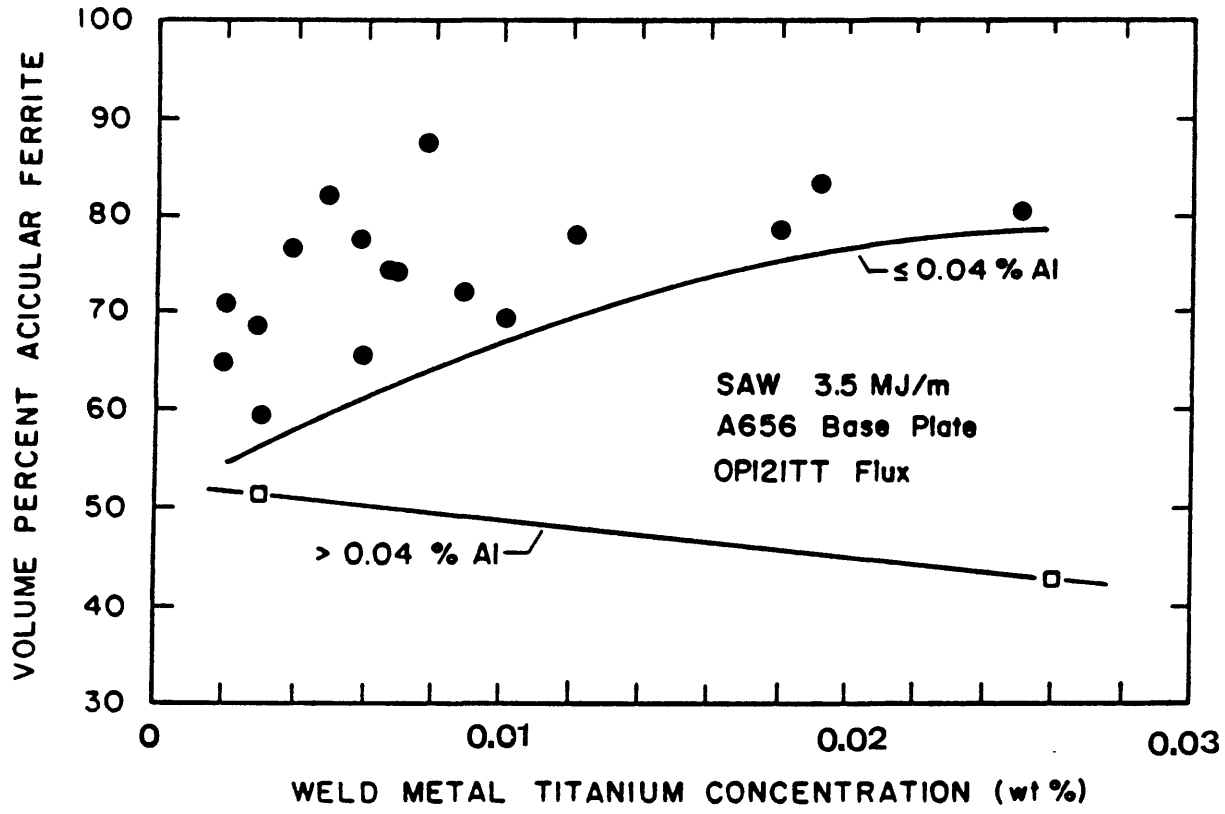

Figure 11. The effect of Ti changes depending upon the amount of Al concentration exist in the welds. (after Brownlee [68])

intragranular acicular ferrite nucleation. Ito and Nakanishi [28] not only showed that titanium raised the temperature for the maximum transformation rate but also found that titanium increased the transformation start temperature. These are most important observations, which indicate that titanium contributes more effective nucleation sites for ferrite nucleation. Grong and Matlock [16] reported that there is a minimum amount of titanium ($\geq$ 0.0045 wt. pct.) above which the beneficial effect of titanium becomes apparent, Figure 12. Tsuboi and Terashima [60] indicated that there is an optimum range of titanium which will produce maximum toughness in welds, and that range is dependent upon the exact chemical composition in the weld metal.

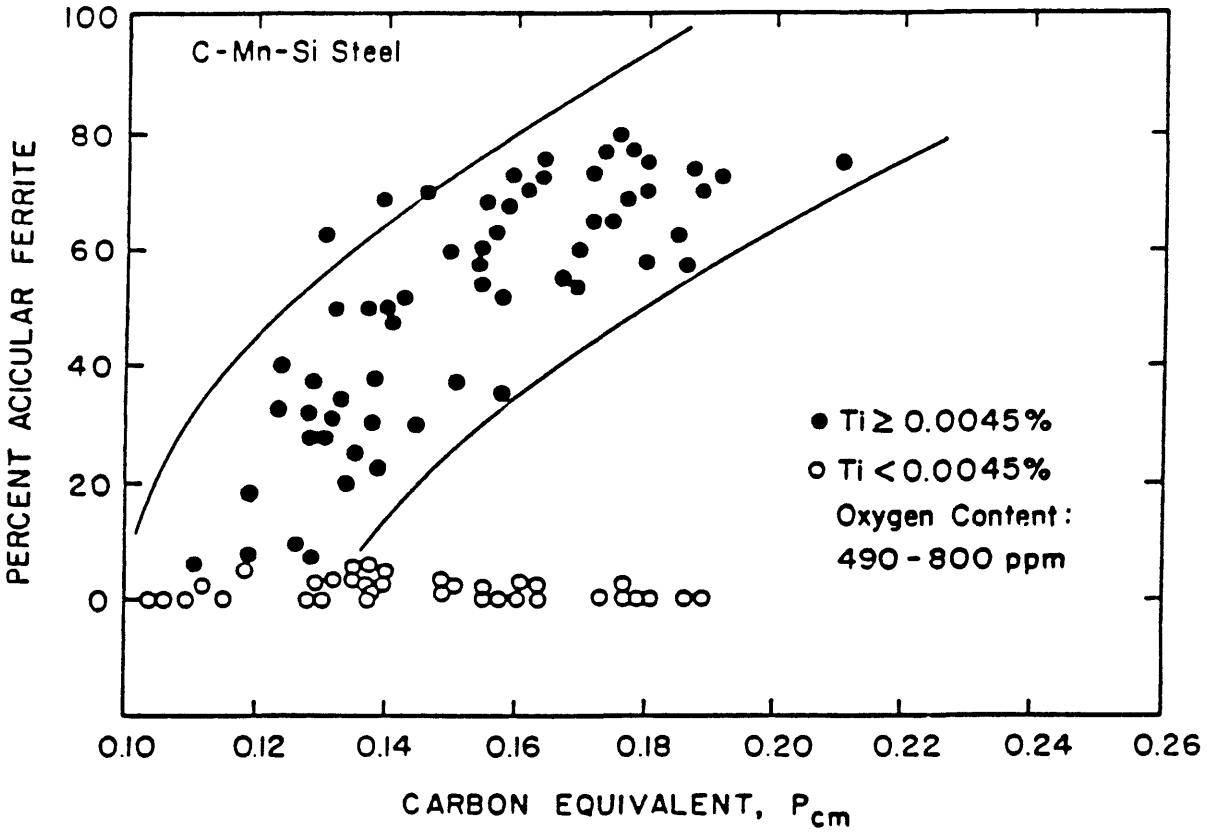

Figure 12. Plot showing the influence of weld metal Ti content on the volume percentage of acicular ferrite in the Mn-Si-Ti microalloyed steel submerged arc welds.
(after Grong and Matlock [16])

III. EXPERIMENTAL PROCEDURE

III.1. Experimental Design Procedure

Review of the available literature shows that in most of the experiments related to weld pool chemistry investigation, the deoxidizers are added altogether in the form of an electrode or welding fluxes. As such, all the deoxidants present in the weld pool compete with each other for the oxygen atoms, and the individual and combined effect of these elements in weld pool deoxidation can not be clearly distinguished. In this research, controlled amounts of aluminum and titanium are introduced into the different passes of the carbon - manganese steel weldments to investigate the individual and combined effects of aluminum and titanium.

The base plate chosen for this research was an ASTM A516 G70 pressure vessel steel. A 3.2 mm (1/8 inch) diameter E70S-3 electrode and a high MgO-CaF_2, low SiO_2 commercial flux were used in the experiments. The compositions are given in Table 3.

A two-part experiment concerning the weld pool deoxidation sequence was designed. The first part examined the titanium - aluminum addition sequence and the second

Table 3. Chemical compositions of the bass metal, the electrode filler wire and the OP121TT flux in this research.

base metal	C	N	O	S	Mn	P
A516 G70 PVQ1/2"	0.2566	0.0056	0.0019	0.0125	1.200	0.008

Si	Cr	W	Mo	Co	As
0.174	0.023	0.004	0.002	0.001	0.001

Sn	Ti	Cu	Ta	Al
0.002	0.001	0.019	0.038	0.028

filler wire	C	Mn	Si	P	Cu	Al
E70S-3	0.124	1.152	0.560	0.021	0.070	0.010

flux	SiO_2	Al_2O_3	MgO	CaO	MnO
OP121TT	10.7	17.3	31.7	6.6	1.1

TiO_2	CaF_2	Na_2O	Fe_2O_3	C
0.86	24.1	0.78	1.9	0.35

Notes :

(1).The concentration of all elements and compounds are given in weight percent.

(2).Base metal plate dimension is 12.7 mm (0.5 inch thickness) x 102 mm (4 inch width) x 203 mm (8 inch length).

(3).Filler wire diameter = 3.2 mm (1/8 inch).

part, the aluminum - titanium addition sequence. In the case of the titanium - aluminum addition sequence welds, the first pass of each weld was made by submerged arc welding (SAW) to contain eight different levels of titanium, from 0.007 to 0.355 weight percent. These welds were prepared using 3.2 mm (1/8 inch) diameter E70-S3 electrode with different additions of pure titanium strips in a single-v-grooved joint, Figure 13, and covered with OP121TT flux. The nominal heat input for the first pass welding was approximately 3.0 KJ/mm. The detailed welding parameters were shown in Table 4.

After the first passes were made, v-grooves were cut from the center of the beads. Different amounts of pure aluminum in the form of thin strips were positioned in these grooves for the second passes. Gas tungsten arc (GTA) welds with eight levels of aluminum additions, from 0.009 to 0.228 weight percent were made with argon shielding. The nominal heat input for the second pass welding was approximately 2.9 KJ/mm. GTA welding was chosen to ensure that the variations in oxygen and nitrogen content observed at the second passes were caused mainly by aluminum addition since the concentration of other elements was maintained constant for all welds. Due to the nonuniform bead shape of some of the second passes , a third pass is applied in the transverse

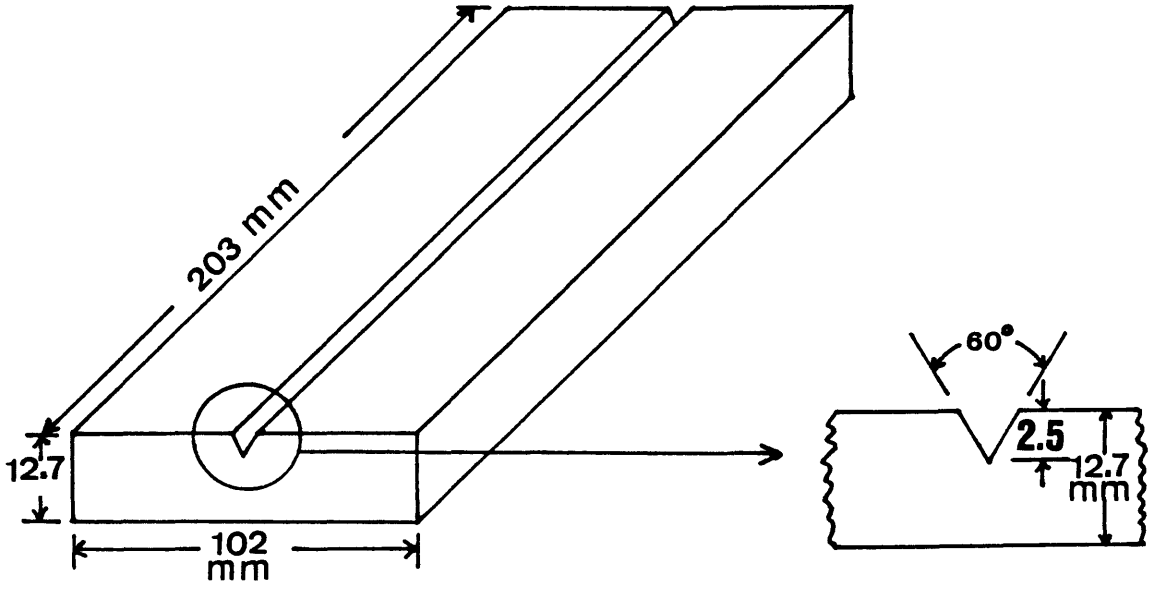

Figure 13. Joint geometry of the single-v-grooved welds for first and second pass.

Table 4. Summary of welding parameters for experimental welds.

Welding Pass	System	Electrode Filler Wire	Power Source & Polarity	Shielding Agent	Single-V-Grooved
1st.	SAW	consumable E70S-3	DCEP	slag & self-generated gas	yes
2nd.	GTAW	non-consumable tungsten electrode	DCEN	argon gas	yes
3rd.	GTAW	non-consumable tungsten electrode	DCEN	argon gas	no

Alloy Element addition	Welding direction	Voltage (V)	Current (A)	Travel Speed (S, mm/s)	Nominal Heat input (KJ/mm)
Ti/Al	longitudinal	30-32	330-350	3.46	3.0
Al/Ti	longitudinal	~16	250	1.36	2.9
	transverse	~16	250	1.36	2.9

Note :

(1). Nominal heat input (KJ/mm) = V x A / S x 1000. [71]

direction of all welds to homogenize the weld metal. The welding parameters were listed in Table 4 and the schematic drawing of the welding sequence was shown in Figure 14.

Similarly, the second part of the experiment examined the aluminum - titanium addition sequence welds. The procedures were the same as the first part with the exception of the sequence of deoxidizers addition (aluminum in the first pass and titanium in the second pass). The experimental matrix is listed in Table 5.

III.2. Analyses Of The Experimental Welds

For reasons explained in the previous section, only the first and third passes of the welds were studied.

All specimens were examined using a Neophot 21 light metallograph. Two volume percent nital solution was used to reveal the microstructure. The two positions from each weld where micrographs were taken are illustrated in Figure 15.

Standard quantitative metallographic techniques were used to evaluate the volume fractions of the various microstructures. The three groups of microstructures considered were :(1) Grain boundary ferrite (GBF) and intragranular polygonal ferrite (PF) ; (2)Intragranular acicular ferrite (AF) ; and (3) Bainite (B), Widmanstatten

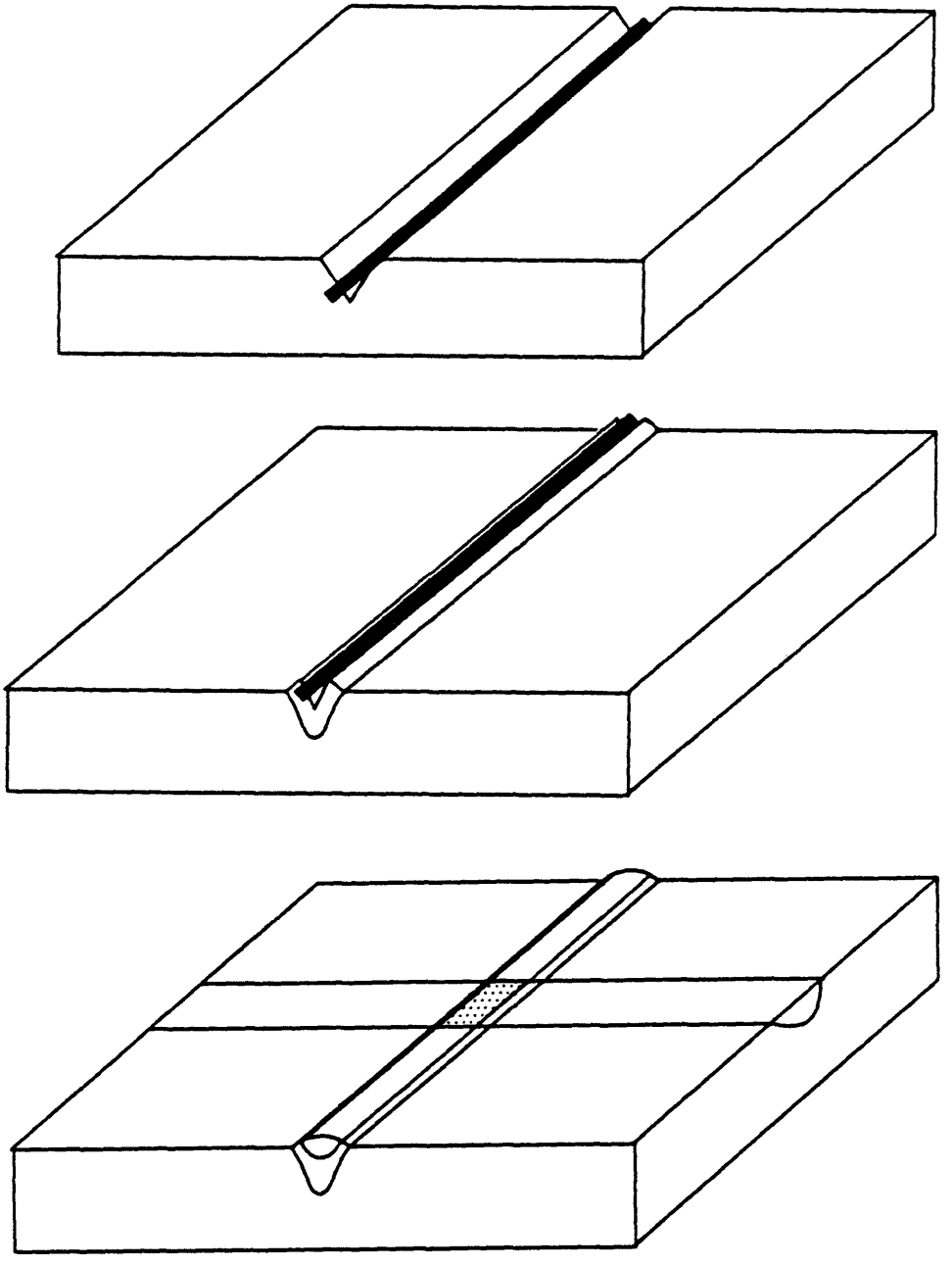

Figure 14. Schematic drawing of the welding sequence.

Table 5. Experimental Matrix.

Sample	Titanium(Ti) addition (mg/mm)	Aluminum(Al) addition (mg/mm)
t1	0.22	–
t2	0.44	–
t3	0.88	–
T1	1.00	–
T2	2.00	–
T3	3.00	–
T4	4.00	–
T5	5.00	–
t1a1	0.22	0.13
t1a2	0.22	0.26
t1a3	0.22	0.52
t2a1	0.44	0.13
t2a2	0.44	0.26
t2a3	0.44	0.52
t3a1	0.88	0.13
t3a2	0.88	0.26
t3a3	0.88	0.52
T1A1	1.00	0.72
T1A2	1.00	1.44
T2A1	2.00	0.72
T2A2	2.00	1.44
T3A1	3.00	0.72
T3A2	3.00	1.44
T4A1	4.00	0.72
T4A2	4.00	1.44
T5A1	5.00	0.72
T5A2	5.00	1.44

Table 5. Experimental Matrix (continued).

Sample	Aluminum(Al) addition (mg/mm)	Titanium(Ti) addition (mg/mm)
a1	0.13	–
a2	0.26	–
a3	0.52	–
A1	0.72	–
A2	1.44	–
A3	2.16	–
A4	2.88	–
A5	3.60	–
a1t1	0.13	0.22
a1t2	0.13	0.44
a1t3	0.13	0.88
a2t1	0.26	0.22
a2t2	0.26	0.44
a2t3	0.26	0.88
a3t1	0.52	0.22
a3t2	0.52	0.44
a3t3	0.52	0.88

Notes :

T (t) series :only titanium added in the first pass.
A (a) series :only aluminum added in the first pass.
TA (ta) series :titanium added in the first pass and followed with aluminum addition in the second pass.
AT (at) series :aluminum added in the first pass and followed with titanium addition in the second pass.

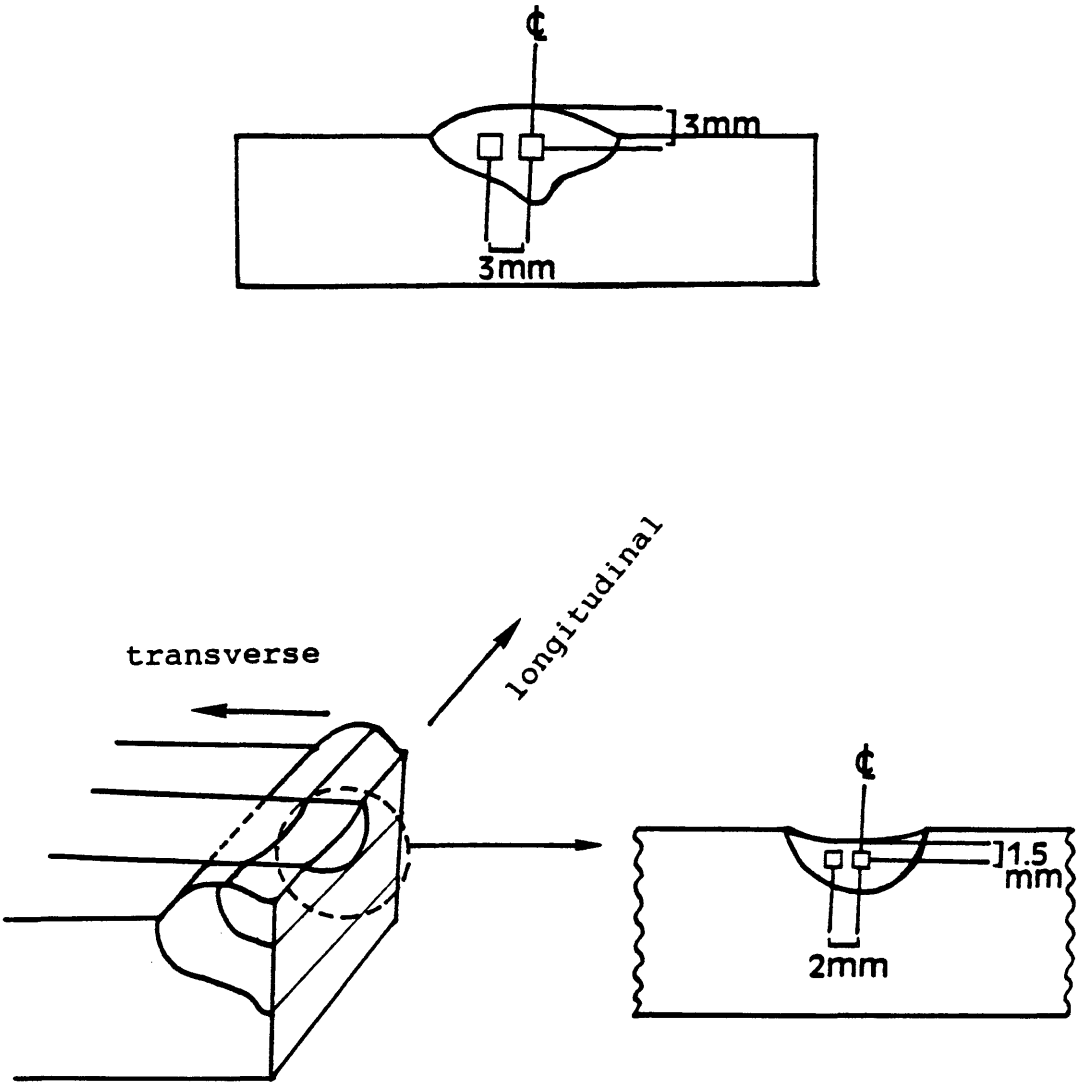

Figure 15. Schematic diagram showing the positions where micrographs were taken for quantitative metallographly.

sideplate ferrite (SP) and the microconstituents (MAC).

All welds were analyzed using an ARL Quantometer 34000 SAS/DPS Emission Spectrometer. The carbon and sulfur content of the weld metals were analyzed using a LECO CS-244 Carbon-Sulfur Determinator, while oxygen and nitrogen content were analyzed using a LECO TC-136 Nitrogen-Oxygen Determinator. The chemical composition of each specimen is given in the appendix.

Carbon extraction replicas were used to determine the size and chemical composition of the inclusions. The carbon coatings were deposited on the welds in a Denton Vacuum Evaporator. Since an adequate thickness carbon film is required, the following procedure was carried out to obtain useful carbon replicas :

(1). Divide the replicated specimen surface into few small regions (about 2 mm x 2 mm).
(2). Immerse the specimen into a ten volume percent nital solution until bubbling occurs, which means the replica film is ready to float.
(3). Transfer the specimen to a ninety volume percent methanol aqueous solution, for floating the small curved replica films.

(4). Use small nylon grids to "fish" the replicas and transfer them to a solution mixed of methanol (10 vol. pct.) and water (90 vol. pct.). The curved replica film will expand and flatten in this solution.

(5). Use nylon grids to transfer the flattened replica films, onto a filter paper and dry.

For the determination of the chemical composition and size distribution of the inclusions, a JEOL JXA-840 Scanning Microanalyzer with Tracor Northern EDS unit was used. The standard quantitative (SQ) analysis program was used to analyze the composition of inclusions. Eight elements were requested in the calculation, which were aluminum, silicon, sulfur, titanium, vanadium, manganese, iron, and copper.

IV. RESULTS AND DISCUSSION

IV.1. INDIVIDUAL EFFECTS

IV.1.1 Relationship Between Weld Metal Chemical Composition And Microstructures

As explained in the previous section, two sets of results will be presented :from the first and third passes of all the weldments. To correlate weld metal microstructures to chemical composition, the carbon equivalent (CE) equation was first considered. There are currently many different forms of CE equations [72-75], but only the CE equation originally devised by Dearden and O'Neill, and adopted by IIW in 1967 was chosen in this research.

$$CE = \%C + \frac{\%Mn}{6} + \frac{\%Cu + \%Ni}{15} + \frac{\%Cr + \%Mo + \%V}{5} \qquad ---(12)$$

This formula is applicable to plain carbon and carbon-manganese steels.

It is well established that CE can strongly affect the weld metal microstructures, but the purpose in this research is to determine the aluminum and titanium effects. Therefore

welds with similar CE values were chosen for evaluation. In the first pass weldments, all the CE values were approximately 0.30 wt. pct. and thus the individual effects of titanium or aluminum additions on microstructures could be determined.

Different microstructures were obtained at different levels of titanium or aluminum addition. Figure 16 shows the variation of weld metal microstructures with only titanium addition. There is a critical titanium concentration approximately 0.05 wt. pct. of titanium above which bainite (B) structure increased at the expense of intragranular acicular ferrite (AF) and grain boundary ferrite (GBF). It is possible that excess titanium, in the form of solid solution, promotes the formation of bainite. Below 0.05 wt. pct. of titanium, both AF and GBF increased at the expense of bainite with titanium addition.

The variation of weld metal microstructures with only aluminum addition is shown in Figure 17. Below approximately 0.05 wt. pct. of aluminum, AF and bainite increase with decreasing GBF. Above this point, GBF and bainite increase at the expense of AF. This result agrees with the data reported by Brownlee [68]. Figures 18 and 19 are light micrographs with different levels of titanium and aluminum

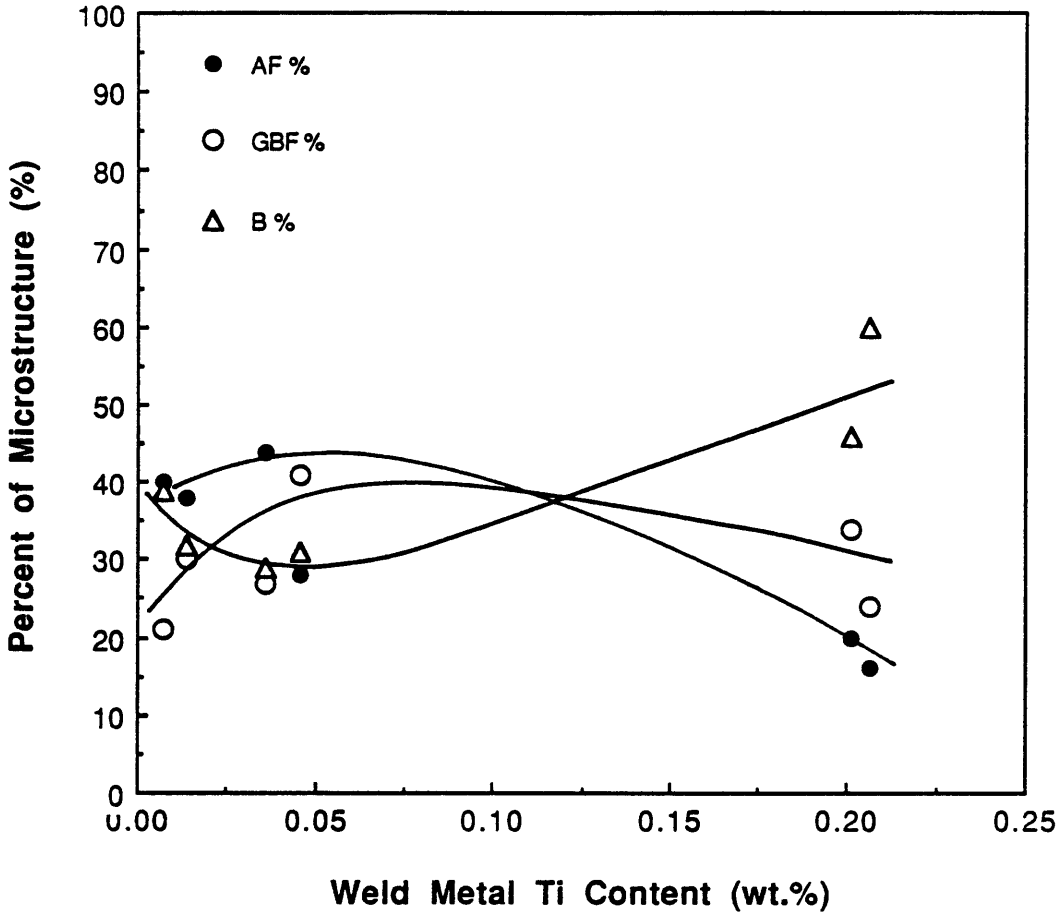

Figure 16. Summary plot of the variation in the weld metal microstructures as a function of the weld metal titanium concentration.

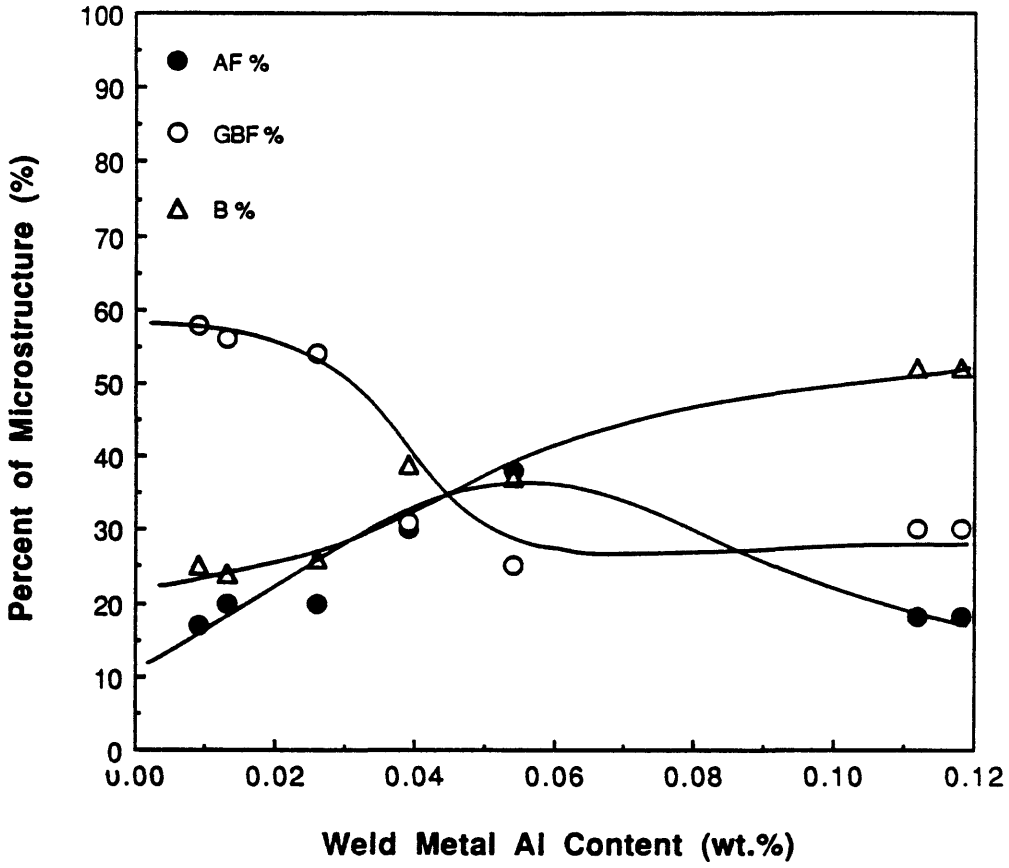

Figure 17. Summary plot of the variation in the weld metal microstructures as a function of the weld metal aluminum concentration.

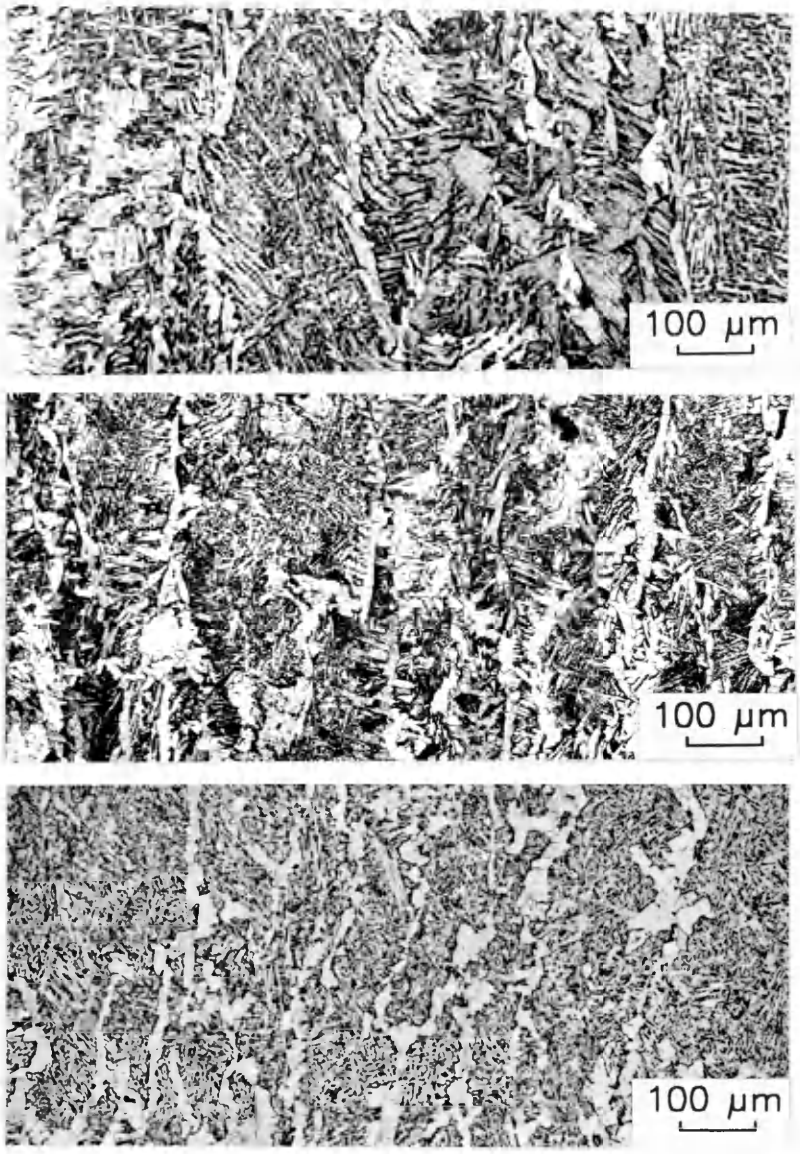

Figure 18. Weld metal microstructure showing mixture of GBF, PF, SP, AF and B for different level of titanium addition. (a) t1 specimen (b) t3 specimen (c) T2 specimen.

(a)

(b)

(c)

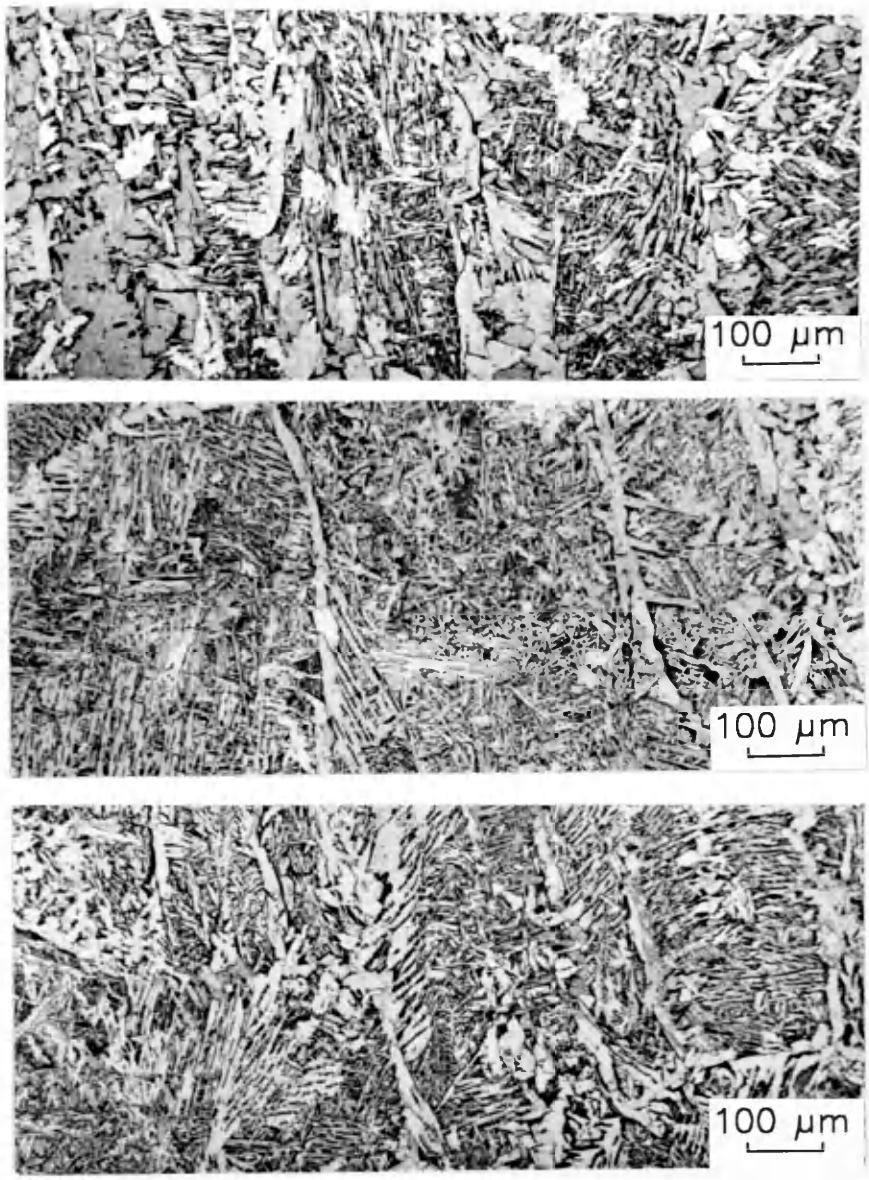

Figure 19. Weld metal microstructure showing mixture of GBF, PF, SP, AF and B for different level of aluminum addition. (a) a1 specimen (b) A2 specimen (c) A4 specimen.

addition.

IV.1.2 Relationship Between Prior Austenite Grain Size And Weld Metal Microstructures

Another factor to be considered in weld metal phase transformation is the prior austenite grain size. For a similar heat input (and cooling rate), the different alloying elements and their levels of additions showed different effects on prior austenite grain size. The measured values of the prior austenite grain sizes are listed in Table 6. Figures 20 and 21 show the variation of prior austenite grain size as a function of titanium and aluminum addition. In Figure 20, prior austenite grain size decreased with increasing titanium content. This seems to indicate that titanium addition controls the austenite grain size by inclusions formation. Figure 21, however, shows that prior austenite grain size does not seem to be altered by aluminum addition. Apparently, titanium has a much better pinning effect to restrict austenite grain growth than aluminum.

Figures 22 and 23 show the effect of prior austenite grain size on the final weld metal microstructures with titanium and aluminum addition. In Figure 22, the amount of bainite decreased, substituted by acicular ferrite, and the

Table 6. The measured values of the prior austenite grain size of the investigated weldments.

	Prior Austenite Grain Size (μm)		Prior Austenite Grain Size(μm)
t1	126	a1	125
t2	90	a2	119
t3	117	a3	132
T1	121	A1	128
T2	79	A2	137
T3	79	A3	130
T4	59	A4	125
T5	38	A5	93

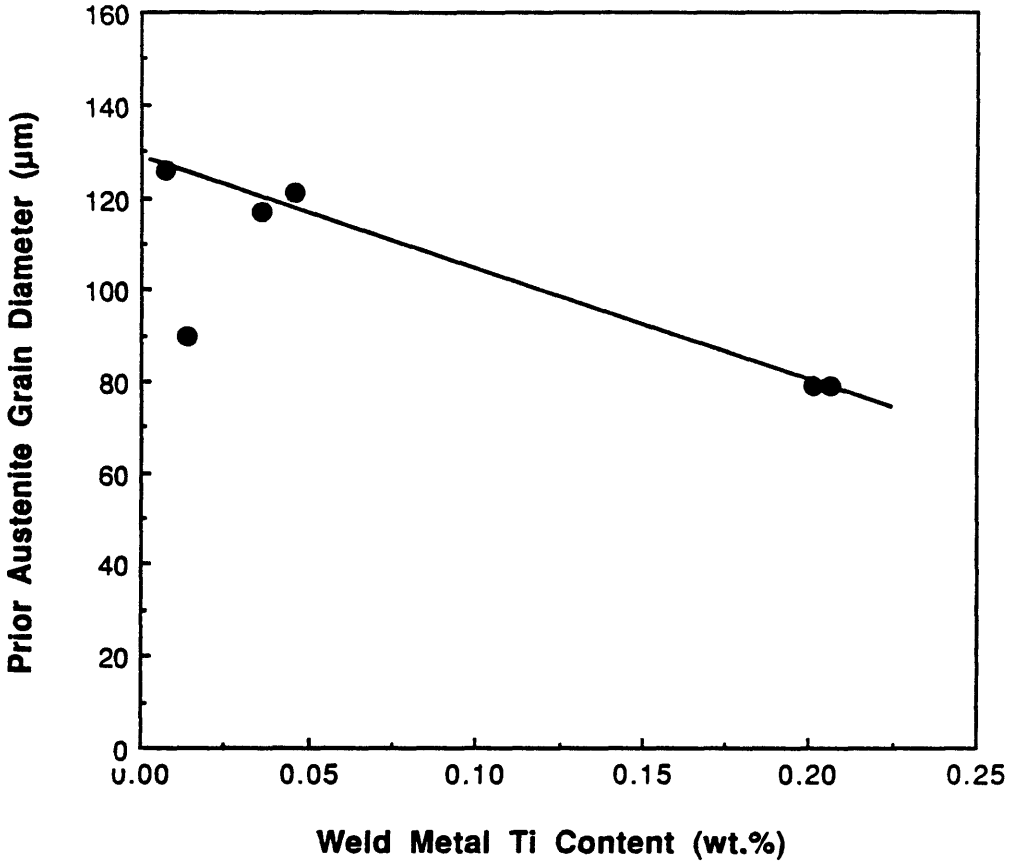

Figure 20. The effect of titanium addition to the prior austenite grain size.

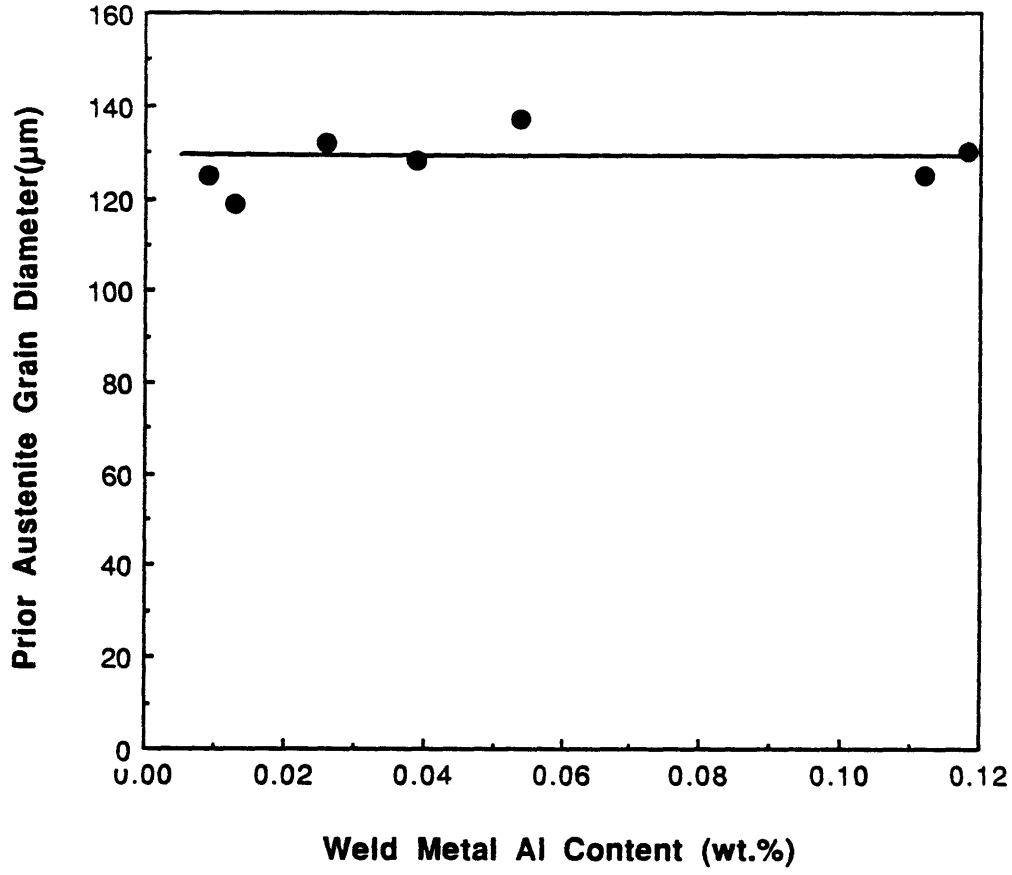

Figure 21. The effect of aluminum addition to the prior austenite grain size.

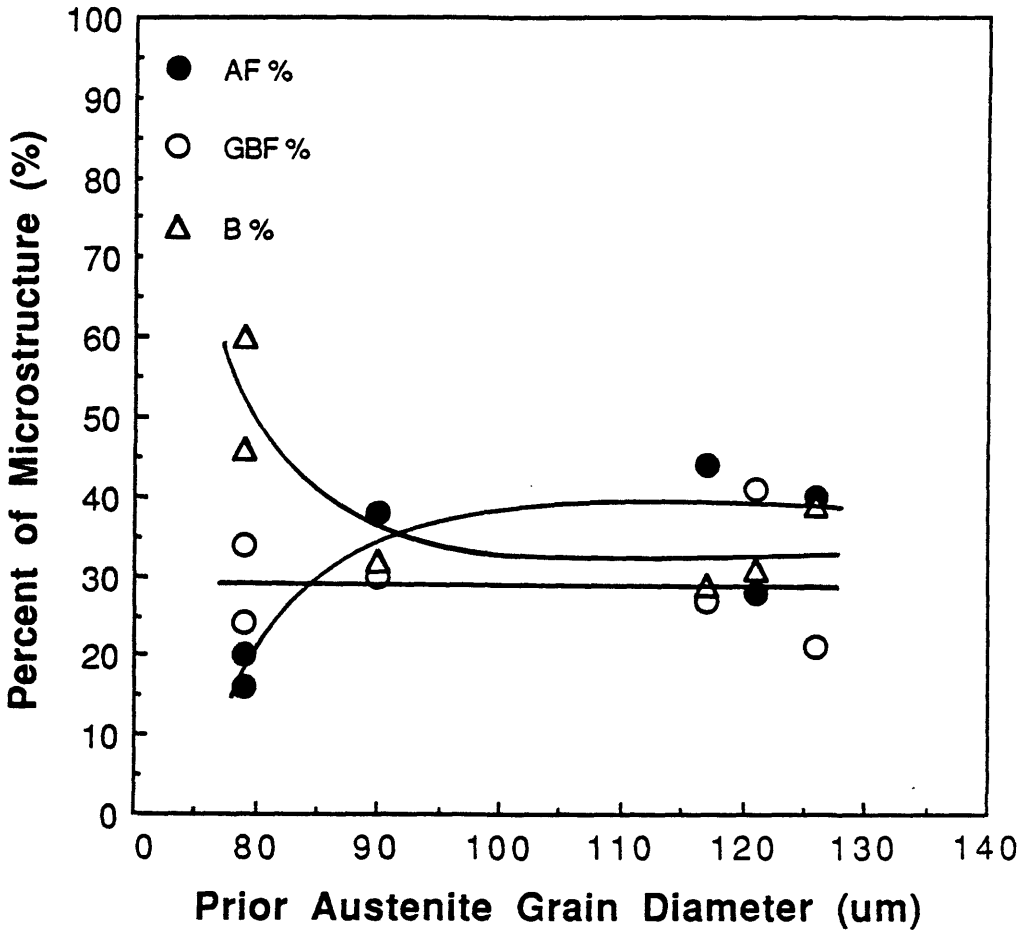

Figure 22. The effect of prior austenite grain size to the weld metal microstructures with only titanium addition.

prior austenite grain size increased. Austenite grain size did not seem to affect significantly the volume fraction of GBF. After austenite grain size reached approximately 90 μm, the weld metal microstructures were no longer altered by austenite grain size changes.

The final weld metal microstructures do not seem to have clear correlation with austenite grain size in the aluminum addition series, Figure 23.

IV.1.3 Relationship Between Inclusions And Weld Metal Microstructures

Many authors [22,35,36,39,42,53,76-79] emphasize that nonmetallic inclusions have strong effects on the final weld metal microstructures because inclusions can affect both the thermodynamic and kinetic aspects of the weld metal transformations. Inclusion size distribution, number density (Nv), volume fraction (Vv), and mean particle size (da) are all important factors that affect phase transformations in the weld metal.

IV.1.3.1. Influence Of Inclusion Size Distribution On Weld Metal Transformation

Two inclusion size distributions were chosen to

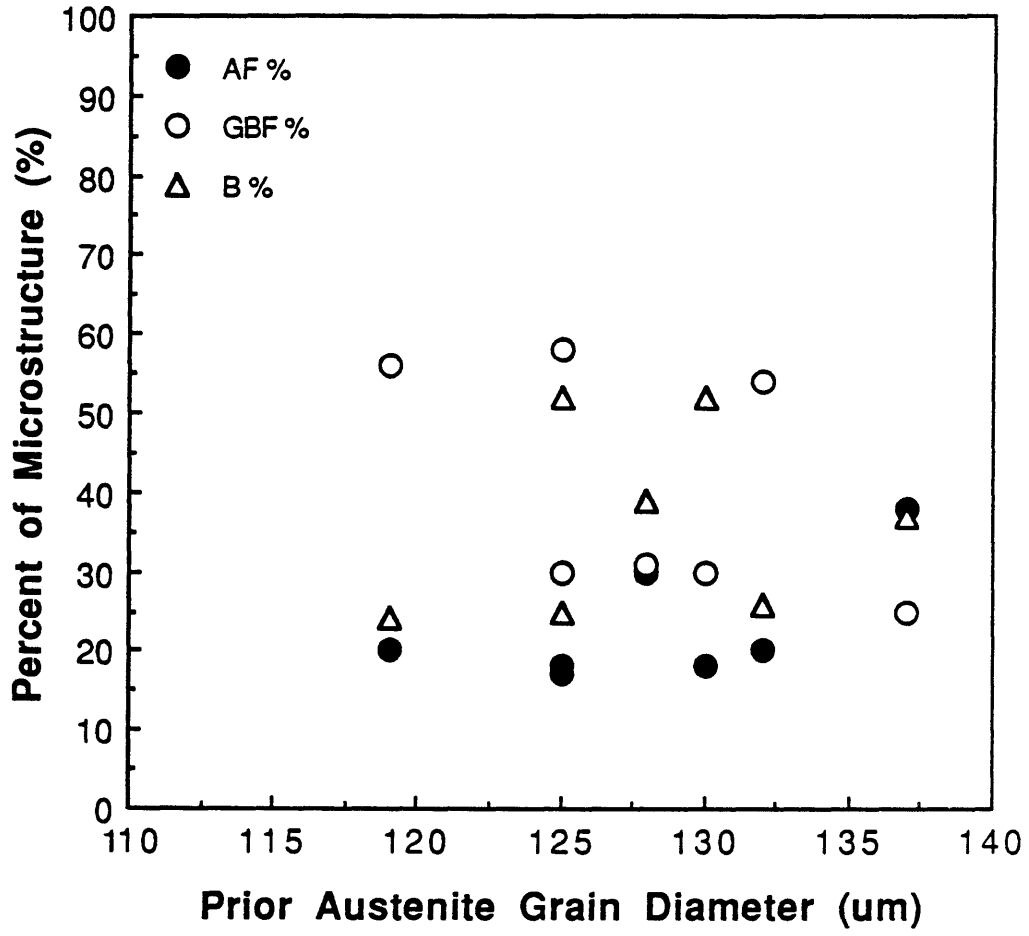

Figure 23. The effect of prior austenite grain size to the weld metal microstructures with only aluminum addition.

illustrate the effect of inclusions and are shown in Figures 24 and 25.

Comparing Figures 24 and 25, it is clear that the aluminum addition series welds exhibited inclusion population with larger particles, for example, those of diameter larger than 0.8 μm. Figures 24(a) and 25(a) do not show smaller particles (diameter < 0.2 μm) and corresponded to welds with higher volume fraction of AF. Barbaro et al. [2] and Jang et al. [87] suggested that inclusions of diameter greater than o.45 μm (within the range of 0.4 to 0.6 μm) are more efficient in AF formation. Cochrane et al. [69] also reported similar observation in their investigation. Figures 24 and 25 seem to indicate that not only the inclusion size but also the size distribution are important factors to affect the final weld metal microstructures.

IV.1.3.2 Influence Of Weld Metal Composition On The Inclusion Oxide Types

With different levels of titanium or aluminum addition, the form of oxide compounds in the inclusions and their ratio were quite different and are shown in Table 7. In C-Mn-Si steels weld metals, the inclusion contain SiO_2, MnO, etc. As aluminum is added, the composition of the inclusions also

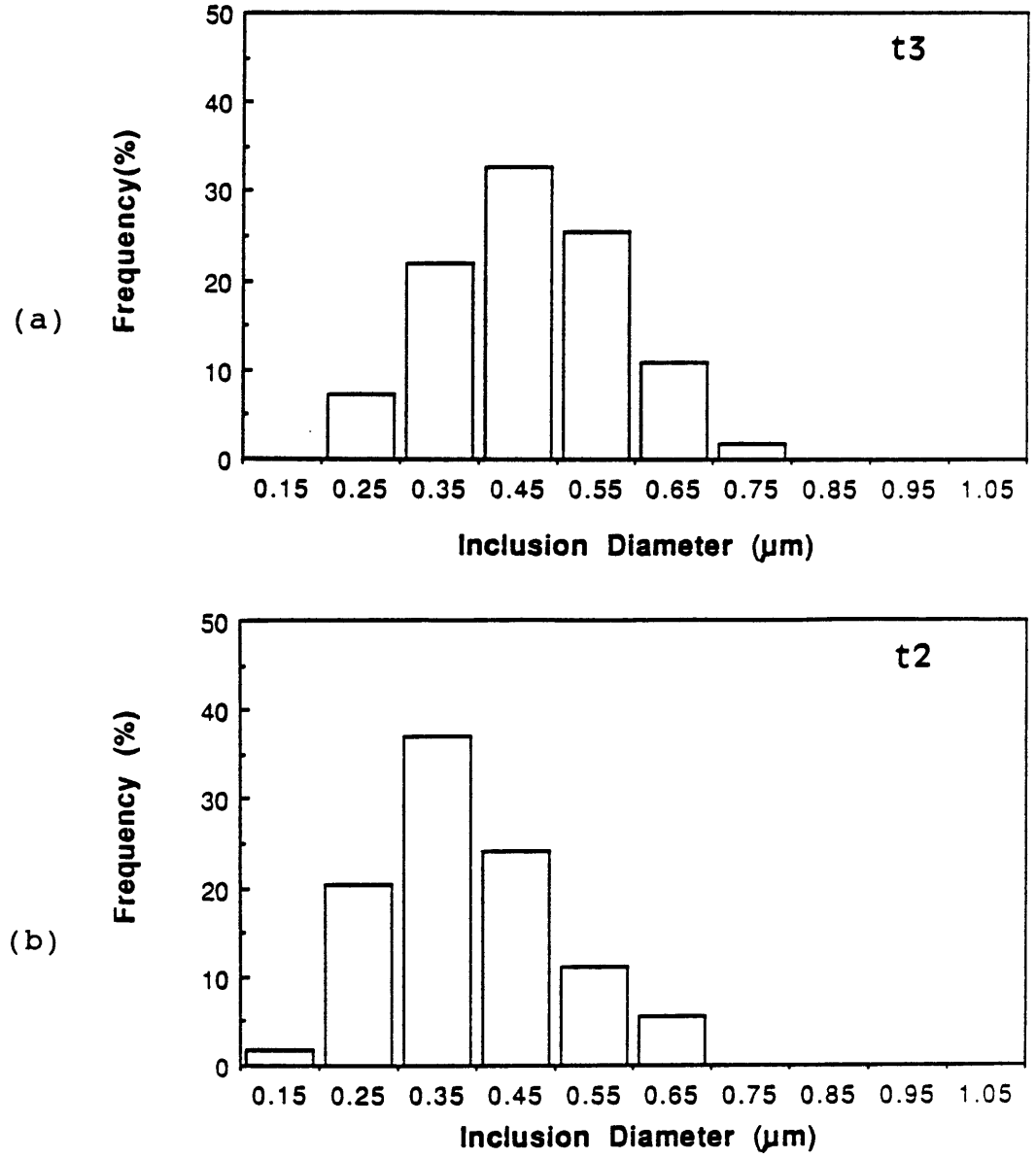

Figure 24. Simple size distribution of the inclusions extracted from (a) t3 specimen (b) t2 specimen with only titanium addition.

(a)

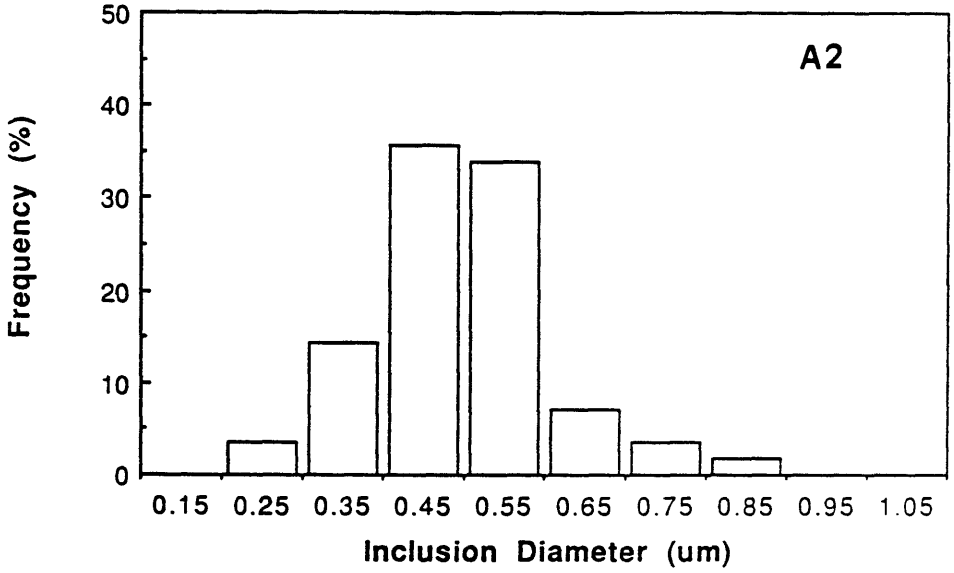

(b)

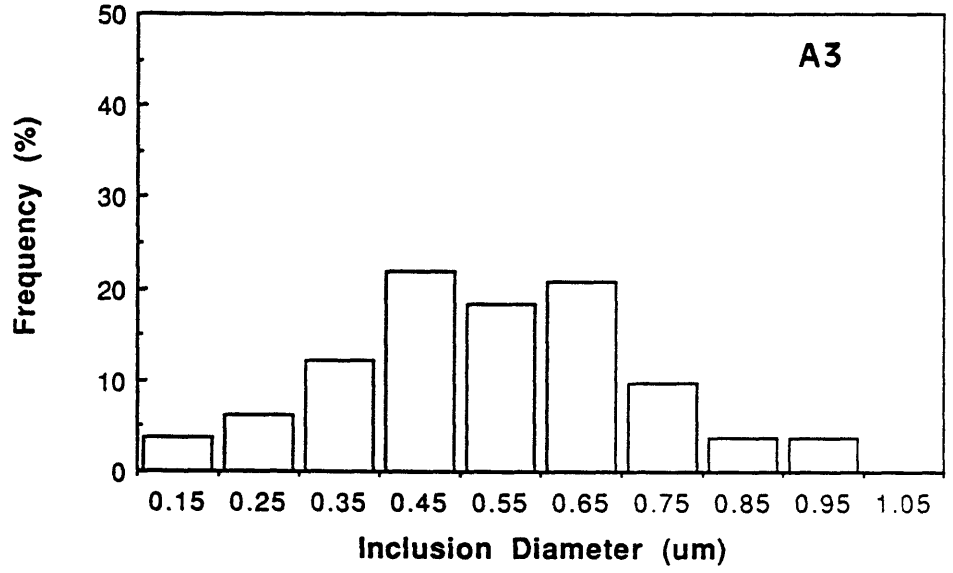

Figure 25. Simple size distribution of the inclusions extracted from (a) A2 specimen (b) A3 specimen with only aluminum addition.

Table 7. Summary of inclusions form in the investigation specimens.

	inclusion form (titanium addition)
t1	$(MnO)_1\ (SiO_2)_1\ (Al_2O_3)_1\ (TiO/TiO_2)_1$
t2	$(TiO/TiO_2)_3\ (Al_2O_3)_2\ (MnO)_1\ (SiO_2)_1$
t3	$(TiO/TiO_2)_7\ (Al_2O_3)_4\ (MnO)_2$
T1	$(TiO/TiO_2)_5\ (Al_2O_3)_2$
T2	$(TiO/TiO_2)_7\ (Al_2O_3)_1$
T3	(TiO/TiO_2) • (♦)
T4	(TiO/TiO_2) • (♦)
T5	(TiO/TiO_2) • (♦)
	inclusion form (aluminum addition)
a1	$(SiO_2)_1\ (Al_2O_3)_1\ (MnO)_1$ • TiO/TiO_2
a2	$(Al_2O_3)_2\ (SiO_2)_1\ (MnO)_1$
a3	$(Al_2O_3)_1\ (SiO_2)_1\ (MnO)_1$
A1	(Al_2O_3) • (*)
A2	(Al_2O_3) • (*)
A3	(Al_2O_3) • (*)
A4	(Al_2O_3) • (*)
A5	(Al_2O_3) • (*)

Notes :
( ) :major component.
(♦) :contain very small amount of Al_2O_3.
(*) :contain very small amount of MnO.

changed with increasing Al_2O_3. Cochrane et al. [69] observed similar behavior in their investigation.

Increasing the weld metal titanium concentration, titanium content in the inclusions is also observed to increase, being TiO /TiO_2 the predominant phase in the inclusions. Liu and Olson [5,80] and Bhatti et al. [54] also have observed the similar result in their investigations. Due to the techniques used in this work, it was impossible to distinguish between TiO and TiO_2.

Figures 26 and 27 show the variation of oxide type in inclusions as a function of weld metal aluminum and titanium content changed. It was considered in these two Figures the results of characterization of aluminum, titanium, silicon, and manganese in the inclusions. Only simple oxides such as Al_2O_3, TiO/TiO_2, SiO_2 and MnO are assumed as deoxidation products. Figure 26 shows that the Al_2O_3 is the major component in inclusions with aluminum additions. Figure 27 shows that the TiO/TiO_2 will be the main component with only titanium additions with some Al_2O_3. No matter how high the weld metal aluminum content in the weld pool, there is always a certain amount of MnO in the inclusions.

If only the mean composition is considered, inclusions extracted form the aluminum addition series welds can be

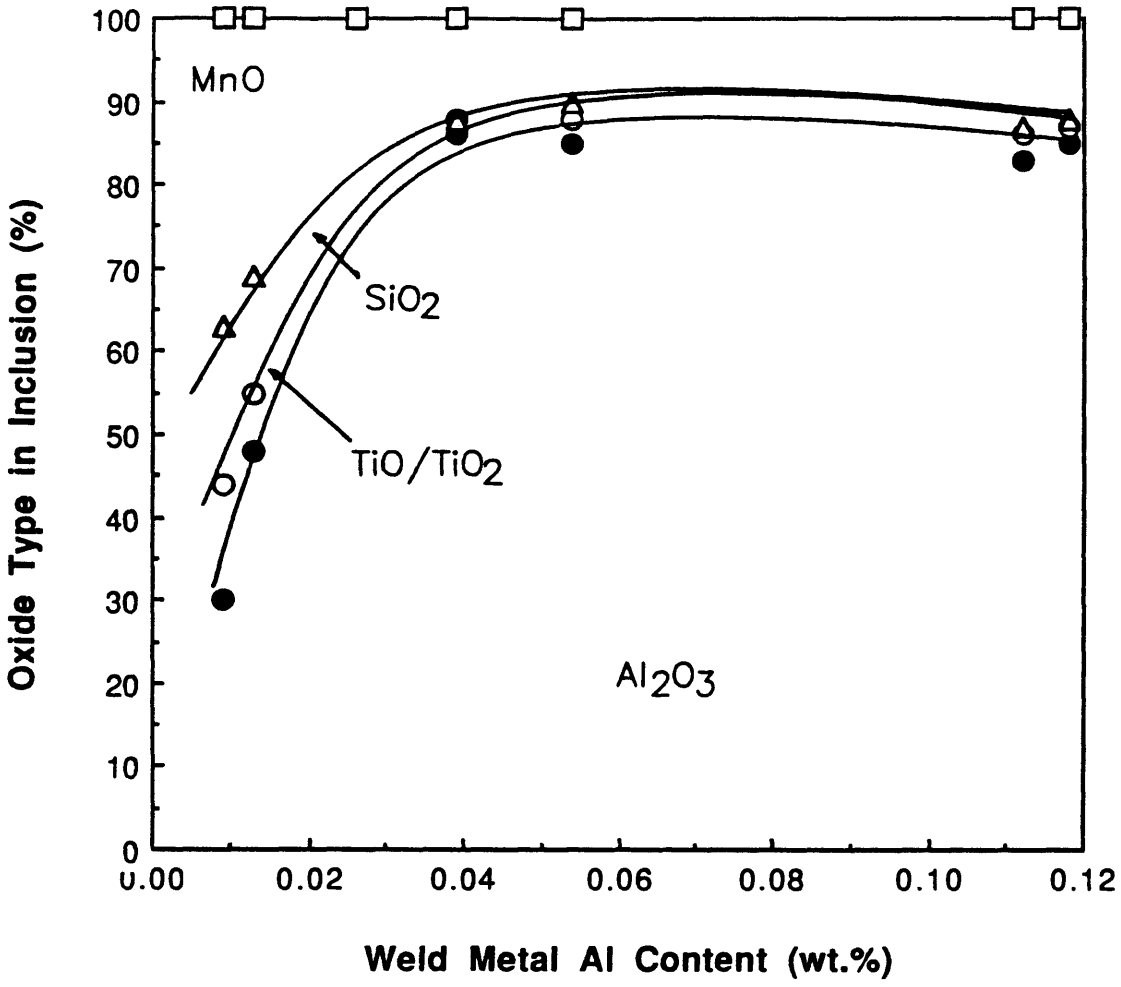

Figure 26. Effects of aluminum content on the oxide composition.

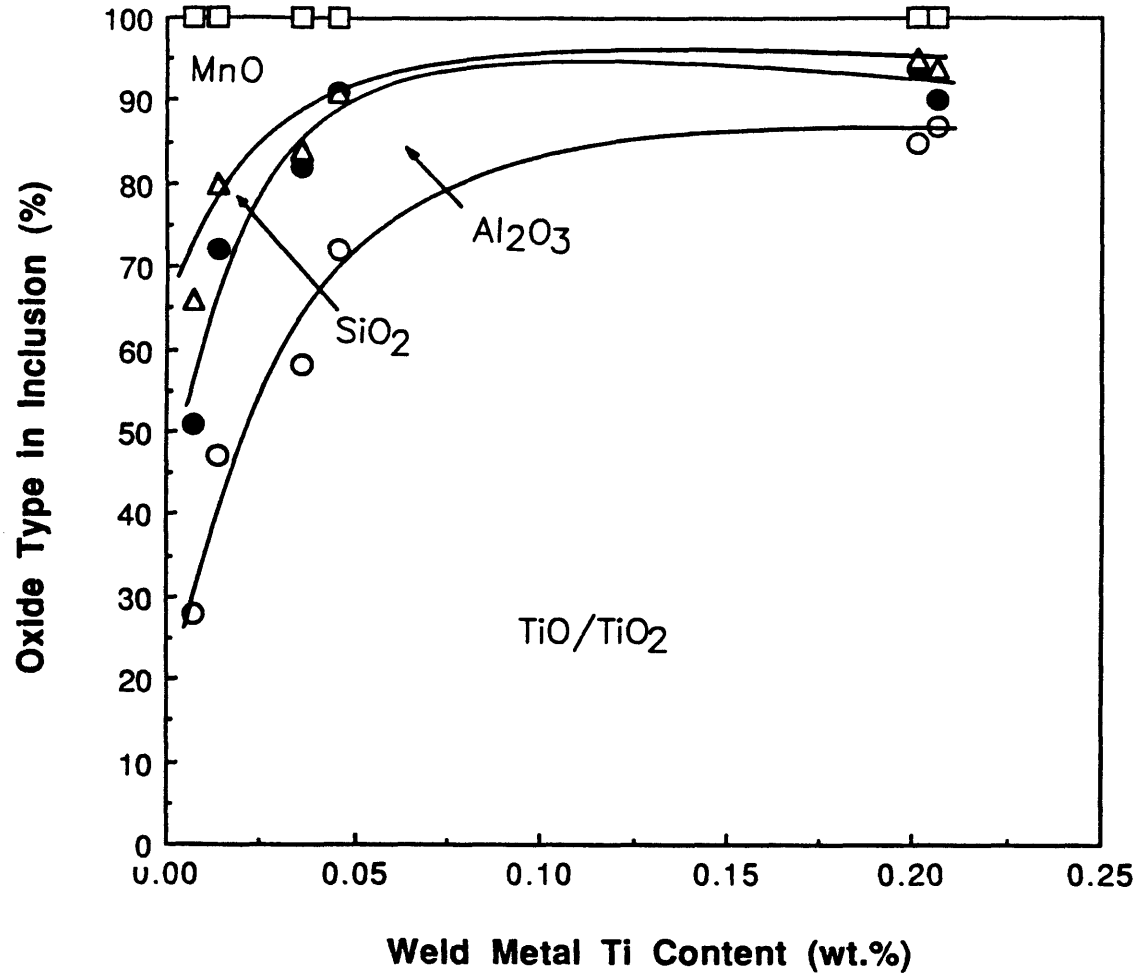

Figure 27. Effects of titanium content on the oxide composition.

represented on the Al_2O_3-MnO-SiO_2 or Al_2O_3-MnO-SiO_2+(TiO/TiO_2) ternary diagram. In Figure 28 and 29, the majority of inclusion compositions are located between the lines joining the Rhodonite ($MnO \cdot SiO_2$) to Corundum (Al_2O_3) and Tephroite ($2MnO \cdot SiO_2$) to Corundum (Al_2O_3). This result agreed with Kluken and Grong [19], Saggese et al. [21], and Keissling and Lange [24]. In the titanium addition series welds, the inclusion compositions are plotted on both (TiO/TiO_2)-Al_2O_3-MnO and (TiO/TiO_2)+SiO_2-Al_2O_3-MnO ternary diagrams, Figure 30 and 31.

IV.1.3.3. Relationship Between Mean Particle Size (da) And Volume Fraction (Vv) To The Weld Metal Oxygen Content

Figure 32 shows that with increasing weld metal oxygen content, the inclusion volume fraction (Vv) increased for both titanium and aluminum addition welds. Devillers et al. [41] also reported similar results. In Figure 33, the mean particle size is also observed to increase as the weld metal oxygen content increases to approximately 0.5 μm for both titanium and aluminum addition welds. Cochrane et al. [69] and Ferrante and Farrar [40] also showed the same results. Liu and Olson [38] reported, however, a different trend that

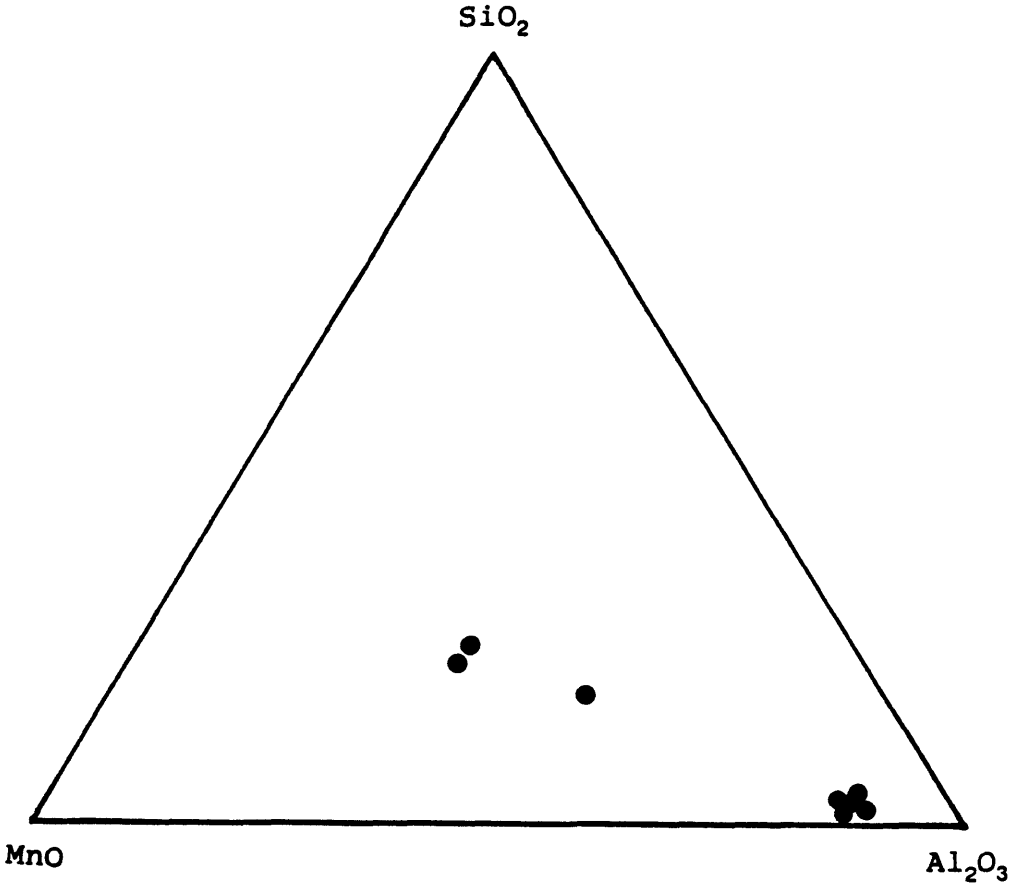

Figure 28. Measured average compositions of inclusions in aluminum addition submerged arc welds and plotting in the Al_2O_3-MnO-SiO_2 ternary system.

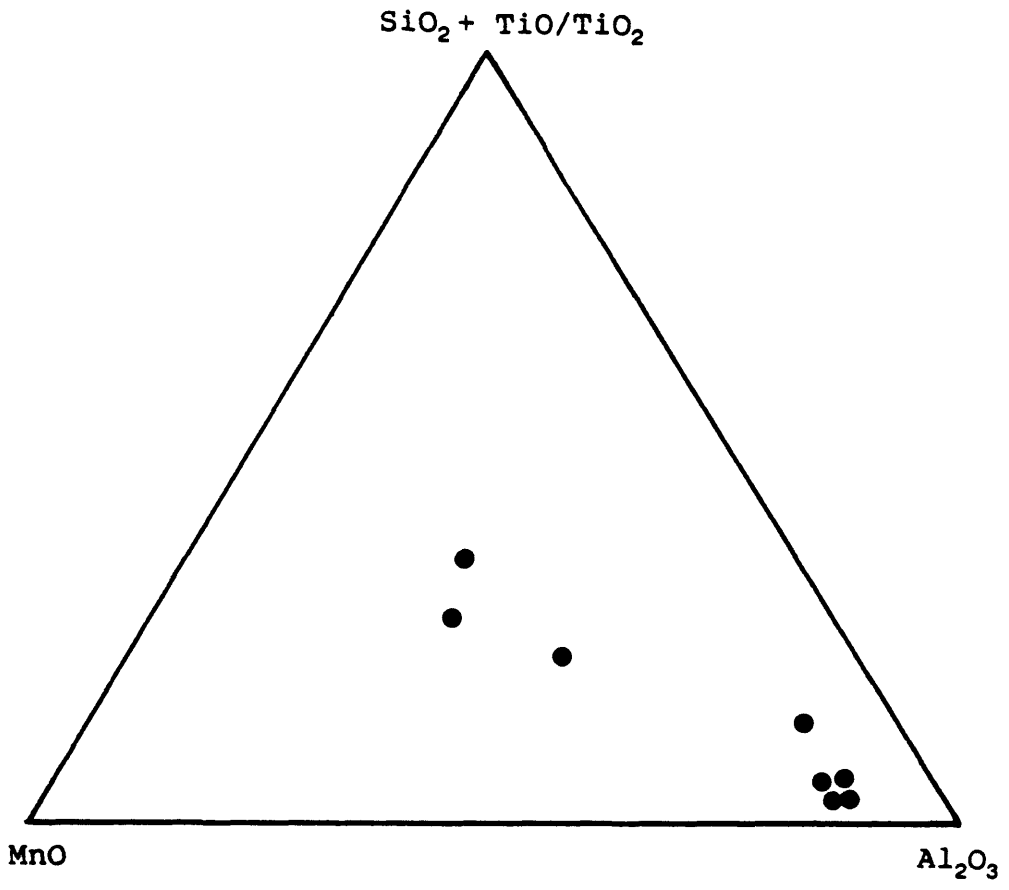

Figure 29. Measured average compositions of inclusions in aluminum addition submerged arc welds and plotting in the Al_2O_3-MnO-SiO_2+(TiO/TiO_2) ternary system.

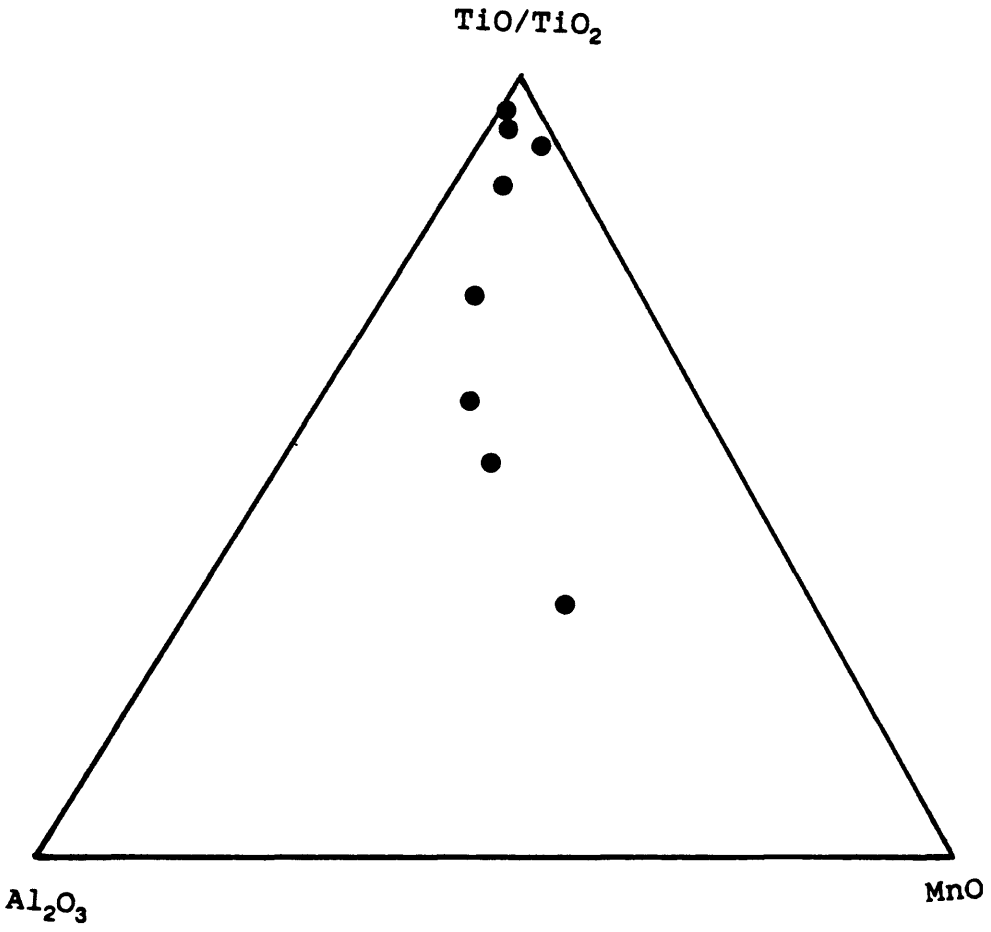

Figure 30. Measured average compositions of inclusions in titanium addition submerged arc welds and plotting in the (TiO/TiO_2)-Al_2O_3-MnO ternary system.

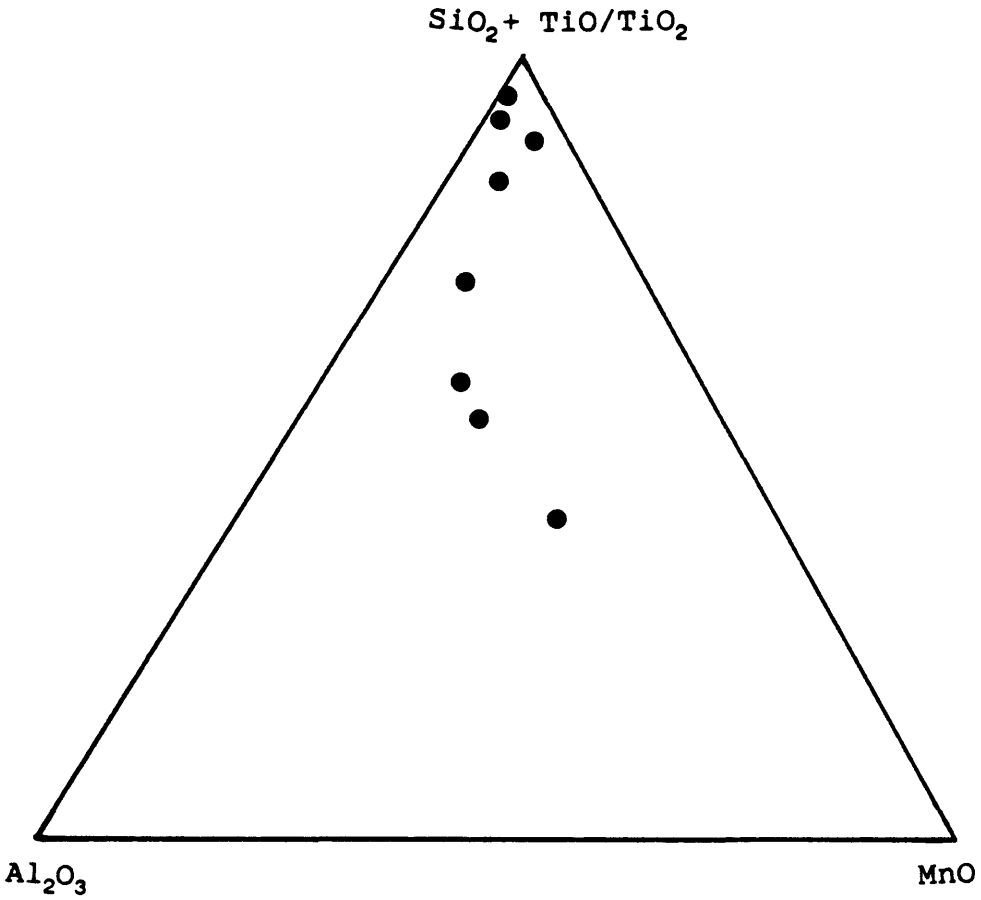

Figure 31. Measured average compositions of inclusions in titanium addition submerged arc welds and plotting in the $(TiO/TiO_2)+SiO_2-Al_2O_3-MnO$ ternary system.

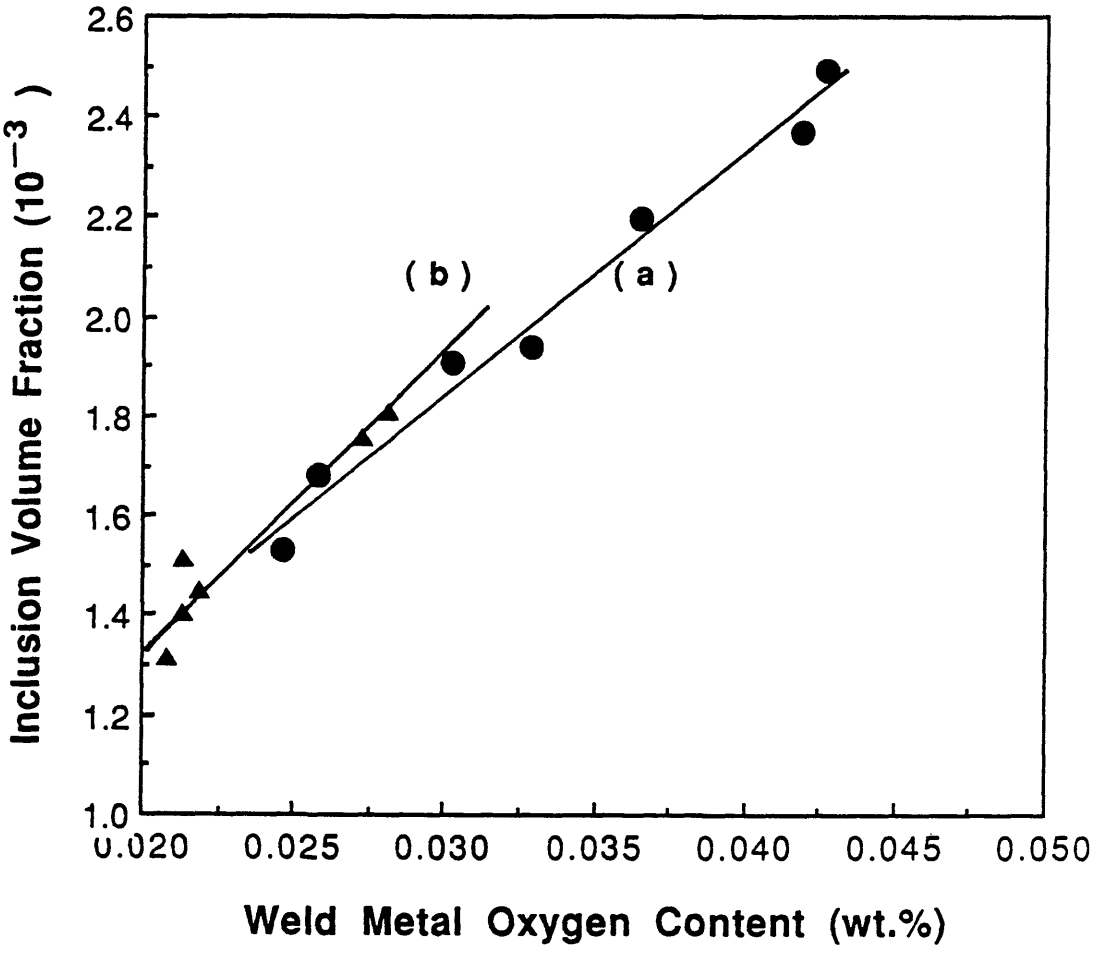

Figure 32. The variation of inclusion volume fraction (Vv) as a function of oxygen content in the weld metal.

(a). Aluminum addition series.

(b). Titanium addition series.

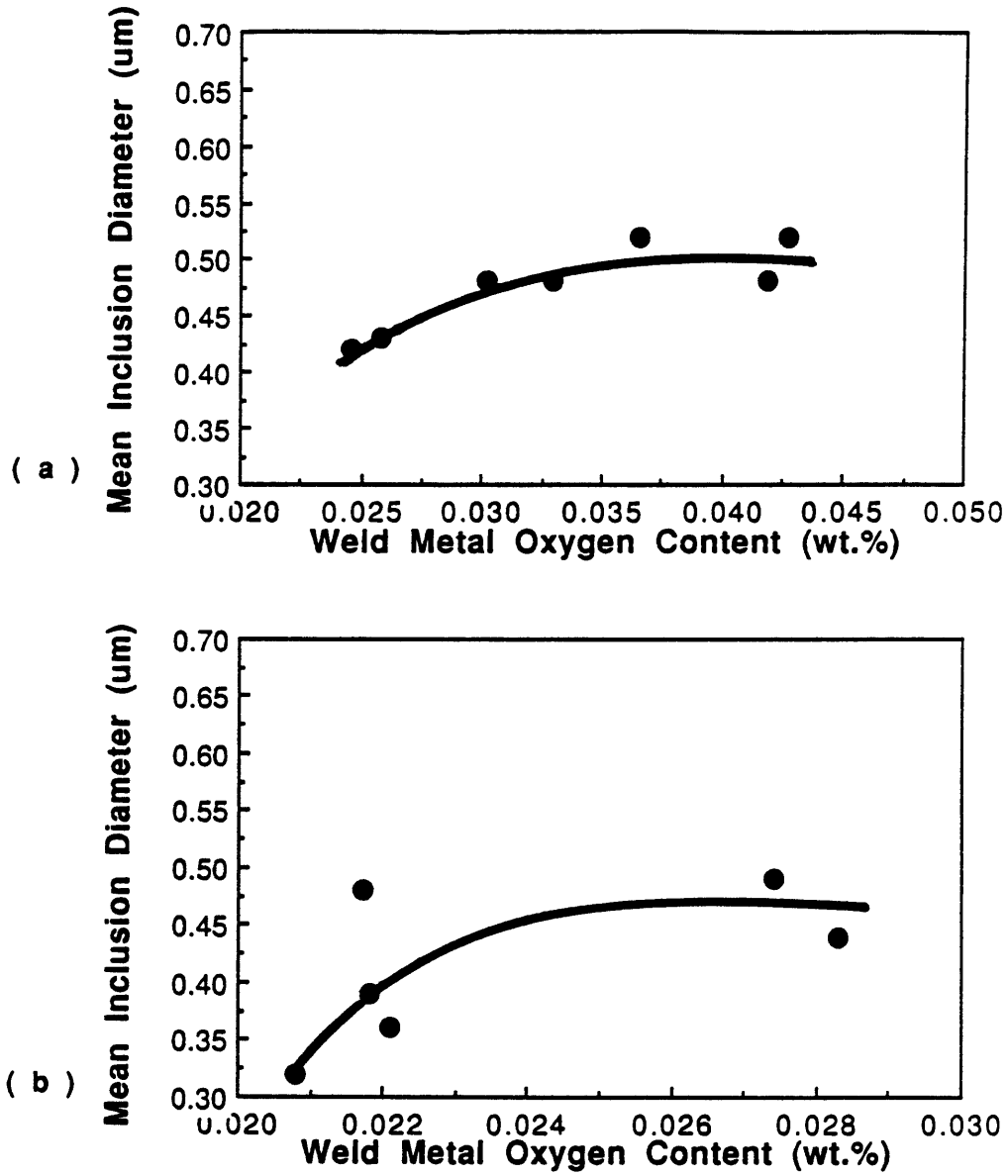

Figure 33. The variation of mean particle diameter (da) as a function of oxygen content in the weld metal.

(a). Aluminum addition series.

(b). Titanium addition series.

inclusion size decreased with weld metal oxygen content. These authors attributed the difference to the layer range of particle sizes examined, including inclusions smaller than 0.2 μm.

IV.1.3.4. Relationship Between Weld Metal Inclusion And Weld Metal Oxygen Content

In Figure 34 , the oxygen content in the weld metal quickly increases with aluminum addition, then reaching a maximum at approximately 0.05 wt. percent. After that the curve levels off, it might be that the free oxygen in the weld pool was consumed and additional aluminum will go into the weld pool and become solid solution atoms. At the same time, aluminum-rich oxide inclusions coalesce and float, decreasing the oxygen content. Figure 35 shows that the inclusion size remained constant after 0.05 wt. pct. of weld metal aluminum content. This also indicates that the proposed mechanism is correct. Figure 36 shows that weld metal oxygen content did not significantly increase with titanium addition, meaning that titanium fixed oxygen to form small oxides and trapped in weld pool.

In Figure 37(b), the aluminum in inclusions rapidly increased with weld pool aluminum content. However, at

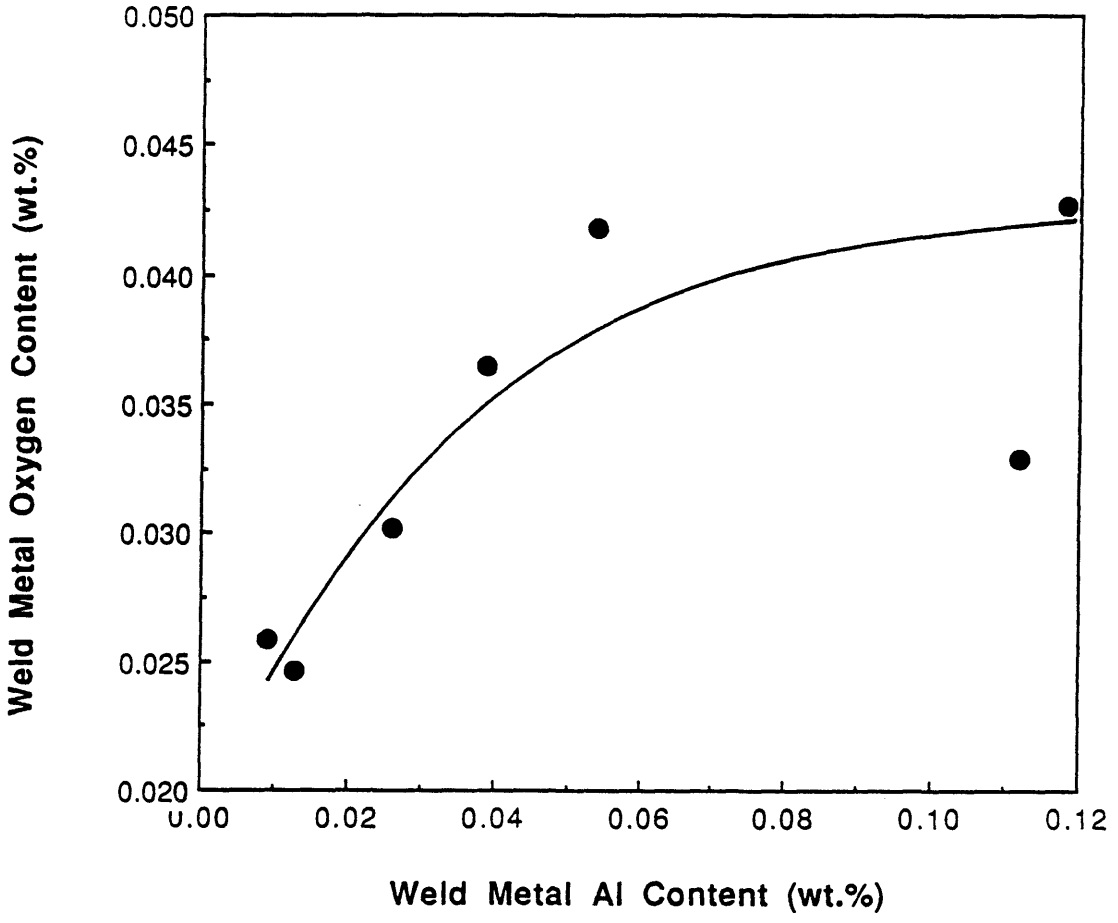

Figure 34. The variation of weld metal oxygen content as a function of weld metal aluminum content.

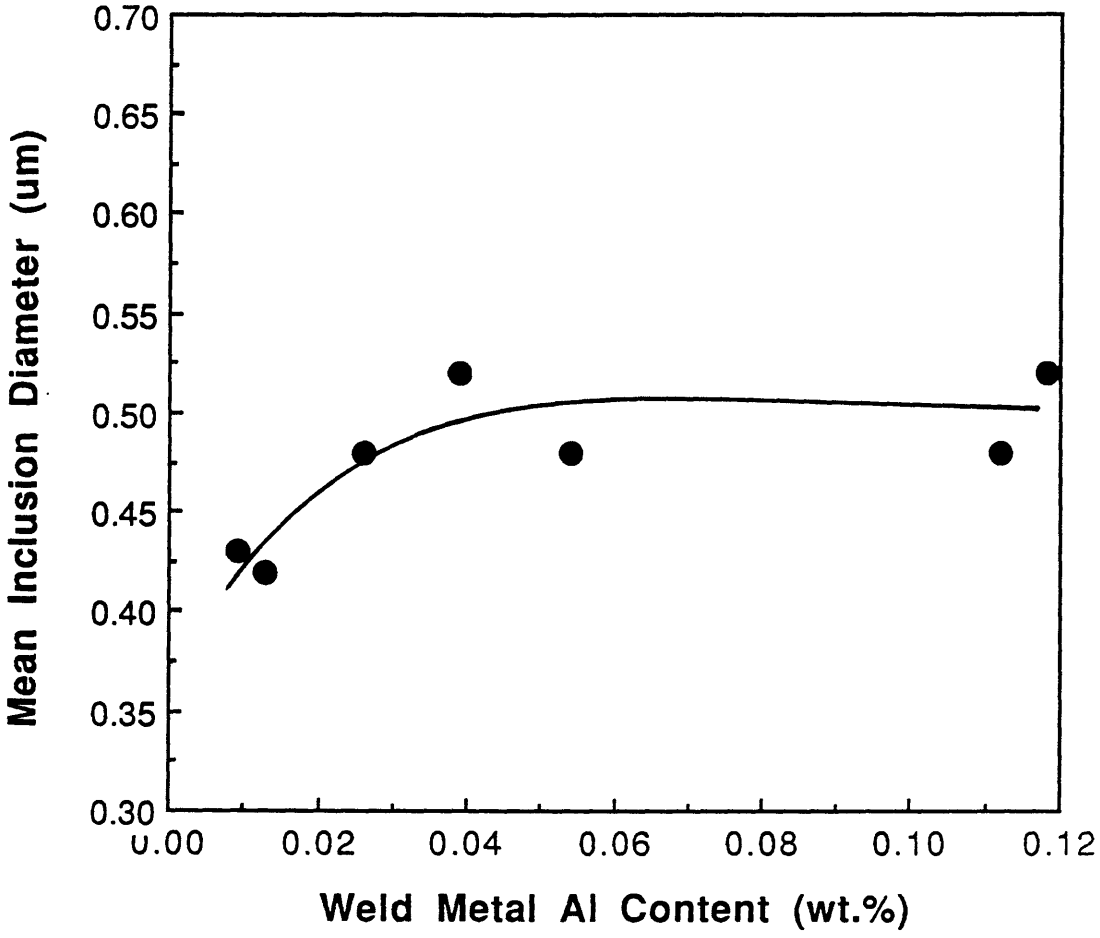

Figure 35. Mean particle diameter as a function of weld metal aluminum content.

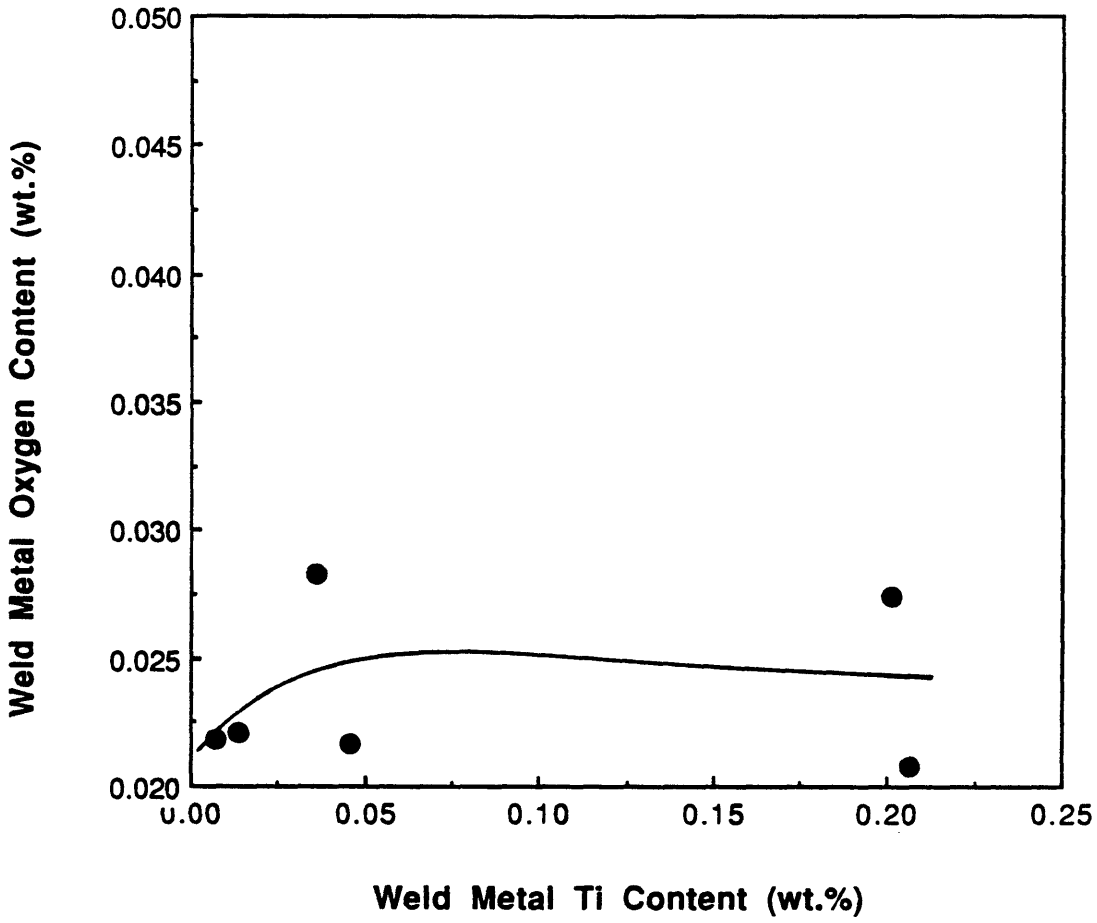

Figure 36. The variation of weld metal oxygen content as a function of weld metal titanium content.

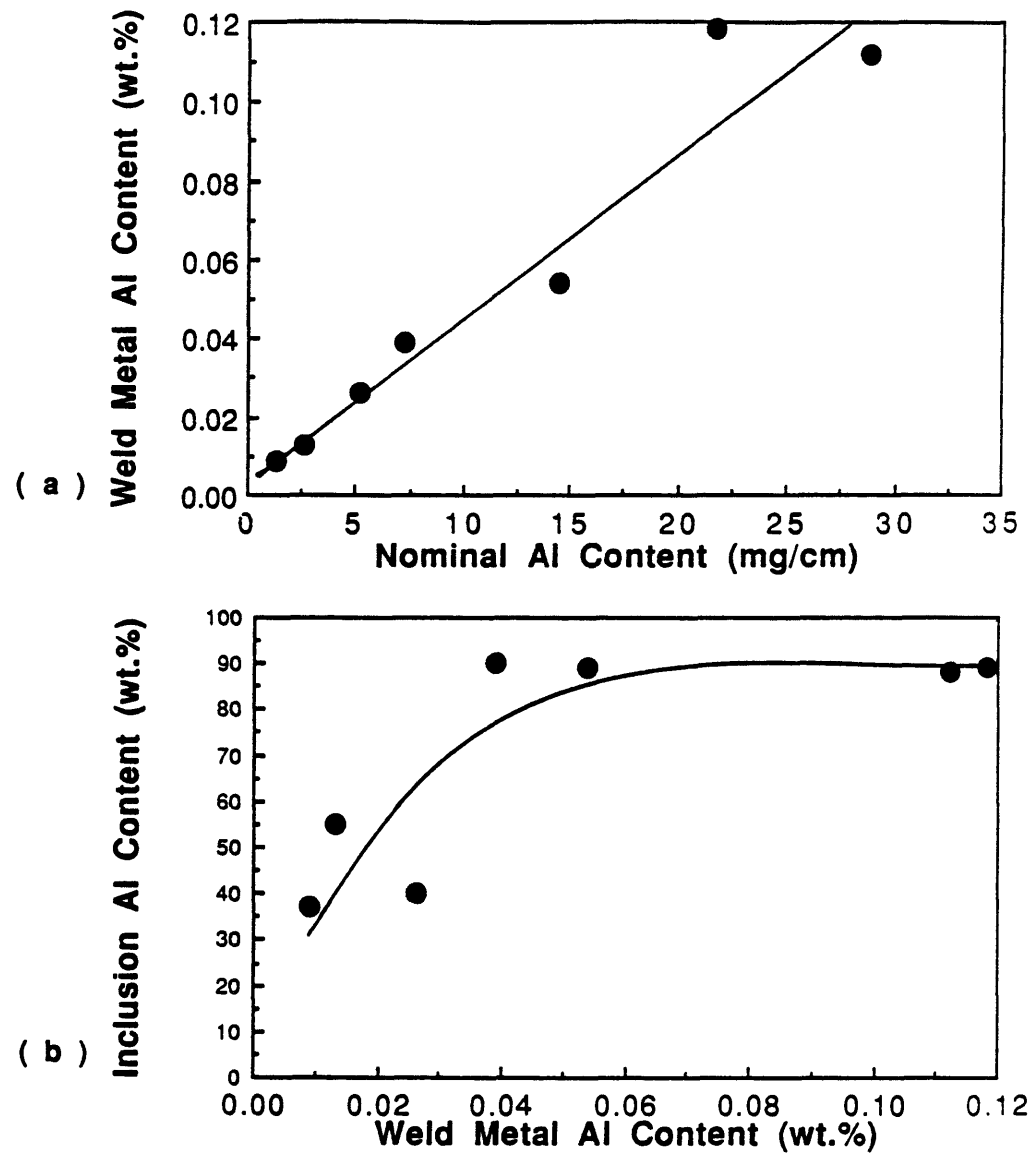

Figure 37. (a). The relationship between weld metal aluminum content and nominal aluminum addition.

(b). The relationship between inclusion aluminum content and weld metal aluminum content.

higher aluminum content, the aluminum content in inclusions became almost constant. If more aluminum is added, the excess aluminum would enter the weld pool to become solid solution atoms, detrimental to the weld metal properties. In Figure 38(b), the titanium content in inclusion increased with increasing weld pool titanium. This seems to indicate that titanium inclusions do not coalesce, nor float. They remain in the weld pool, reason why the titanium content in inclusions increases with weld metal titanium content.

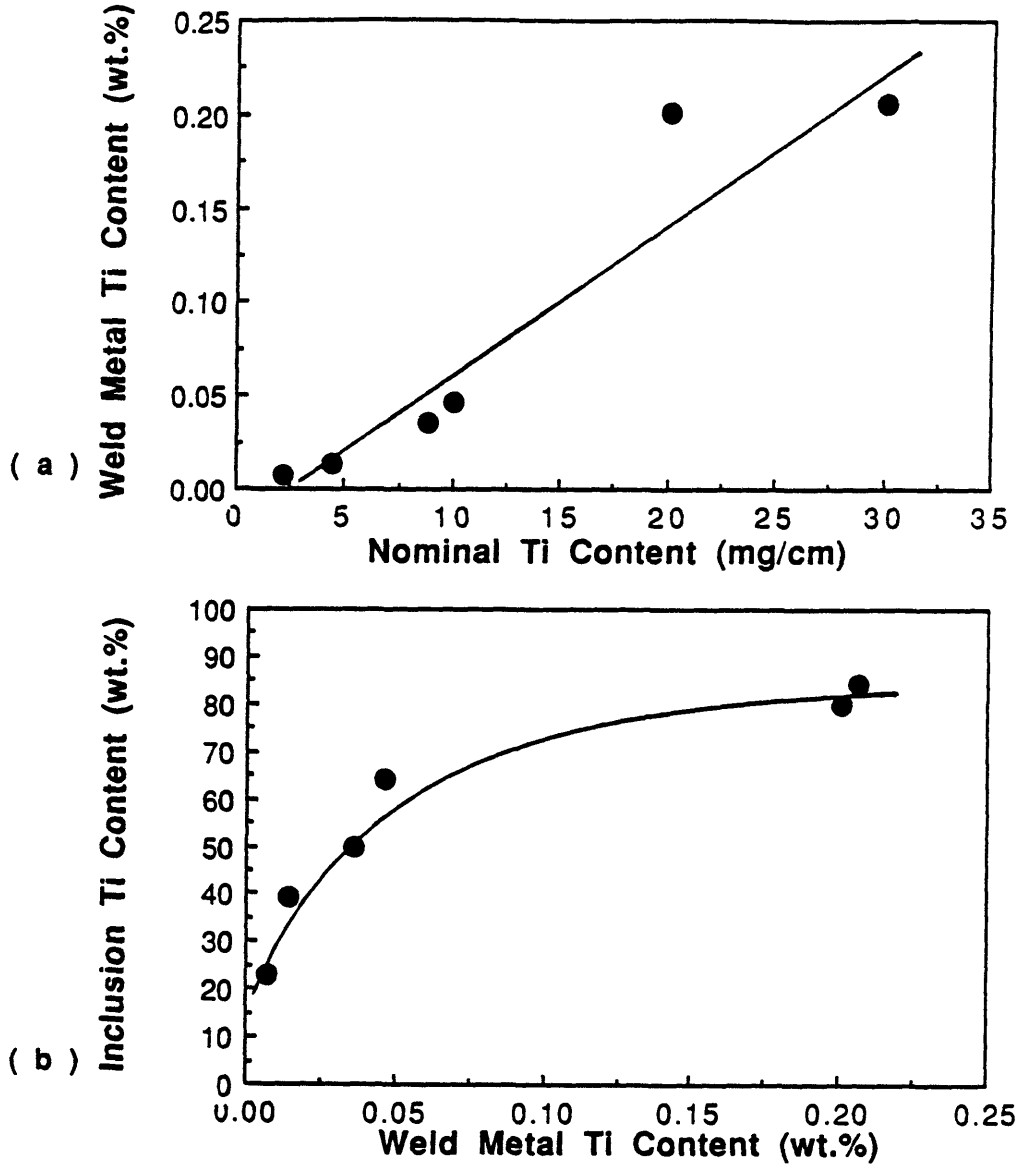

Figure 38. (a). The relationship between weld metal titanium content and nominal titanium addition.

(b). The relationship between inclusion titanium content and weld metal titanium content.

IV.2. Combined Effects

In the previous section, the individual effects of titanium and aluminum additions are explained. In this section, the combined effects of these two elements will be discussed. Due to the large number of welds made in both aluminum-titanium (A-T) sequence and titanium-aluminum (T-A) sequence ,a typical set was chosen from each group to illustrate the behavior of these welds.

IV.2.1. Weld Metal Composition Effect In A-T Welds

The A-T sequence welds showed that titanium further decreased the residual oxygen content from the first pass (aluminum addition) ,Figure 39. Figure 40 shows that maximum acicular ferrite was observed at approximately 0.04 wt. pct. of titanium. Above this point, acicular ferrite is replaced by bainite. Below this point, AF increases at the expense of GBF.

To explain the observed microstructures change as a function of weld metal oxygen and titanium content the following approach is proposed.

It is assumed that in the discussion with enough oxygen in the system, all aluminum atoms in the weld metal will

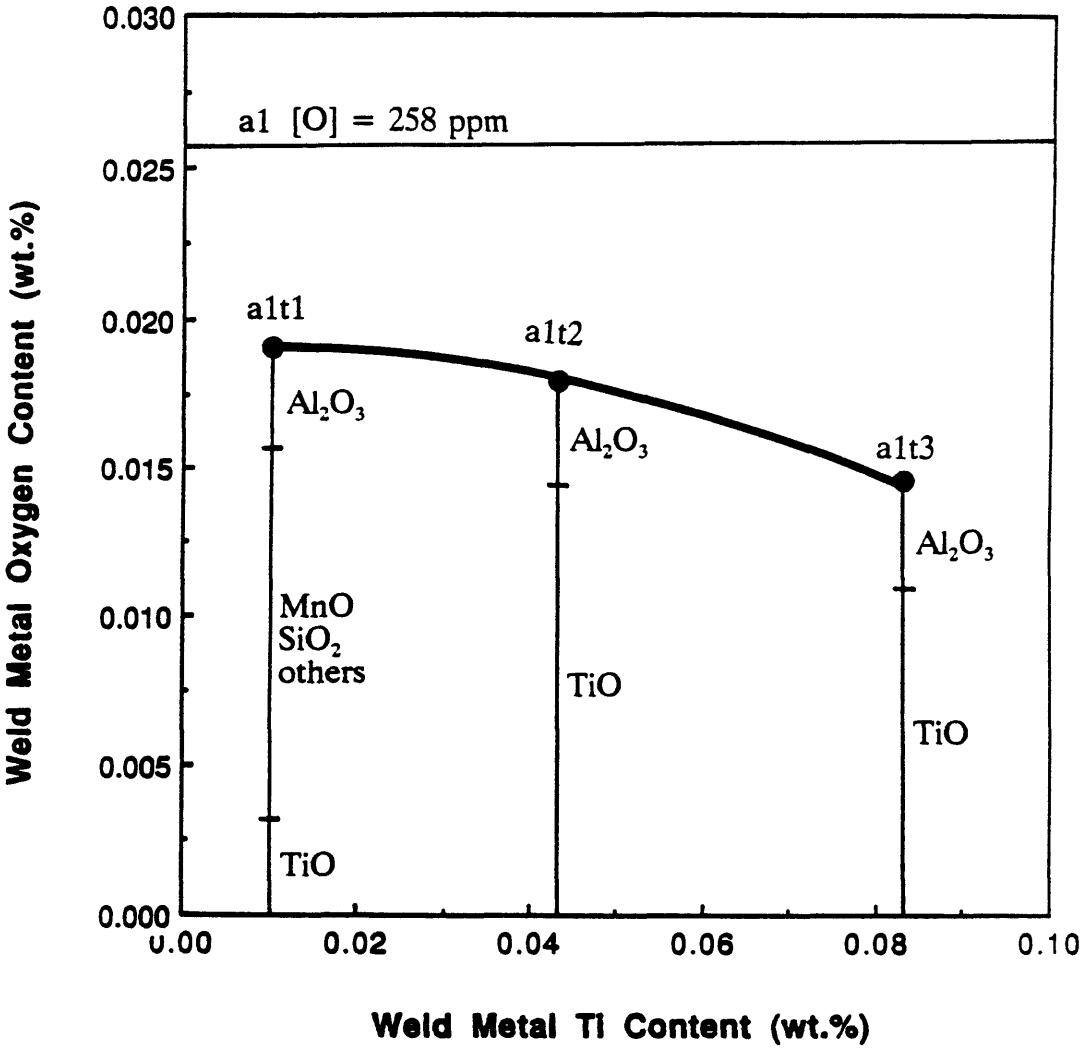

Figure 39. The variation of the oxygen content as a function of the weld metal titanium content in A-T group welds.

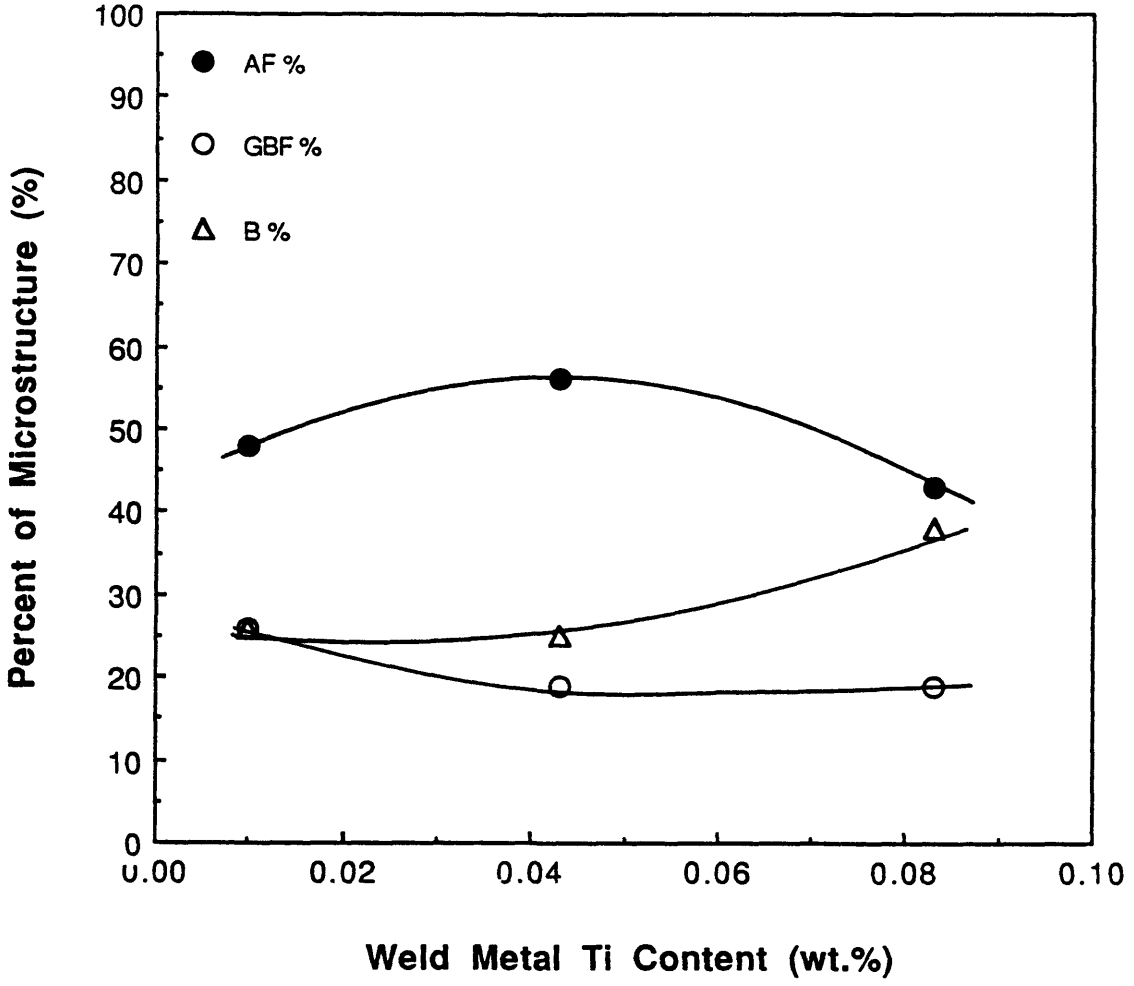

Figure 40. The variation of the weld microstructures as a function of the weld metal titanium content in A-T group welds.

form Al_2O_3. Since Al_2O_3 is a very stable oxide, it will not be reduced by the titanium addition during the second pass. It is also assumed that all titanium atoms in the weld metal are in the form of TiO. Finally, MnO and SiO_2 are reduced to manganese and silicon by titanium addition.

As described previously, the first pass (with aluminum addition) has the following composition.

a1 weld :[Al] = 0.009 wt. pct. (90 ppm)
[Ti] = 0.002 wt. pct. (20 ppm)
[O] = 258 ppm
[N] = 54 ppm

Since approximately 80 ppm of oxygen are required to combine with the 90 ppm of aluminum and 7 ppm of oxygen are needed to combine with 20 ppm of titanium, only 171 ppm of oxygen remained to combine with other elements. Therefore, MnO, SiO_2 are formed. The presence of manganese oxide and silica was confirmed by the inclusion analysis shown in a previous section.

During the second pass welding, the oxygen content dropped from 258 to 191 ppm. The loss is due to inclusions coalescence and flotation, and convective flow in the weld

pool. This is verified by the reduction of aluminum after the titanium addition.

The composition of the alt1 weld is :

[Al] = 0.004 wt. pct. (40 ppm)

[Ti] = 0.010 wt. pct. (100 ppm)

[O] = 191 ppm

Based on stoichiometric calculation , 36 ppm of oxygen are needed to combine with 40 ppm of aluminum. If all titanium (100 ppm) are in the form of titanium oxide, then 33 ppm of oxygen will be needed, which means that not enough titanium is available to react with all the 155 ppm oxygen in this weld. Thus, MnO and SiO_2 are also formed. This subject is also confirmed by inclusion analysis.

The composition of alt2 weld is :

[Al] = 0.004 wt. pct. (40 ppm)

[Ti] = 0.043 wt. pct. (430 ppm)

[O] = 179 ppm

Following the procedure used in the alt1 weld , it was determined that 143 ppm of oxygen was necessary to combine

with 430 ppm of titanium. Mass balance showed that no oxygen is available for other elements. Since there is a small amount of MnO and SiO_2, some titanium atoms might have remained in the form of solid solution. However, the increase in acicular ferrite in the weld is attributed to the large amount of TiO inclusions in the weld.

For the composition of alt3 weld is :

[Al] = 0.004 wt. pct. (40 ppm)

[Ti] = 0.083 wt. pct. (830 ppm)

[O] = 146 ppm

Following a similar calculation, 36 ppm of oxygen is needed to combine with 40 ppm of aluminum to form Al_2O_3. Assuming that all the other oxygen atoms available had reacted with titanium to form TiO, then the 110 ppm of oxygen would have consumed 330 ppm of titanium, which means that at least 500 ppm of titanium remained in the weld metal in different forms.

During solidification, only a small part of the titanium atoms will form nitride or carbide (as isolated particles or on the surface of already existing inclusions). Taking into account the solubility product of TiN and TiC in austenite

[83] and that the nucleation and growth of TiN and TiC are controlled by titanium diffusion [84], only part of the titanium atoms will form TiN and TiC on the outer layer of existing inclusions (oxide particles) [19,84]. The remaining titanium atoms will be dispersed in the weld metal as solid solution atoms and hardenability agent. The above model is supported by experimental evidences of Kluken and Grong [19]. They investigated the differences between total and acid soluble contents of aluminum and titanium. Despite the high affinity of titanium for carbon and nitrogen, a significant amount of titanium atoms remain in solution, determined as acid soluble titanium. Their results shown in Table 8 [19], agreed with the observations made by Es-Souni and Beaven [84].

From the calculation above, it is easy to explain the variation of microstructures in Figure 40. Below the optimum content (0.04 wt. pct.), TiO increased with the titanium addition. The volume fraction of AF increased with the nonmetallic inclusion TiO increasing. Above the optimum value, excess titanium atoms enter the weld pool and behave as hardenability agent promoting bainite formation. In all A-T group welds, higher titanium addition also led to higher volume fraction of bainite, sometimes as high as 100 percent.

Table 8. Chemical composition of selected experimental welds showing the total and acid soluble contents of aluminum and titanium in low carbon low alloy steel weld metal [19]. (in weight percent)

[C]	[O]	[N]	$[Al]_{(total)}$	$[Al]_{(soluble)}$	$[Ti]_{(total)}$	$[Ti]_{(soluble)}$
0.09	0.037	0.005	0.020	0.002	0.025	0.018
0.09	0.039	0.005	0.037	0.004	0.022	0.018
0.09	0.040	0.006	0.044	0.006	0.058	0.046
0.10	0.031	0.005	0.062	0.013	0.032	0.029
0.09	0.031	0.006	0.053	0.008	0.053	0.052

IV.2.2. Weld Metal Composition Effect In T-A Welds

In the section above , the combined effects of aluminum-titanium (A-T) additions are explained. In this section, the effects of titanium-aluminum(T-A) additions will be discussed.

The T-A welds showed that aluminum increased the second pass weld metal oxygen content to a maximum point followed by a slight drop, Figure 41. From Figure 42, it can be seen that above 0.024 wt. pct. of aluminum addition, AF is replaced by bainite. Below 0.024 wt. pct. of aluminum, AF increases at the expense of bainite. GBF does not seem to be altered by aluminum addition.

To explain the observed microstructural change as a function of weld metal oxygen and aluminum content the following assumptions were made.

(1). All aluminum atoms in the weld metal will form Al_2O_3, if there is enough oxygen atoms available.
(2). Al_2O_3 is a stable oxide and will not be reduced during the welding process.
(3). Titanium atoms in the weld metal are in the form of TiO, if there is enough oxygen atoms available.

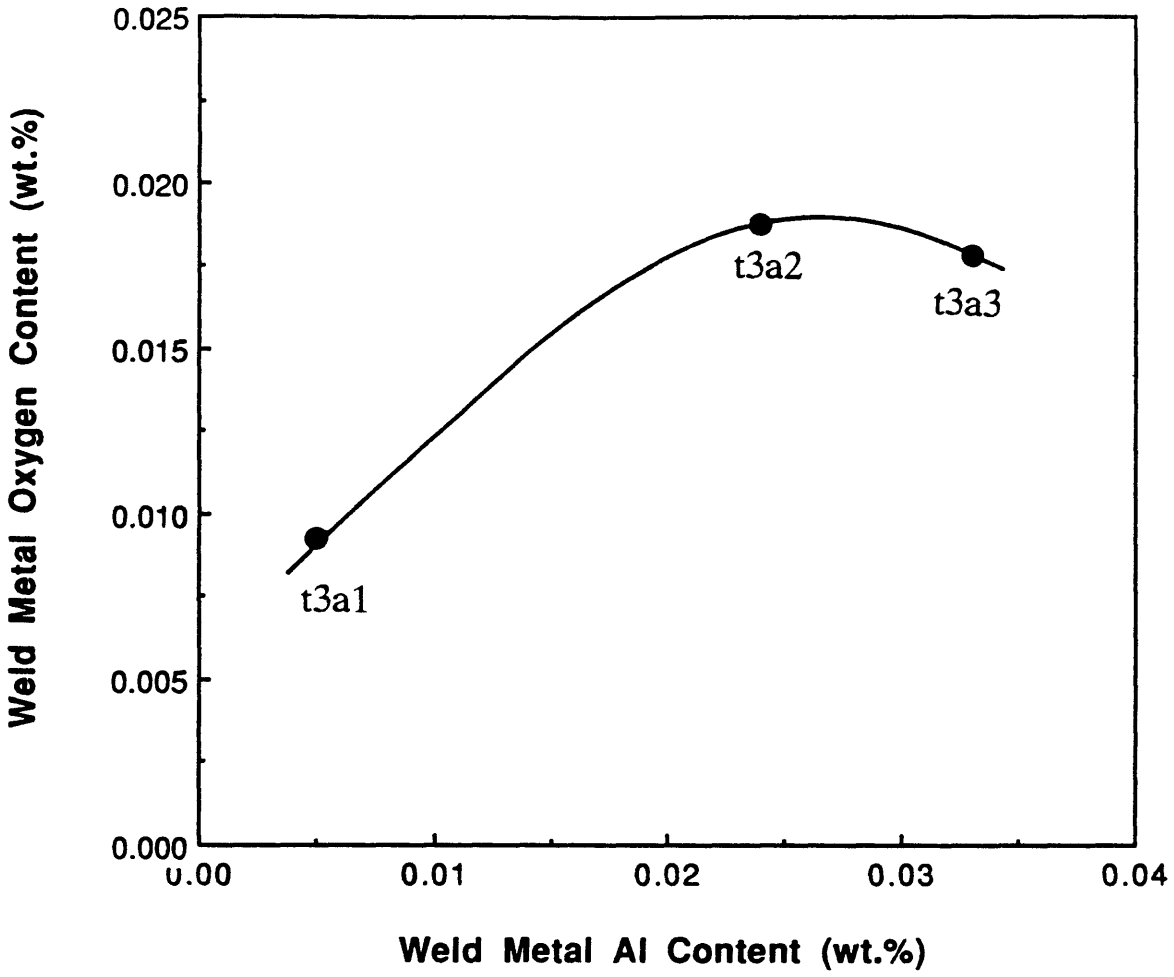

Figure 41. The variation of the oxygen content as a function of the weld metal aluminum content in T-A group welds.

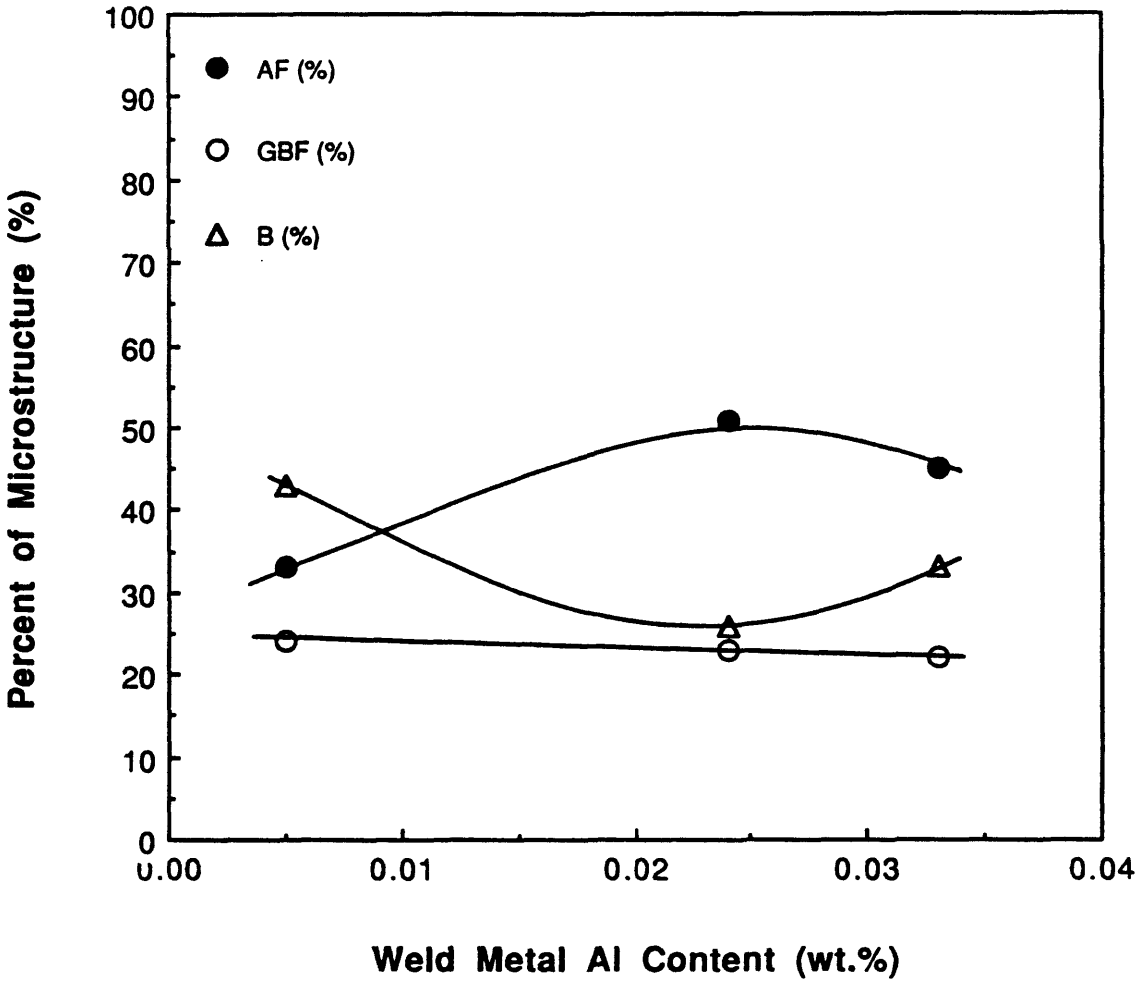

Figure 42. The variation of the weld metal microstructures as a function of the weld metal aluminum content in T-A group welds.

(4). TiO, MnO and SiO_2 are reduced to titanium, manganese and silicon with the aluminum addition.

The first pass (with titanium addition) has the following composition :

t3 weld :[Al] = 0.009 wt. pct. (90 ppm)
[Ti] = 0.036 wt. pct. (360 ppm)
[O] = 283 ppm
[N] = 49 ppm

Since approximately 80 ppm of oxygen are required to combine with the 90 ppm of aluminum to form oxide, only 203 ppm of oxygen remained to combine with titanium, manganese, silicon, etc. Stoichiometric calculation showed that only 120 ppm of oxygen are needed to combine with titanium to form TiO. Therefore, MnO, SiO_2 are formed, which is confirmed by the inclusion analysis.

During the second pass welding, the oxygen content dropped from 283 to 93 ppm. The loss may be due to inclusion loss by coalescence and flotation, and convective flow in the weld pool.

After adding aluminum in the second pass, the following

composition is determined in weld t3a1.

t3a1 weld :[Al] = 0.005 wt. pct. (50 ppm)
[Ti] = 0.013 wt. pct. (130 ppm)
[O] = 93 ppm

Aluminum was observed to decrease indicating that indeed inclusions were lost by flotation or convective flow in the weld pool.

Assuming that all 50 ppm of aluminum are in the form of oxide, then 44 ppm of oxygen are needed to combine with aluminum. If all titanium are in the form of titanium oxide, then 43 ppm of oxygen will be needed. Mass balance showed that there is only 6 ppm of oxygen remaining which means that only very little amount of oxygen is in the form of MnO and SiO_2. This is also confirmed by inclusion analysis.
The weld t3a2 has the following composition :

[Al] = 0.024 wt. pct. (240 ppm)
[Ti] = 0.022 wt. pct. (220 ppm)
[O] = 188 ppm

Assuming that all oxygen available have reacted with

aluminum to form Al_2O_3. The 188 ppm of oxygen will combine with 212 ppm of aluminum, which means that in weld metal do not have enough oxygen to react with all aluminum. Therefore, some aluminum atoms and most of titanium, manganese and silicon atoms will go into the weld pool as solid solution atoms and become hardenability agents. This explains the increase of acicular ferrite in the weld metal. Weld t3a3 has the following composition :

[Al] = 0.033 wt. pct. (330 ppm)
[Ti] = 0.019 wt. pct. (190 ppm)
[O] = 178 pm

Following similar procedure, the 178 ppm of oxygen combined with 200 ppm of aluminum to form Al_2O_3, which means that at least 130 ppm of aluminum and most of titanium, manganese and silicon atoms went into the weld pool becoming solid solution atoms. This promoted bainite formation.

Based on the calculation shown, the optimum aluminum concentration and AF volume fraction can be explained as the result of the increase in inclusion volume fraction, Figure 43. Above this point, excess aluminum, titanium, manganese and silicon in solution will promote bainite formation at the

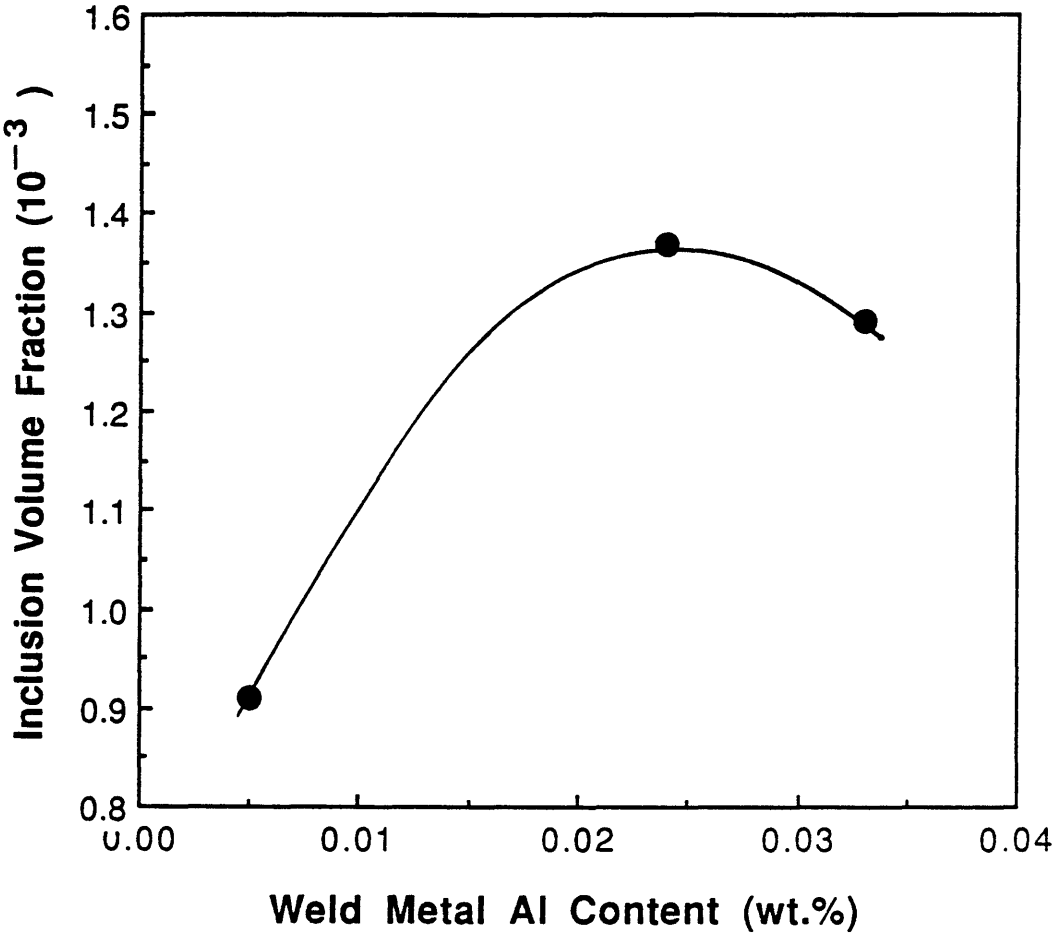

Figure 43. The variation of inclusion volume fraction (Vv) as a function of aluminum content in the T-A group welds.

expense of AF. Additionally, the decrease in inclusion density confirm the coalescence & floatation of aluminum oxide particles [19]. Generally speaking, in the T-A sequence welds, the microstructure is always a mixture of bainite, acicular ferrite and grain boundary ferrite.

From Figures 44 to 47 show the eight micrographs with same aluminum and titanium addition to the weld pool but the different deoxidation sequence.

(a)

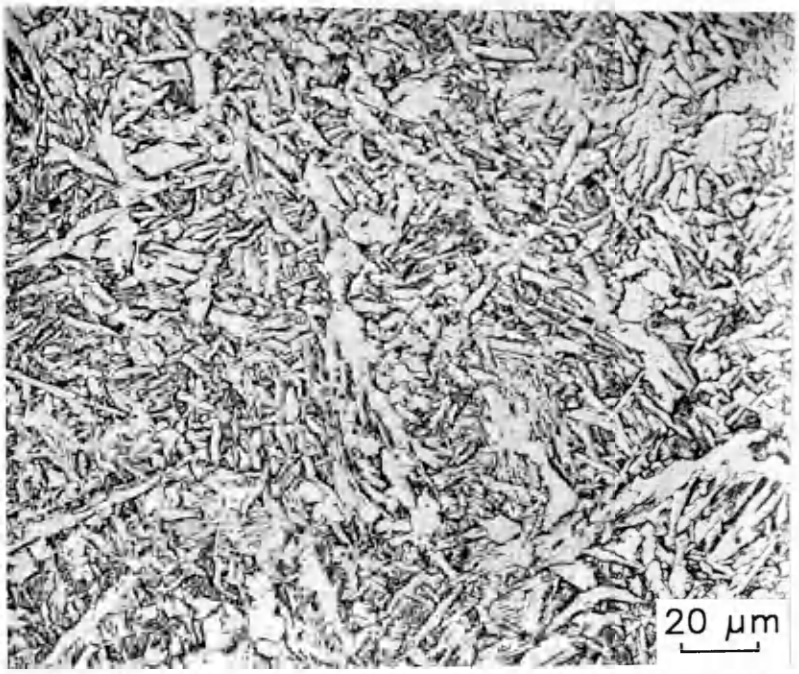

(b)

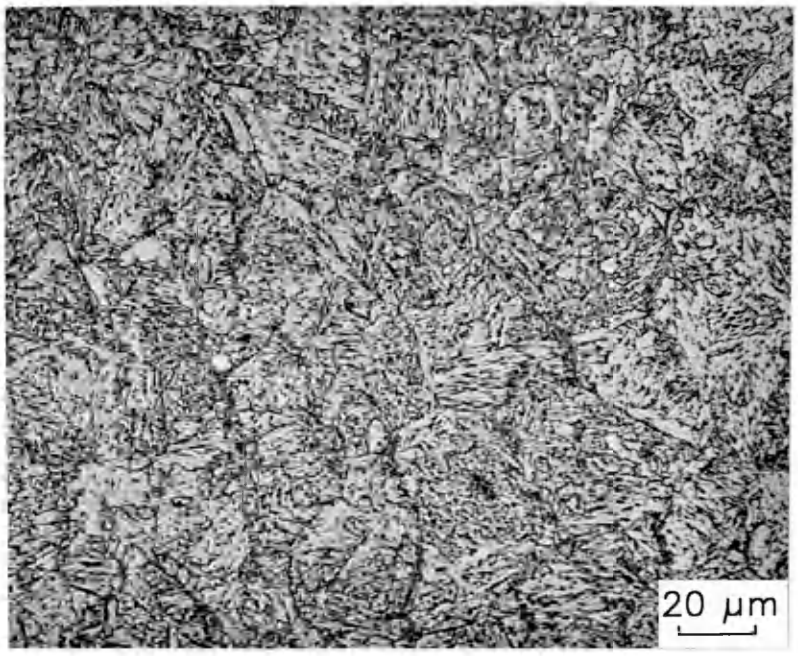

Figure 44. Optical micrographs

(a).T1A1 vs (b).A1T1

(a)

(b)

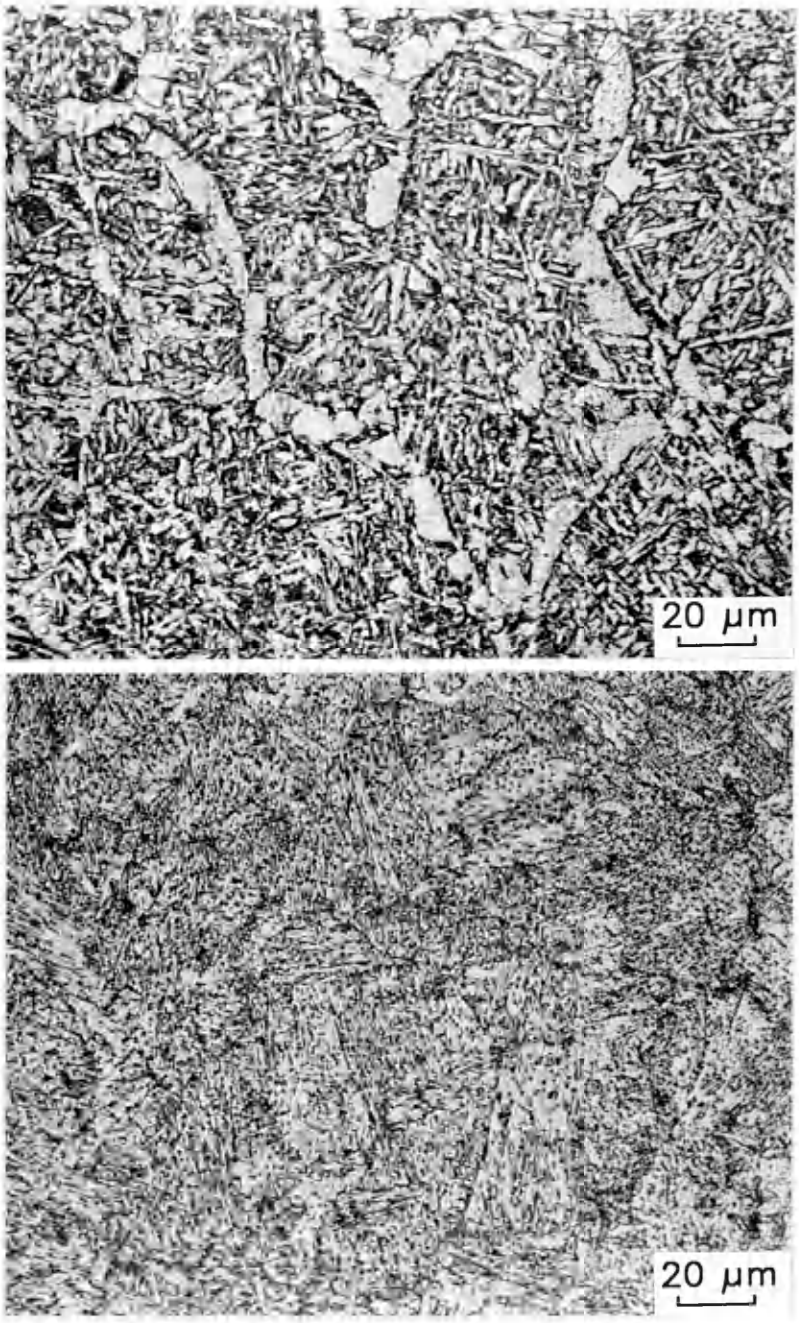

Figure 45. Optical micrographs

(a).T2A1 vs (b).A1T2

(a)

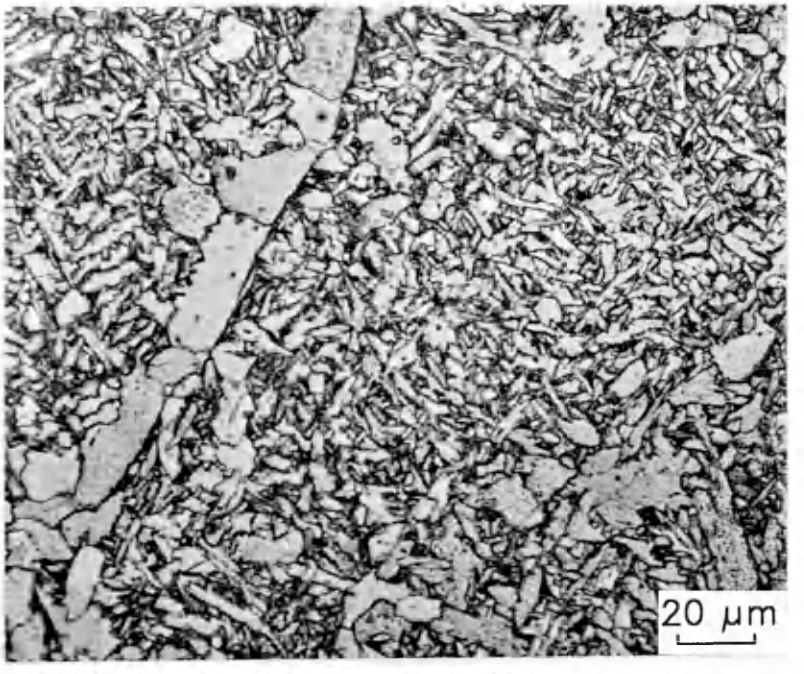

(b)

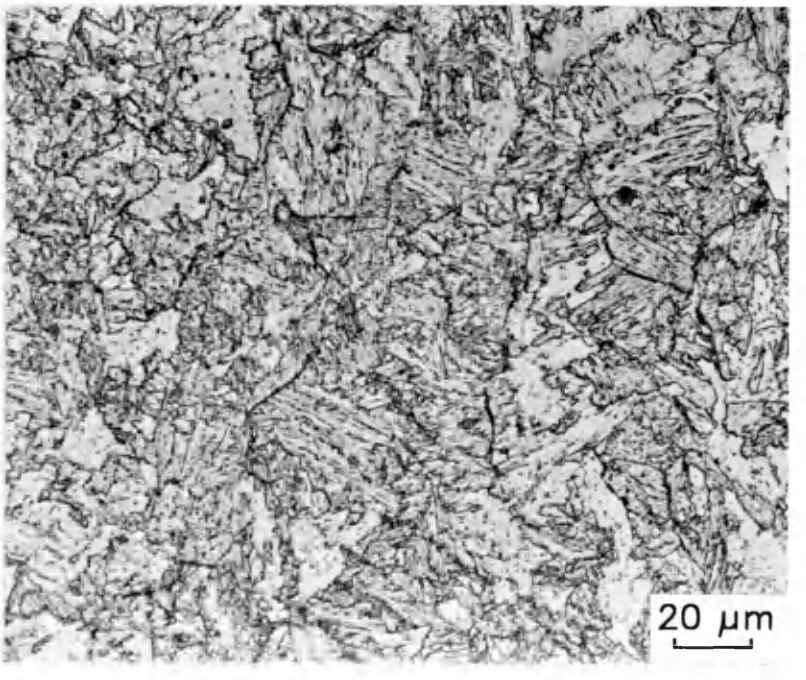

Figure 46. Optical micrographs

(a).T2A2 vs (b).A2T2

(a)

(b)

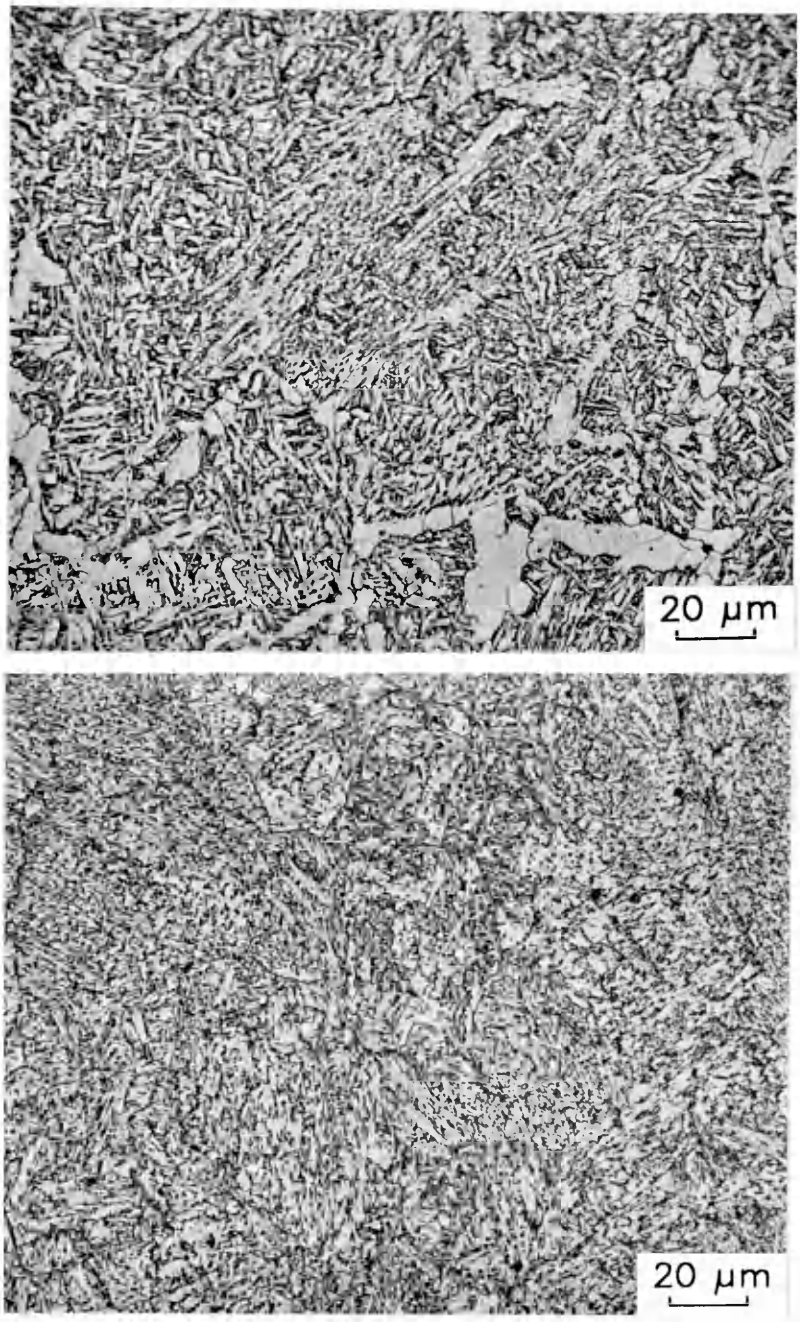

Figure 47. Optical micrographs

(a).T3A3 vs (b).A3T3

V. CONCLUSIONS

The results of this investigation on aluminum and titanium deoxidation sequence can be summarized in the following.

I. Individual Effect :

(1). Increasing weld metal titanium content up to approximately 0.05 wt. pct. increased the amount of acicular ferrite and grain boundary ferrite at the expense of bainite. At high titanium content, both acicular ferrite and grain boundary ferrite which were substituted by bainite.

(2). Increasing weld metal aluminum content up to approximately 0.05 wt. pct. increased the amount of acicular ferrite and bainite at the expense of grain boundary ferrite. High aluminum content resulted in less acicular ferrite (replaced by bainite).

(3). Titanium-bearing inclusions have better austenite grain boundary pinning effect than aluminum-bearing inclusions.

(4). Weld metal with higher amount of acicular ferrite are found to be related to coarser prior austenite grains and/or

with larger number of 0.45 μm nonmetallic inclusions.

(5). In the aluminum addition series welds, all the bulk inclusion compositions are located around the line where the [$\%SiO_2+\%TiO/TiO_2$] : [%MnO] ratio is approximately equal to 1.25.

II. Combined Effect :

(1). Deoxidation sequence is important in weld pool deoxidation and microstructural refinement. Excessive aluminum and/or titanium (in solution) increase the weld metal hardenability which results in increasing bainite.

(2). In A-T group welds, the higher titanium additions led to higher volume fraction of bainite.

(3). In T-A group welds, no matter how high the aluminum addition, the weld metal microstructure always show a mixture of bainite, grain boundary ferrite and acicular ferrite.

(4). The concept of welding systems using multiple wires (in tandem) that contain different deoxidizers can be used to better control and refine the weld metal microstructure.

VI. REFERENCES CITED

1. K. Easterling :"Introduction to the physical metallurgy of welding", Butterworths, London, U.K., p. 98, (1983).
2. F.J. Barbaro, P. Krauklis and K.E. Easterling :"Formation of acicular ferrite at oxide particles in steels", Materials Science and Technology , Vol. 5 , (Nov. 1989).
3. W.F. Savage and A.H. Aronson :"Preferred orientation in the weld fusion zone", Welding Journal, 45(2), pp. 76s-89s, (1966).
4. C.E. Cross, O. Grong, S. Liu and J.F. Capes :"Metallography and welding process control", Applied Metallography, Van Nostrand Reinhold, pp. 197-210, (1984).
5. Stephen K.C. Liu :"The role of non-metallic inclusions in controlling weld metal microstructures in niobium microalloyed steels", Colorado School of Mines, Ph.D. Thesis T-2923, (1984).
6. G.J. Davies and J.G. Garland :"Solidification structures and properties of fusion welds", International Metallurgical Review, Vol. 20, pp. 83-

106, (1975).

7. E. Levine and D.C. Hill :"Structure-property relationships in low carbon weld metal", Metallurgical Transaction A, Vol. 8A, pp. 1453-1463, (1973).
8. A.C. Hunt :"The effects of heat input and dilution on the microstructure and properties of microalloyed steel weld metal", M.S. Thesis No. T-3305, Colorado School of Mines, Golden, Colorado, (1987).
9. R.J. Pargeter :"Quantification of weld metal microstructure", IIW Doc. No. IXJ-78-83. (1983).
10. "Guidelines for classification of ferritic steel weld metal microstructural constituents using the light microscope", IIW Doc. No. IX-1377-85. (1985).
11. "Guide to the light microscope examination of ferritic steel weld metals", IIW Doc. No. IX-1533-88. (1988).
12. Committee of Welding Metallurgy of Japan Welding Society :"Classification of microstructures in low carbon - low alloy steel weld metal and terminology", IIW Doc. No. IX-1282-83. (1983).
13. D.A. Porter and K.E. Easterling :"Phase Transformations in Metals and alloys", Van Nostrand Reinhold, Berkshire , (1981).

14. P.G. Shewmon :"Transformations in metals", Mc Graw-Hill , New York, (1969).

15. H.I. Aaronson :"Proentectoid ferrite and the proentectoid cementite reactions" in Proc. Symp. "Decomposition of austenite by decompositional processes", Philadelphia, AIME, p. 387, (1960).

16. O. Grong and D.K. Matlock :"Microstructural developments in mild and low alloy steel weld metals", Intl. Metals reviews, Vol. 31, pp. 27-48, (1986).

17. C.S. Choi and T.W. Eagar :"Slag metal equilibrium during submerged arc welding", Met. Trans., Vol. 12B, pp. 539-547, (1981).

18. R. Kiessling :"Non-metallic inclusions in steel. Part I-IV", London, The Metal Society, (1978).

19. A.O. Kluken and O. Grong :"Mechanisms of inclusion formation in Al-Ti-Si-Mn deoxidized steel weld metals", Metallurgical Transactions A, Vol. 20A, pp. 1335-1349, (Aug. 1989).

20. US Steel Corp. :"The making, shaping, and treating of steels", 9th edition, Pittsburgh, US Steel Corp., p.281, (1971).

21. M.E. Saggese, A.R. Bhatti, D.N. Hawkins and J.A. Whiteman :"Factors influencing inclusion chemistry and

microstructure in submerged arc welds", Proc. Conf. on "The effects of residual, impurity and microalloying elements on weldability and weld properties", London, The Welding Institute, Abington, Paper 15, (1983).

22. J.M. Dowling, J.M. Corbett and H.W. Kerr :"Inclusion phases and the nucleation of acicular ferrite in submerged arc welds in high strength low alloy steels", Metallurgical Transactions A, Vol. 17A, pp. 1611-1623, (Sept. 1986).
23. N. Iwamoto :"Oxide inclusions formed in steels (Report I) -- Deoxidation products by Al, Si, Mn, Ti, V --", Transactions of JWRI, Vol. 3, No. 1, (1974).
24. R. Keissling and N. Lange :"Non-metallic inclusions in steels", The Metals Society, London, (1978).
25. D.J. Abson :"Non-Metallic inclusions in ferritic steel weld metals - a review", IIW Doc. IX-1486-87, (May 1987).
26. J.R. Rait and H.W. Pinder :JISI, Vol. 154, pp. 371-398, (1946).
27. C.L. Choi and D.C. Hill :"A study of microstructural progression in as-deposited weld metal", Welding Journal, Vol. 57, p. 2329, (1978).
28. Y. Ito and M. Nakanishi :"Study on charpy impact

properties of weld metal with submerged arc welding", The sumitomo Search, 15, pp. 27, (1976).

29. D.J. Widgery :"New ideas on submerged arc welding", in Proc. Intl. Conf. on "Trends in steels and consumables for welding", London, The Welding Institute, p. 217, (1978).
30. Y. Ito and M. Nakanishi :"Study on charpy impact properties of weld metal with submerged arc welding", The Sumitomo Search, 15, pp. 42-62, (1976).
31. Y. Ito, M. Nakanishi and Y. Komizo :"Effects on oxygen on low carbon steel weld metal", Met. Con., 14(9), pp. 472-478, (1982).
32. C.W. Ramsay :"The influence of oxygen and non-metallic inclusions on high strength steel weld metal microstructures and properties", Ph.D. Thesis No. T-3391, Colorado School of Mines, Golden, Colorado, (1989).
33. S. Ohkita, H. Homma, S. Tsushima and N. Mori :"The effect of oxide inclusions on the microstructure of Ti-B-containing weld metals", Austrialian Weld J. 29(3), pp. 29-36, (1984).
34. P.F. Chaveriate, G.S. Kim, S. Shah and J.E. Indacochea :"Low carbon steel weld metal microstructures :"The

role of oxygen and manganese", J. Materials Engineering, Vol. 9, No. 3, pp. 253-267, (1987).

35. G.S. Barritte, R.A. Ricks and P.R. Howell :"The effect of inclusions on the structure and properties of HSLA steel weld metals", Proc. 6th Intl. Conf. Melbourne, Australian, pp. 121-126, (Aug. 1982).
36. D.J. Abson, R.E. Dolby and P.H.M. Hart :"The role of nonmetallic inclusions in ferrite nucleation in carbon steel weld metals", in Proc. Intl. Conf. on "Trends in steels and consumables for welding", London, The Welding Institute, Paper 25, pp. 75-101, (1978).
37. R.C. Cochrane and P.R. Kirkwood :"The effect of oxygen on weld metal microstructure" in Proc. Intl. Conf. on "Trends in steels and consumables for welding", London, The Welding Institute, p. 103, (1978).
38. S. Liu and D.L. Olson :"The role of inclusions in controlling HSLA steel weld microstructure", Welding J. Res. Suppl., pp. 139S-149S, (June 1986).
39. P.L. Harrison and R.A. Farrar :"Infuence of oxygen-rich inclusions on the r --> α phase transformation in high strength low alloy (HSLA) steel weld metals", J. of Materials Science 16, pp. 2218-2226, (1981).

40. M. Ferrante and R.A. Farrar :"The role of oxygen-rich inclusions in determining the microstructure of weld metal deposits", J. of Materials Science, Vol. 17, pp. 3293-3298, (Nov. 1982).

41. L. Devillers, D. Keplan, B. Marandet, A. Ribes and P.V. riboud :"The effect of low level concentrations of some elements on the toughness of submerged-arc welded C-Mn steel welds", Conf. on "The effects of residual, impurity and micro-alloying elements on weldability and weld properties", London, The Welding Institute, Abington, Paper 1, (1983).

42. R.J. Pargeter :"Investigation of submerged arc weld metal inclusions", WIRR 151/1981, (July 1981).

43. E.S. Kayali, J.M. Corbett and H.W. Herr :"Observations on inclusions and acicular ferrite nucleation in submerged arc HSLA welds", J. of Material Science, 2(3), pp. 123-128, (1983).

44. A. Terashima and P.H.M. Hart :"Effect of flux TiO_2 and wire Ti content on tolerance to high Al content of submerged arc welds made with basic fluxes", Proc. Conf. on "The effects of residual, impurity and microalloying elements on weldability and weld properties", London, The Welding Institute, Abington,

Paper 27, (1983).

45. R.C. Cochrane and B.R. Keville :"Influence of inclusion morphology on microstructure and toughness of submerged arc weldments", Proc. Conf. on "Steels for line pipe and pipeline fittings", London, The Metals Society, pp. 51-60, (1981).
46. G.S. Barritte and D.V. Edmonds :"The microstructure and toughness of HSLA steel weld metals", Proc. Conf. on "Advances in the physical metallurgy of steel", Liverpool, The Metals Society, London, pp. 126-135, (1981).
47. Norbert A. Fleck II :"The effect of filler wire and flux compositions on the microstructure and properties of microalloyed steel weld metal", Colorado School of Mines, M.S. Thesis T-2942, (1984).
48. B.L. Bramfitt :"The effect of carbide and nitride additions on the heterogeneous nucleation behavior of liquid iron", Met. Trans. A, Vol. 1, p. 1987, (1970).
49. I. Watanabe and T. Kojima, Journal of Welding Society, Part I. 49, p. 772, (1980).
50. N. Mori, H. Homma, S. Okita and M. Wadabayshi :"Mechanism of notch toughness improvement in Ti-B bearing weld metals", IIW Doc. IX-1196-81, (May 1981).

51. G. Thewlis :"The influence of pipe plate and consumable chemistry on the composition, microstructure and toughness of weld metal", Proc. Conf. on "Welding and performance of pipelines", The Welding Institute, London, Paper 9, (1986).

52. G.M. Evans :"The effect of sulphur and phosphorus on the microstructure and properties of C-Mn all weld metal deposits", Oerlikon Schweissmitteilungen, 44 (No. 111), pp. 22-35, (1986).

53. A.R. Mills, G. Thewlis and J.A. Whiteman :"The nature of inclusions in steel weld metals and their influence on the formation of acicular ferrite", Material Science and Technology, Vol. 3, (Dec. 1987).

54. A.R. Bhatti, M.E. Saggese, D.N. Hawkins, J.A. Whiteman and M.S. Golding :"Analysis of inclusions in submerged arc welds in microalloyed steels", Welding J. Res. Supp., 63(7), p. 224s-230s, (1984).

55. D. Brooksbank and K.W. Andrews :"Stress field around inclusions and their relation to mechamical properties", Journal of The Iron and Steel Institute, p.246, (1972).

56. R.C. Cochrane, J.L. Ward and B.R. Keville :"The influence of deoxidation and/or desulphurisation

practice on the weld metal toughness of high dilution welds", in Proc. Intl. Conf. on "The effect of residual, impurity and micro-alloying elements on weldability and weld properties", London, The Welding Institute, Paper 16, (1983).

57. N.A. Fleck, O.Grong, G.R. Edwards and D.K. Matlock :"The role of filler metal wire and flux composition in submerged arc weld metal transformation kinetics", Welding J. Res. Supp., 65(5), pp. 113s-121s, (1986).
58. M.L.E. Davis and F.R. Coe :"The chemistry of submerged arc welding flexes", The Welding Institute Research Report, 39/1977/M, (1977).
59. D.C. Hill and D.E. Passoja :"Understanding the role of inclusions and microstructure in ductile fracture", Welding J. Res. Supp., 53(1), pp. 481s-485s, (1974).
60. J. Tsuboi and H. Terashima :"Review of strength and toughness of Ti and Ti-B microalloyed deposits", Int. Inst. of Welding, IIW Doc. IIS/IIW-764-83, (1983).
61. I. Watanabe and T. Kojima :"Effects of titanium, boron, and oxygen on notch toughness", Proc. Intl. Conf. on "Effects of residual,impurity and microalloying elements on weldability and weld properties", The Welding Institute, London, Paper 51,

(Nov. 1983).

62. N. Bailey :"Titanium flux additions during submerged arc welding of ferritic steels", Welding Institute Research Report, No. 221, pp. 1-5, (July, 1983).
63. T.H. North, H.B. Bell, A.H. Koukabi, and I. Craig :"Notch toughness of low oxygen content submerged arc deposits", Welding Journal, 58(12), pp. 343s-354s, (1979).
64. W. Cole and P. Colvin :"Submerged arc welding of higher tensile steels", Met. Con. and Brit. Weld. J. 3(4), pp. 131-136, (1971).
65. J.M. Dowling, J.M. Corbett and H.W. Kerr :"Effects of inclusion compositions and size distribution on the microstructure and properties of submerged arc welds", Proc. Conf. on "Inclusions and residuals in steels :Effects on fabrication and service behavior, CANMET/CSIRA, Ottawa, Canada, pp. 469-486, (1985).
66. H. Terashima and P.H. Hart :"Effect of aluminum on C-Mn-Nb steel submerged arc weld metal properties", Welding Journal, 63(6), pp. 173s-183s, (1984).
67. Y. Yoshino and R.D. Stout :"Effect of microalloys on t the notch toughness of line pipe seam welds", Welding Journal, 58(2), pp. 59s-68s, (1979).

68. J.K. Brownlee :"Effects of Aluminum and Titanium on the microstructure and properties of microalloyed steel weld metal". Colorado School of Mines, M. Sc. Thesis No. T-3064, (April, 1985).

69. R.C. Cochrane, J.L. Ward and B.R. Keville :"The influence of deoxidation and/or desulphurisation practice on the weld metal toughness of high dilution welds", in Proc. Intl. Conf. on "The effect of residual, impurity and micro-alloying elements on weldability and weld properties", London, The Welding Institute, Paper 16, (1983).

70. S.S. Tuliani, T. Boniszewski, and N.F. Eaton : Weld. Met. Fabr., Vol. 37, pp. 327-339, (1969).

71. "Estimating the average grain size of metals". Annual Book of ASTM Standards, E 112-81, (1981).

72. Y. Ito and K. Bessyo :"Weldability formula of high strength steels related to heat affected zone cracking", IIW DOC IX-576-68, (1968).

73. H. Grajon :"Note on the carbon equivalent", IIW DOC IX-555-67, (1967).

74. J. Tanaka and T. Kitada :"Implant test for studying cold cracking", IIW DOC IX-959-76, (1976).

75. H. Sekiguchi :"Fundamental research on the welding heat affected zone of steels", Nikkan Kogyo Shimbum, Tokyo, (1976).

76. J. Jang and J.E. Indacochea :"Inclusion effects on submerged-arc weld microstructure", Journal of Materials Science 22, pp. 689-700, (1987).

77. R.E. Dolby :"Factors controlling weld toughness - the present position, pt. II-weld metals", WIRR, 14/1976/M, (1976).

78. P.R. Kirkwood :"Microstructural and toughness control in low carbon weld metals", Metal Construction, pp. 260-264, (1978).

79. J.G. Garland and P.R. Kirkwood :"A reappraisal of the relationship between flux basicity and mechanical properties in submerged arc welding", Welding and Metal Fabrication, pp. 44-49, (April 1976).

80. S. Liu and D.L. Olson :"The influence of inclusion chemical composition on weld metal microstructure", J. Materials Engineering, Vol. 9, No. 3, pp. 237-251, (1987).

81. F.D. Richardson and J.H.E. Jeffes, substatantially as in J. Iron Steel Institute 160, 261, (1948).

82. G.M. Evans :"Effect of manganese on the microstructure and properties of C-Mn all weld metal deposits", Intl. Inst. of Welding, IIW Doc. II-A-432-77, (1977).

83. S. Suzuki, G.C. Weatherly and D.C. Houghton :"The response of carbo-nitride particls in HSLA steels to weld thermal cycles", Acta. Metall. , Vol. 35, No. 2, pp. 341-352, (1987).

84. M. Es-Souni and P.A. Beaven :"Microanalysis of inclusion/matrix interfaces in weld metals", Intl. Conf. on "Application of Surface and Interface Analysis - ECASIA 89", Antibes, France, (Oct. 1989).

85. C. B. Dallam :"The effect of stress on the weld metal acicular ferrite phase transformation", M.S. Thesis No. T-3293, Colorado School of Mines, Golden, Colorado, (1986).

86. G. Thewlis :"Transformation kinetics of submerged arc weld metal preliminary investigation", IXJ-165-90, (May 1990).

87. J.W. Jang, S. Shah, and J.E. Indacochea :"Influence of saw fluxes on low-carbon steel weld microstructure", J. Materials for Energy Systems, Vol. 8, No. 4, pp. 391-401, (March 1987).

Appendix I. : Chemical compositions of the weld metals.

	[C]	[Ti]	[Al]	[Mn]	[Si]	[P]	[S]	[Cu]	[Ni]	[Cr]	[B]*
t1	0.143	0.007	0.005	0.84	0.198	0.013	0.011	0.133	0.04	0.026	12
t2	0.151	0.014	0.007	0.88	0.200	0.013	0.009	0.114	0.03	0.025	7
t3	0.149	0.036	0.009	0.95	0.219	0.013	0.010	0.097	0.02	0.024	12
T1	0.127	0.046	0.006	0.90	0.198	0.010	0.009	0.090	0.02	0.031	0
T2	0.141	0.201	0.012	0.85	0.278	0.014	0.011	0.115	0.04	0.029	0
T3	0.148	0.206	0.010	0.88	0.283	0.011	0.008	0.103	0.03	0.031	0
T4	0.144	0.344	0.015	0.87	0.315	0.010	0.012	0.095	0.02	0.030	0
T5	0.131	0.355	0.016	0.86	0.355	0.009	0.009	0.095	0.02	0.030	0

[Mo]	[V]	[W]	[Co]	[As]	[Sn]	[Nb]	[Ta]	[Zr]	[O]*	[N]*
0.010	0.003	0.006	0.006	0.008	0.009	0.003	0.036	0.002	218	50
0.008	0.002	0.005	0.005	0.007	0.008	0.003	0.034	0.002	221	49
0.008	0.001	0.006	0.004	0.007	0.007	0.002	0.033	0.002	283	49
0.004	0.000	0.000	0.004	0.001	0.009	0.000	0.040	0.000	217	58
0.008	0.001	0.004	0.005	0.000	0.012	0.003	0.058	0.000	274	56
0.005	0.000	0.001	0.005	0.001	0.010	0.000	0.041	0.000	208	58
0.004	0.000	0.000	0.005	0.002	0.009	0.000	0.039	0.000	355	58
0.003	0.000	0.000	0.004	0.000	0.008	0.000	0.031	0.000	234	57

Notes :

* Boron, Oxygen, and Nitrogen concentration given in ppm.

All other concentrations expressed in weight percent.

Appendix I. : Chemical compositions of the weld metals (continued).

	[C]	[Ti]	[Al]	[Mn]	[Si]	[P]	[S]	[Cu]	[Ni]	[Cr]	[B]*
t1a1	0.119	0.007	0.005	0.70	0.133	0.013	0.010	0.074	0.03	0.023	13
t1a2	0.141	0.007	0.007	0.75	0.146	0.012	0.011	0.081	0.03	0.023	9
t1a3	0.127	0.007	0.028	0.69	0.139	0.012	0.011	0.083	0.02	0.023	1
t2a1	0.113	0.008	0.004	0.68	0.119	0.012	0.012	0.071	0.02	0.023	14
t2a2	0.122	0.009	0.009	0.63	0.104	0.011	0.009	0.071	0.02	0.022	4
t2a3	0.132	0.012	0.032	0.69	0.148	0.011	0.011	0.078	0.02	0.023	3
t3a1	0.109	0.013	0.005	0.58	0.122	0.010	0.011	0.070	0.02	0.022	0
t3a2	0.148	0.022	0.024	0.74	0.172	0.011	0.011	0.068	0.02	0.023	10
t3a3	0.122	0.019	0.033	0.64	0.145	0.011	0.011	0.078	0.03	0.023	4

[Mo]	[V]	[W]	[Co]	[As]	[Sn]	[Nb]	[Ta]	[Zr]	[O]*	[N]*
0.008	0.024	0.007	0.007	0.006	0.007	0.003	0.042	0.002	150	60
0.008	0.018	0.006	0.007	0.006	0.006	0.003	0.040	0.002	198	57
0.006	0.022	0.005	0.006	0.005	0.007	0.001	0.032	0.001	187	65
0.007	0.026	0.008	0.008	0.006	0.007	0.003	0.041	0.002	190	64
0.005	0.035	0.005	0.008	0.005	0.007	0.002	0.040	0.002	202	75
0.007	0.025	0.007	0.007	0.006	0.006	0.002	0.035	0.002	178	53
0.005	0.025	0.003	0.007	0.005	0.006	0.002	0.035	0.001	93	52
0.007	0.022	0.007	0.007	0.006	0.007	0.002	0.038	0.002	188	55
0.007	0.028	0.006	0.008	0.005	0.006	0.002	0.035	0.002	178	53

Notes :

* Boron, Oxygen, and Nitrogen concentration given in ppm.

All other concentrations expressed in weight percent.

Appendix I. : Chemical Compositions of the Weld Metals (continued).

	[C]	[Ti]	[Al]	[Mn]	[Si]	[P]	[S]	[Cu]	[Ni]	[Cr]	[B]*
a1	0.132	0.002	0.009	0.88	0.177	0.013	0.010	0.105	0.03	0.025	13
a2	0.132	0.003	0.013	0.88	0.224	0.015	0.009	0.119	0.03	0.026	15
a3	0.107	0.003	0.026	0.88	0.195	0.013	0.011	0.134	0.03	0.026	6
A1	0.156	0.003	0.039	0.96	0.206	0.011	0.010	0.095	0.03	0.027	4
A2	0.138	0.003	0.054	0.87	0.253	0.013	0.008	0.102	0.03	0.029	0
A3	0.150	0.005	0.118	0.98	0.364	0.012	0.010	0.108	0.03	0.028	10
A4	0.138	0.005	0.112	0.86	0.345	0.013	0.008	0.117	0.03	0.028	0
A5	0.120	0.007	0.228	0.83	0.503	0.013	0.008	0.111	0.03	0.029	0

[Mo]	[V]	[W]	[Co]	[As]	[Sn]	[Nb]	[Ta]	[Zr]	[O]*	[N]*
0.008	0.002	0.005	0.005	0.007	0.008	0.002	0.036	0.001	258	54
0.010	0.003	0.007	0.006	0.008	0.008	0.003	0.040	0.002	246	51
0.009	0.003	0.006	0.005	0.008	0.009	0.003	0.040	0.002	302	52
0.008	0.002	0.007	0.004	0.004	0.007	0.002	0.045	0.001	365	55
0.006	0.001	0.005	0.004	0.000	0.010	0.000	0.047	0.000	418	59
0.010	0.002	0.016	0.006	0.006	0.008	0.003	0.047	0.002	427	58
0.006	0.001	0.012	0.004	0.001	0.001	0.000	0.044	0.000	329	54
0.007	0.001	0.016	0.004	0.000	0.011	0.000	0.045	0.000	367	52

Notes :

* Boron, Oxygen, and Nitrogen concentration given in ppm.

All other concentrations expressed in weight percent.

Appendix I. : Chemical Compositions of the Weld Metals (continued).

	[C]	[Ti]	[Al]	[Mn]	[Si]	[P]	[S]	[Cu]	[Ni]	[Cr]	[B]*
a1t1	0.139	0.010	0.004	0.72	0.136	0.012	0.010	0.100	0.03	0.024	6
a1t2	0.118	0.043	0.004	0.72	0.136	0.012	0.009	0.079	0.02	0.023	8
a1t3	0.119	0.083	0.004	0.67	0.121	0.011	0.010	0.087	0.03	0.023	5
a2t1	0.126	0.011	0.009	0.79	0.163	0.013	0.011	0.087	0.03	0.024	19
a2t2	0.113	0.031	0.008	0.67	0.136	0.011	0.010	0.083	0.02	0.023	12
a2t3	0.125	0.084	0.008	0.67	0.136	0.011	0.011	0.088	0.03	0.023	11
a3t1	0.124	0.014	0.009	0.62	0.136	0.012	0.010	0.066	0.02	0.023	8
a3t2	0.135	0.048	0.011	0.66	0.138	0.011	0.011	0.077	0.02	0.022	1
a3t3	0.123	0.121	0.011	0.62	0.136	0.001	0.009	0.074	0.02	0.022	11

[Mo]	[V]	[W]	[Co]	[As]	[Sn]	[Nb]	[Ta]	[Zr]	[O]*	[N]*
0.007	0.017	0.005	0.006	0.007	0.008	0.002	0.035	0.002	191	68
0.006	0.018	0.005	0.007	0.006	0.006	0.002	0.037	0.001	179	87
0.007	0.021	0.004	0.007	0.006	0.006	0.002	0.034	0.002	146	66
0.009	0.013	0.007	0.007	0.007	0.007	0.003	0.041	0.002	186	104
0.006	0.022	0.005	0.007	0.005	0.006	0.002	0.033	0.002	185	78
0.007	0.020	0.007	0.006	0.006	0.007	0.002	0.031	0.002	214	61
0.007	0.024	0.007	0.008	0.006	0.007	0.003	0.041	0.002	194	67
0.006	0.027	0.006	0.007	0.005	0.007	0.002	0.035	0.001	236	66
0.007	0.033	0.006	0.008	0.006	0.006	0.003	0.037	0.002	173	58

Notes :

* Boron, Oxygen, and Nitrogen concentration given in ppm.

All other concentrations expressed in weight percent.

Appendix I.: Chemical Compositions of the Weld Metals (continued).

	[C]	[Ti]	[Al]	[Mn]	[Si]	[P]	[S]	[Cu]	[Ni]	[Cr]	[B]*
T1A1	0.144	0.042	0.128	0.63	0.131	0.007	0.010	0.058	0.02	0.022	0
T2A1	0.136	0.075	0.126	0.60	0.144	0.008	0.012	0.065	0.02	0.022	4
T2A2	0.129	0.082	0.131	0.59	0.169	0.009	0.011	0.057	0.02	0.023	0
T3A1	0.143	0.166	0.137	0.66	0.204	0.009	0.012	0.061	0.02	0.023	0
T3A2	0.134	0.169	0.123	0.73	0.220	0.011	0.012	0.072	0.03	0.026	0
T4A1	0.123	0.174	0.095	0.74	0.241	0.011	0.012	0.066	0.03	0.026	0
T4A2	0.135	0.147	0.134	0.85	0.260	0.013	0.011	0.069	0.03	0.027	2
T5A1	0.140	0.190	0.099	0.79	0.269	0.009	0.010	0.063	0.02	0.027	0

[Mo]	[V]	[W]	[Co]	[As]	[Sn]	[Nb]	[Ta]	[Zr]	[O]*	[N]*
0.003	0.026	0.006	0.005	0.000	0.005	0.000	0.030	0.000	263	61
0.003	0.025	0.006	0.005	0.000	0.006	0.000	0.032	0.000	248	85
0.003	0.031	0.333	0.007	0.000	0.007	0.000	0.039	0.000	200	78
0.004	0.025	0.007	0.006	0.000	0.007	0.000	0.037	0.000	291	86
0.004	0.020	0.057	0.007	0.000	0.011	0.003	0.057	0.000	259	75
0.004	0.022	0.009	0.006	0.000	0.011	0.003	0.052	0.000	175	91
0.005	0.011	0.012	0.006	0.000	0.012	0.003	0.061	0.000	221	81
0.002	0.018	0.005	0.006	0.000	0.007	0.000	0.038	0.000	221	91

Notes :

* Boron, Oxygen, and Nitrogen concentration given in ppm.

All other concentrations expressed in weight percent.